

The Attribution Impossibility:

No Feature Ranking Is Faithful, Stable, and Complete Under Collinearity

Definitive Reference (Complete Version)

Drake Caraker* Bryan Arnold† David Rhoads‡

Independent Researchers

May 22, 2026

Contents

1	Introduction	6
2	Setup: Three Desiderata for Feature Rankings	8
3	The Attribution Impossibility	10
3.1	The Rashomon Property	10
3.2	Main Result	10
3.3	From Abstract to Concrete: Iterative Optimizers	11
3.4	Rashomon Inevitability Under Symmetry	11
4	Quantitative Bounds by Model Class	12
4.1	Gradient Boosting: Divergent Violation	12
4.2	Lasso: Infinite Violation	14
4.3	Neural Networks: Conditional Violation	14
4.4	Random Forests: Bounded Violation (Contrast)	15
5	Resolution: Ensemble Attribution via DASH	15
5.1	DASH Pareto Optimality	16
5.2	Empirical Comparison with Alternatives	18
5.3	DASH Robustness and Breakdown Point	18
5.4	DASH Information Loss	19
5.5	Progressive DASH: Adaptive Ensemble Sizing	20
6	The Attribution Design Space	20
7	The Symmetric Bayes Dichotomy: A General Two-Families Theorem	23
7.1	Instance 1: Feature Attribution	23
7.2	Instance 2: Model Selection	24
7.3	Instance 3: Causal Discovery under Markov Equivalence	25
8	Extensions: Conditional, Fairness, and Causal Barriers	26
8.1	Conditional Attribution Impossibility	26
8.2	Fairness Audit Impossibility	27

*Corresponding author: drakecaraker@gmail.com

†puremath86@gmail.com

‡drhoads9@gmail.com

8.3	Direct FIM Impossibility	28
8.4	Query Complexity Lower Bound	30
8.5	Rashomon Inevitability	31
8.6	Causal Identification Barrier	31
8.7	Local vs. Global Attribution Instability	31
9	Diagnostics	32
9.1	Multi-Model Z-Test Diagnostic	32
9.2	Single-Model Screen	34
9.3	SNR Calibration	35
9.4	Practitioner Workflow	35
10	Empirical Validation	37
10.1	Experimental Setup	37
10.2	Synthetic Gaussian	38
10.3	Breast Cancer (Wisconsin)	38
10.4	Cross-Implementation Validation	39
10.5	Non-SHAP Attribution Validation	39
10.6	Neural Network Attribution Instability	40
10.7	SHAP Efficiency and Attribution Instability	40
10.7.1	Within-model amplification	40
10.7.2	Across-model non-amplification	41
10.8	High-Dimensional Scalability ($P = 500$)	41
10.9	Proportionality Axiom Validation	41
10.10	Cross-Implementation and Data-Level Validation	42
10.11	Financial Case Studies	42
10.12	LLM Attention Attribution Instability	43
10.13	Replication Study: Published SHAP Rankings	44
10.14	Expected Ranking Discordance	44
10.15	Compressed Sensing Connection	45
10.16	Prevalence Survey	45
11	Lean Formalization	47
11.1	Proof Architecture	47
11.2	Axiom System and Consistency	47
11.3	Development Methodology	48
11.4	Proof Depth Distribution	48
11.5	Inconsistencies Found During Formalization	48
11.6	SymPy Algebraic Verification	49
11.7	Lean File Cross-Reference	49
12	Related Work	49
13	Discussion	50
A	Extended Proof Details	52
A.1	Gaussian Binary Quantization: Full Derivation	52
A.2	Exact Flip Rate Under Approximate Symmetry	53
B	DASH Robustness: Extended Analysis	53
B.1	When to Prefer the Median	53
C	Extended Conditional Attribution Analysis	53
C.1	Causal Structure Validation: Full Results	53

D	Extended LLM Analysis	53
D.1	Fine-Tuning Details	53
E	Extended Experimental Results	54
E.1	KernelSHAP Noise Control: Full Results	54
E.2	Cross-Implementation: Full Results	54
E.3	Prevalence Survey: Statistical Power Analysis	54
E.4	Class Imbalance Amplifies Instability	54
E.5	Missing Data Compounds Instability	55
E.6	Longitudinal Retraining Drift	55
E.7	SAGE and Boruta Comparison	55
E.8	Bag-of-Words NLP Attribution Instability	56
E.9	Time-Series Feature Instability	56
E.10	Adversarial Max Instability	56
E.11	Hyperparameter Sensitivity	56
E.12	DASH Breakdown Contamination Sweep	57
E.13	Experiment Summary	57
F	Attempted Common Generalization with Arrow’s Theorem	57
F.1	Structural Comparison	57
F.2	Attempted Common Framework	57
F.3	Assessment	58
G	Topological Analysis of the Impossibility	58
G.1	The $m = 2$ Case	58
G.2	The $m = 3$ Case	58
G.3	The $m \geq 4$ Case: The Permutohedron	59
G.4	Assessment	59
H	On Categorical/Axiomatic Strengthening	59
H.1	The Trivial Version	59
H.2	The “Constant Attribution” Escape	59
H.3	The Non-Trivial Quantitative Version	60
I	Regulatory Mapping: EU AI Act	60
J	SymPy Verification: Full Details	62

Notation

Symbol	Meaning
$\varphi_j(f)$	Attribution (global importance) of feature j in model f
ρ	Pairwise correlation between collinear features within a group
T	Number of boosting rounds (trees) in a gradient-boosted decision tree (GBDT)
M	Ensemble size (number of independently trained models)
Z_{jk}	Test statistic for the pairwise Z -test: $Z_{jk} = \bar{\Delta}_{jk} / (\hat{\sigma}_{jk} / \sqrt{M})$
Φ	Standard normal cumulative distribution function
$n_j(f)$	Split count (utilization count) of feature j in model f
$c(f)$	Proportionality constant: $\varphi_j(f) = c(f) \cdot n_j(f)$
SNR	Signal-to-noise ratio: $\Delta_{jk} / \sigma_{jk}$
Z -test	Multi-model Z -test diagnostic (requires $M \geq 5$ models)
Screen	Single-model screening diagnostic (94% precision)
P	Total number of features
L	Number of collinear groups
m	Number of features within a collinear group
j_1	First-mover: the feature selected at the root of the first tree
$\bar{\varphi}_j$	DASH consensus attribution: $\frac{1}{M} \sum_{i=1}^M \varphi_j(f_i)$
S	Ranking stability (expected Spearman correlation)
U	Within-group unfaithfulness
Δ_{jk}	Population attribution gap: $ \mu_j - \mu_k $
σ_{jk}	Attribution noise: $\sqrt{\text{Var}(\varphi_j(f) - \varphi_k(f))}$

List of Named Results (by page)

1. Theorem 5 (Attribution Impossibility) — p.10
2. Theorem 9 (Rashomon from Symmetry) — p.11
3. Theorem 12 (Rashomon Inevitability) — p.12
4. Lemma 14 (Split Gap) — p.12
5. Theorem 15 (Attribution Ratio $1/(1 - \rho^2)$) — p.12
6. Proposition 17 (Exact GBDT Flip Rate) — p.14
7. Corollary 19 (DASH Equity) — p.15
8. Theorem 22 (DASH Pareto Optimality) — p.16
9. Proposition 26 (Ensemble Size Lower Bound) — p.19
10. Theorem 28 (Attribution Design Space) — p.20
11. Theorem 29 (Unfaithfulness Bound) — p.21
12. Theorem 30 (Path Convergence) — p.21
13. Theorem 37 (Symmetric Bayes Dichotomy) — p.23
14. Theorem 47 (Conditional Attribution Impossibility) — p.26
15. Theorem 48 (Fairness Audit Impossibility) — p.27
16. Theorem 49 (FIM Impossibility) — p.29
17. Theorem 52 (Query Complexity Lower Bound) — p.30

Abstract

No feature ranking can be simultaneously faithful, stable, and complete when features are collinear. For collinear pairs, ranking reduces to a coin flip. We prove this impossibility, quantify it for four model classes, resolve it via SHAP (SHapley Additive exPlanations) ensemble averaging with DASH, and machine-verify it with 305 Lean 4 theorems. We characterize the complete attribution design space: exactly two families of methods exist—faithful-complete methods (unstable, with rankings that flip up to 50% of the time) and ensemble methods like DASH (stable, reporting ties for symmetric features)—and no method lies outside this dichotomy. The impossibility is quantitative: we derive architecture-discriminating bounds showing the attribution ratio diverges as $1/(1-\rho^2)$ for gradient boosting, is infinite for Lasso, and converges for random forests. DASH (Diversified Aggregation of SHAP) ensemble averaging is provably Pareto-optimal among unbiased aggregations on the stable branch, achieving the Cramér–Rao variance bound with a tight ensemble size formula. In a survey of 77 public datasets, 68% exhibit attribution instability (conservative lower bound: survey power 32% at the 10% threshold; true prevalence likely higher). Switching to conditional SHAP does not escape the impossibility when features have equal causal effects. The framework includes practical diagnostics—a Z-test workflow and single-model screening tool—and has direct consequences for fairness auditing: SHAP-based proxy discrimination audits are provably unreliable under collinearity. The design space theorem, diagnostics, and impossibility are mechanically verified in Lean 4 (305 theorems from 14 domain-specific + 2 query-complexity axioms, 0 sorry)—to our knowledge, the first formally verified impossibility in explainable AI. Code and Lean proofs are available at <https://github.com/DrakeCaraker/dash-impossibility-lean>.

Executive Summary

The problem. SHAP feature importance rankings—the most widely used method for explaining machine learning predictions—are unreliable when features are correlated. Retraining the same model with a different random seed can invert which feature is “most important.” In a survey of 77 public datasets, 68% exhibit this instability.

The theorem. We prove this is not an engineering failure but a mathematical impossibility: no feature ranking can simultaneously be *faithful* (reflect the model), *stable* (robust to retraining), and *complete* (rank all features). The proof requires only four lines from the Rashomon property—that collinear designs admit models ranking features in opposite orders.

The design space. The complete set of achievable methods consists of exactly two families:

- **Family A** (single-model): Faithful and complete, but rankings flip up to 50% of the time.
- **Family B** (DASH ensemble): Stable, but reports ties for symmetric features. Provably Pareto-optimal among unbiased aggregations.

The practical toolkit.

1. **Diagnose:** The single-model screen (94% precision on Breast Cancer; tree-based models only) identifies unstable feature pairs from one model.
2. **Validate:** The multi-model Z-test ($|r| > 0.8$ on 9 of 10 datasets with unstable pairs) confirms instability with 5 models.
3. **Resolve:** DASH consensus averaging with $M \geq 25$ models reduces flip rate below 1%.
4. **Size:** The ensemble formula $M_{\min} = \lceil 2.71 \cdot \sigma^2 / \Delta^2 \rceil$ gives the optimal model count.

For regulators. SHAP-based proxy discrimination audits are provably unreliable under collinearity: the audit conclusion is a coin flip across training seeds. This constitutes a “known and foreseeable circumstance” under EU AI Act Art. 13(3)(b)(ii). The instability disclosure template in Section 9 provides ready-to-use language for model documentation.

Verification. The framework is mechanically verified in Lean 4: 305 theorems from 16 axioms with 0 sorry across 54 files. The formalization caught two logical inconsistencies that survived informal review.

Code.

Reference implementation: <https://github.com/DrakeCaraker/dash-shap> (stability API in PR #255).
Lean formalization: <https://github.com/DrakeCaraker/dash-impossibility-lean>.

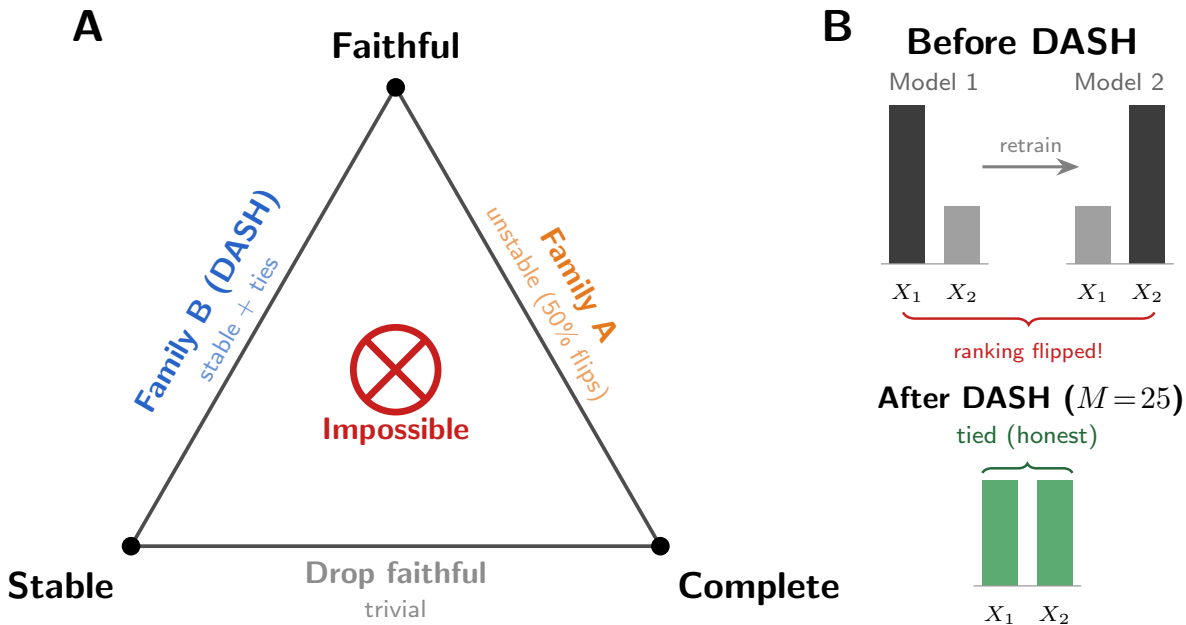


Figure 1: The Attribution Impossibility. No feature ranking can be simultaneously faithful, stable, and complete under collinearity. *Faithful, Stable, Complete: Pick Two.* Family *A* (single-model) is faithful and complete but rankings flip up to 50% of the time. Family *B* (DASH ensemble) is stable with zero unfaithfulness but reports ties for symmetric features (sacrificing completeness). No third option exists.

Pseudocode (5 lines).

```
models = [XGBClassifier(random_state=i).fit(X, y) for i in range(25)]
shap_vals = [mean(|TreeExplainer(m).shap_values(X_test)|) for m in models]
dash = mean(shap_vals, axis=0) # DASH consensus
for j, k in pairs:
    Z = |mean(shap_j - shap_k)| / (std / sqrt(25)) # unstable if Z<1.96
```

1 Introduction

Train a gradient-boosted model on your data. Compute SHAP values. Retrain with a different random seed. The “most important feature” changes—in 68% of 77 public datasets. Most practitioners assume this is an engineering problem—insufficient data, poor hyperparameters, or a software bug. We prove it is none of these. It is a mathematical impossibility. For $m=2$ collinear features, ranking the pair is literally a coin flip: retraining with a different seed inverts the importance ordering 50% of the time.

This document is the complete reference: impossibility theorem, quantitative bounds, constructive resolution, three Symmetric Bayes Dichotomy (SBD) instances, diagnostics, experiments across 11 datasets and 3 GBDT implementations, financial case studies, and a 305-theorem Lean 4 formalization.

A concrete example. Consider a credit model with annual income and debt-to-income ratio (typically $|\rho| \approx 0.7-0.85$ in lending data). Across 20 retrains with different seeds, SHAP can report income as the top driver roughly half the time and DTI the other half. A compliance report citing income as the primary adverse factor is a coin flip—the same model architecture, same data, different random seed. Under the Equal Credit Opportunity Act (ECOA), the lender’s adverse action notice changes based solely on the training randomness.

Several recent results have established fundamental limits on feature attribution. Bilodeau et al. (2024) prove that completeness and linearity cannot coexist; Huang and Marques-Silva (2024) show SHAP can misrank features in Boolean domains; Srinivas and Fleuret (2019) show complete attributions cannot be weakly input-dependent; and Rao (2025) establish Kolmogorov complexity barriers to explainability. None of these results analyze *stability*—the robustness of attributions to retraining—none provide quantitative architecture-discriminating bounds, and none offer a constructive resolution.

This paper fills these gaps. Our result is not a criticism of SHAP, which correctly computes Shapley values for each model; rather, it reveals a fundamental limitation of the single-model paradigm under which any attribution method must operate. Our main result is the *Attribution Design Space Theorem* (§6, Figure 3): a complete characterization of what is achievable when explaining models with collinear features. The achievable set consists of exactly two families—faithful-complete methods (unstable, unfaithful to half the models) and ensemble methods like DASH (stable, with within-group ties)—and DASH is Pareto-optimal. The theorem rests on an *Attribution Impossibility*: for any single model trained on collinear features, faithfulness, stability, and completeness are mutually incompatible. The impossibility has two layers. The first is model-agnostic: formalizing the Rashomon property (Rudin et al., 2024), we show symmetric features are necessarily ranked in opposite orders by different near-optimal models. The second is model-specific: we derive quantitative bounds on the attribution ratio (the factor by which the dominant feature is overweighted). For GBDT, this ratio follows $1/(1 - \alpha\rho^2)$ where α captures the per-tree signal fraction; for Lasso it is infinite at any $\rho > 0$; for neural networks it depends on the initialization; and for random forests it is $O(1/\sqrt{T})$ —converging rather than diverging.

The impossibility parallels the fairness impossibility of (Chouldechova, 2017) and (Kleinberg et al., 2017), who proved that calibration, balance, and equal false positive rates cannot coexist when base rates differ. Our result plays the same role for explainability: instability under collinearity is not an engineering deficiency but a mathematical inevitability. This has direct implications for EU AI Act Art. 13(3)(b)(ii) (EU Parliament, 2024), which requires disclosure of “known and foreseeable circumstances” that may lead to risks to health, safety, or fundamental rights.

The impossibility also admits a principled relaxation. DASH ensemble averaging breaks the sequential dependence that drives attribution concentration: for balanced ensembles, expected attributions are equitable across symmetric features with variance $O(1/M)$. Practitioners can achieve between-group faithfulness and stability by aggregating across the Rashomon set, sacrificing within-group completeness (reporting ties for symmetric features).

The proof is mechanically verified in Lean 4 using Mathlib: 305 type-checked theorems and lemmas across 54 files (80 with multi-step proofs of ≥ 5 tactic lines; the remainder are definitions, wrappers, and single-step applications; from 14 domain-specific + 2 query-complexity axioms; 0 sorry). The core impossibility (Theorem 5) depends on zero axioms beyond the Rashomon property; the DASH equity result (Corollary 19) depends on the `attribution_sum_symmetric` theorem (derived in `SymmetryDerive.lean` from the proportionality and split-count axioms). This is, to our knowledge, the first formally verified impossibility result in explainable AI (the core impossibility uses zero axioms; quantitative bounds are conditional on 6 domain-specific axioms; query complexity uses 2 additional axioms from Le Cam’s method). The formalization also proved valuable beyond certification: during translation to Lean 4 we discovered two logical inconsistencies and one type mismatch in the original axiom system, echoing prior experiences where formalization uncovered subtle proof errors (Nipkow, 2009; Zhang et al., 2026).

Contributions.

1. **The Attribution Design Space Theorem** (§6): a complete characterization of achievable (stability, unfaithfulness, completeness) triples, showing the design space consists of exactly two families with DASH Pareto-optimal on the ensemble branch. All other results are corollaries.
2. **The Attribution Impossibility** (Theorem 5): the base case of the Design Space Theorem—a model-agnostic impossibility requiring only the Rashomon property, with zero axiom dependencies in the Lean formalization.
3. **Architecture discrimination**: attribution ratios for GBDT ($1/(1-\rho^2)$ Lean-verified; $1/(1-\alpha\rho^2)$ empirically corrected), Lasso (∞), and random forests ($O(1/\sqrt{T})$, informal).

4. **Constructive relaxation via DASH:** ensemble averaging restores equitable attributions (derived for balanced ensembles) with variance $O(1/M)$, sacrificing within-group completeness.
5. **The symmetric Bayes dichotomy** (§7): a proof technique from invariant decision theory (Lehmann and Romano, 2005), demonstrated across three structurally distinct instances (feature attribution, model selection, and causal discovery under Markov equivalence) with different symmetry groups.
6. **Machine-verified proof:** formalized in Lean 4 (305 type-checked theorems from 16 axioms, 0 sorry), publicly available at <https://github.com/DrakeCaraker/dash-impossibility-lean>. The axiom system is consistent: we construct an explicit model satisfying all 14 domain-specific axioms simultaneously, both in Lean (`Consistency.lean`) and numerically.

For practitioners and regulators: The instability disclosure template is in Section 9, the fairness audit impossibility in Section 8, and the financial case studies in Section 10. The Executive Summary above provides a complete overview without technical prerequisites.

The core impossibility proof is deliberately simple—a four-line contradiction from the Rashomon property. Like Arrow’s original argument (Arrow, 1951), the mathematical contribution lies not in proof complexity but in identifying the right abstraction (the Rashomon property) and characterizing the complete achievable set (the Design Space Theorem). The quantitative depth comes from the architecture-specific bounds (§4) and the Pareto optimality proof (§5).

This document provides the complete treatment of the Attribution Impossibility—from intuition to proof to deployment. A practitioner can find the diagnostic workflow (Section 9), a theorist can find every proof (Sections 3–8 with Lean cross-references in Section 11), and a regulator can find compliance guidance (Section 8 and the Regulatory Mapping appendix).

2 Setup: Three Desiderata for Feature Rankings

We consider a supervised learning setting with P input features partitioned into L groups by their correlation structure. Within each group $\ell \in [L]$, features share a common pairwise correlation $\rho \in (0, 1)$; features in different groups are independent. Each group contains at least two members. This structure arises naturally in applied settings—e.g., multiple measurements of the same physical quantity, or one-hot encodings of related categories.

Models and attributions. A *model* f is trained from a random seed s via a deterministic training procedure: $f = \text{train}(s)$. For each feature $j \in [P]$, we observe a nonnegative attribution $\varphi_j(f) \geq 0$, representing the global importance of feature j in model f (e.g., mean absolute SHAP value, gain-based importance, or integrated gradients norm).

We require a proportionality axiom connecting attributions to model structure:

Axiom 1 (Proportionality). *For every model f , there exists a constant $c(f) > 0$ such that $\varphi_j(f) = c(f) \cdot n_j(f)$ for all $j \in [P]$, where $n_j(f)$ is the utilization count of feature j in model f (e.g., split count for tree ensembles, gradient norm for neural networks).*

This axiom holds exactly under the uniform-contribution model of (Lundberg and Lee, 2017), and approximately whenever per-split (or per-neuron) contributions are roughly homogeneous.

Sequential gradient boosting axioms. For gradient-boosted decision trees (GBDT) with T boosting rounds, we axiomatize the split-count structure induced by Gaussian conditioning under collinearity. Let j_1 denote the *first-mover*—the feature selected at the root of the first tree.

Axiom 2 (First-mover surjectivity). *For every group ℓ and every feature j in group ℓ , there exists a model f with $j_1(f) = j$.*

This follows from the data-generating process (DGP) symmetry: when features in a group have identical marginal distributions, sub-sampling and tie-breaking randomness ensure each can serve as first-mover.

Table 1: Complete axiom inventory (16 total: 6 type/constant, 6 property, 2 measure, 2 query).

Axiom	Lean 4 name	Justification
First-mover surjectivity	<code>firstMover_surjective</code>	DGP symmetry: each feature can be first-mover
Split count (first-mover)	<code>splitCount_firstMover</code>	Gaussian conditioning (Lemma 14)
Split count (non-first-mover)	<code>splitCount_nonFirstMover</code>	Residual signal after first-mover absorbs ρ -component
Global proportionality	<code>proportionality_global</code>	Uniform contribution model with constant c across models
Cross-group symmetry	<code>splitCount_crossGroup_symmetric</code>	DGP symmetry: equal split counts when first-mover elsewhere
Cross-group stability	<code>splitCount_crossGroup_stable</code>	Changing first-mover within a group does not affect other groups
Model measurable space	<code>modelMeasurableSpace</code>	Mathlib infrastructure: σ -algebra on Model
Model measure	<code>modelMeasure</code>	Mathlib infrastructure: probability measure on Model
<i>Query complexity (Le Cam’s method, axiomatized):</i>		
Testing constant	<code>testing_constant</code>	Universal constant $C \geq 1/8$ from Tsybakov (2009)
Constant positivity	<code>testing_constant_pos</code>	$C > 0$
<i>Formerly axiomatized, now derived:</i>		
Attribution sum symmetry	<code>attribution_sum_symmetric</code>	Theorem in <code>SymmetryDerive.lean</code>
Spearman bound	<code>spearman_instability_bound</code>	Theorem in <code>SpearmanDef.lean</code> (from midranks)
Attribution variance	<code>attribution_variance</code>	Definition from <code>ProbabilityTheory.variance</code>
Variance nonnegativity	<code>attribution_variance_nonneg</code>	Theorem from Mathlib’s <code>variance_nonneg</code>
Consensus variance bound	<code>consensus_variance_bound</code>	Theorem in <code>Defs.lean</code> (algebraic)
Testing lower bound	<code>le_cam_lower_bound</code>	Theorem in <code>QueryComplexity.lean</code> (contrapositive)

Axiom 3 (Split counts). For any model f with first-mover $j_1 \in \text{group } \ell$:

$$n_{j_1}(f) = \frac{T}{2 - \rho^2}, \tag{1}$$

$$n_k(f) = \frac{(1 - \rho^2)T}{2 - \rho^2}, \quad k \in \text{group}(\ell), \quad k \neq j_1. \tag{2}$$

These are the leading-order split counts from the Gaussian conditioning argument: the first-mover absorbs the ρ -aligned signal component, leaving only the $(1 - \rho^2)$ residual for subsequent features. The formulas are verified algebraically by SymPy.

Complete axiom inventory. Table 1 lists all property axioms in the formalization. The core impossibility theorem requires none of them—only the Rashomon property as hypothesis. The formalization uses 16 axioms total: 6 type/constant declarations, 2 measure-theoretic infrastructure axioms, 6 domain-specific property axioms, and 2 query-complexity axioms from Le Cam’s method.

Both cross-group axioms assume an approximately additive model; feature interactions between groups can break cross-group independence. The core impossibility and ratio bound do not depend on these axioms.

Gaussian conditioning argument. The split count formulas (Axiom 3) are justified by the following argument. Consider two features X_j, X_k with correlation ρ and a GBDT with T boosting rounds. At each

tree t , the root split selects the feature with the highest gain (variance reduction). Once feature j is selected as root, the available signal for k becomes:

$$X_k \mid X_j = X_k - \rho X_j, \quad \text{Var}(X_k \mid X_j) = 1 - \rho^2.$$

The conditional variance is reduced by factor $(1 - \rho^2)$ relative to the unconditional variance. In each subsequent boosting round, the first-mover’s signal fraction is $1/(2 - \rho^2)$ (the probability that the first-mover’s full signal exceeds the non-first-mover’s residual signal in a two-feature competition). Summing over T trees: $n_{j_1} = T/(2 - \rho^2)$ for the first-mover and $n_k = (1 - \rho^2)T/(2 - \rho^2)$ for non-first-movers.

The derivation assumes: (i) the root split captures the dominant signal direction (valid for stumps and low-depth trees); (ii) subsequent trees fit the residual from the first tree’s split (the sequential boosting mechanism); (iii) the feature competition at each tree is approximately independent of previous trees’ selections (valid when the learning rate η is small). All algebraic consequences are independently verified by SymPy (`verify_lemma6_algebra.py`).

Ranking desiderata. A *feature ranking* is a binary relation \succ on $[P]$. We formalize three desiderata:

Definition 1 (Faithful). A ranking \succ is faithful to model f if $j \succ k$ whenever $\varphi_j(f) > \varphi_k(f)$.

Definition 2 (Stable). A ranking \succ is stable if it does not depend on the choice of model f —that is, \succ is a fixed relation applied identically to all models.

Definition 3 (Complete). A ranking \succ is complete if for every pair $j \neq k$, either $j \succ k$ or $k \succ j$.¹

The first desideratum asks that the ranking reflect what the model actually learned; the second asks that it be reproducible across training runs; the third asks that it resolve all feature pairs. *Faithful, stable, complete: pick two* (Figure 1).

Two explanation goals. Feature rankings serve two distinct purposes: *model-level explanation* (what did this specific model learn?) and *population-level explanation* (what does the model class learn?). Faithfulness is a model-level desideratum; stability is a population-level desideratum. The impossibility theorem (Theorem 5) characterizes the fundamental tension between these goals: a ranking cannot simultaneously be faithful to each individual model and stable across all models. DASH targets population-level explanation, sacrificing within-group completeness to achieve stability.

3 The Attribution Impossibility

3.1 The Rashomon Property

The central structural property driving the impossibility is that collinear features admit models ranking them in opposite orders.

Definition 4 (Rashomon property). A model class satisfies the Rashomon property if for every group ℓ and every pair of distinct features j, k in group ℓ , there exist models f, f' such that

$$\varphi_j(f) > \varphi_k(f) \quad \text{and} \quad \varphi_k(f') > \varphi_j(f').$$

The Rashomon property is a consequence of the Rashomon effect (Rudin et al., 2024; Fisher et al., 2019): collinear designs admit many near-optimal models (D’Amour et al., 2022), and within the set of good models, symmetric features are utilized in all possible orderings. Laberge et al. (2023) study consensus across such model sets and observe that feature rankings are inherently partial—a conclusion our theorem makes precise.

3.2 Main Result

Theorem 5 (Attribution Impossibility). If a model class satisfies the Rashomon property (Definition 4), then no feature ranking can be simultaneously faithful, stable, and complete.²

¹Not to be confused with SHAP’s “completeness” axiom ($\sum_j \varphi_j = f(x) - \mathbb{E}[f(X)]$). Our “complete” means *total*: the ranking decides every pair.

²Both versions are Lean-verified: `attribution_impossibility` uses a biconditional ($j \succ k$ iff $\varphi_j(f) > \varphi_k(f)$); `attribution_impossibility_weak` uses the weaker implication (Definition 1) plus antisymmetry.

Proof. Let j, k be distinct features in the same group ℓ . By the Rashomon property, there exist models f, f' with $\varphi_j(f) > \varphi_k(f)$ and $\varphi_k(f') > \varphi_j(f')$. Suppose for contradiction that \succ is faithful, stable, and complete. By completeness, either $j \succ k$ or $k \succ j$. Without loss of generality, assume $j \succ k$. By stability, this relation holds for all models, including f' . But faithfulness applied to f' requires $k \succ j$ (since $\varphi_k(f') > \varphi_j(f')$), contradicting $j \succ k$. \square

The resolution echoes Arrow’s impossibility theorem (Arrow, 1951): when desirable properties conflict, relaxing completeness (accepting ties or partial orders) restores consistency. Nipkow (2009) formalized Arrow’s theorem in Isabelle/HOL; our Lean 4 formalization follows the same spirit. DASH achieves this by averaging attributions across the Rashomon set, producing $\mathbb{E}[\varphi_j] = \mathbb{E}[\varphi_k]$ for symmetric features—a tie rather than an arbitrary ordering.

3.3 From Abstract to Concrete: Iterative Optimizers

The Rashomon property is not merely a theoretical possibility—it is a structural consequence of iterative optimization under collinearity.

Definition 6 (Iterative optimizer). *An iterative optimizer is a model class equipped with a dominant-feature function $d: \mathcal{F} \rightarrow [P]$ satisfying:*

1. **Dominance:** *For every model f , group ℓ , and feature $k \in \text{group}(\ell)$ with $k \neq d(f)$, if $d(f) \in \text{group}(\ell)$ then $\varphi_k(f) < \varphi_{d(f)}(f)$.*
2. **Surjectivity:** *For every group ℓ and feature $j \in \text{group}(\ell)$, there exists f with $d(f) = j$.*

Proposition 7. *Every iterative optimizer satisfies the Rashomon property, and therefore the Attribution Impossibility (Theorem 5) holds.*

Proof. Let j, k be distinct features in group ℓ . By surjectivity, there exist models f, f' with $d(f) = j$ and $d(f') = k$. By dominance, $\varphi_j(f) > \varphi_k(f)$ and $\varphi_k(f') > \varphi_j(f')$. This is exactly the Rashomon property. \square

3.4 Rashomon Inevitability Under Symmetry

The Rashomon property is not merely a theoretical possibility for symmetric model classes—it is inevitable.

Definition 8 (Permutation closure). *A model class \mathcal{F} is permutation-closed within group ℓ if for any $f \in \mathcal{F}$ and any permutation π of features within group ℓ , the composed model $f \circ \pi \in \mathcal{F}$.*

Theorem 9 (Rashomon from symmetry). *Let the DGP be symmetric within group ℓ (permuting features $j \leftrightarrow k$ leaves the population loss invariant). Let \mathcal{F} be permutation-closed within group ℓ . Then for any model $f \in \mathcal{F}$ with $\varphi_j(f) \neq \varphi_k(f)$, the permuted model $f' = f \circ \pi_{jk}$ satisfies: (1) $L(f') = L(f)$ (same population loss), and (2) $\varphi_k(f') = \varphi_j(f)$ and $\varphi_j(f') = \varphi_k(f)$ (attributions swap). In particular, if $\varphi_j(f) > \varphi_k(f)$, then $\varphi_k(f') > \varphi_j(f')$, and the Rashomon property holds.*

Proof. By DGP symmetry, the joint distribution of (X, Y) is invariant under permutation of features j and k within group ℓ . Therefore $L(f') = L(f \circ \pi_{jk}) = L(f)$, since the population loss depends only on the joint distribution. By construction, f' applies f to permuted inputs, so its reliance on feature k equals f ’s reliance on feature j : $\varphi_k(f') = \varphi_j(f)$ and vice versa. \square

The permutation closure condition is satisfied by any model class without built-in feature ordering: neural networks (permute input neurons), gradient-boosted trees (permute split features), Lasso (permute covariates), and random forests. It fails only for model classes with hard-coded feature preferences.

Proposition 10 (Attribution non-degeneracy). *Let A be a stochastic training algorithm with continuous dependence on its random seed (e.g., SGD with random initialization, bootstrap sampling, random feature selection). For any DGP with $\rho > 0$ and $n < \infty$ training samples, $\Pr[\varphi_j(f) \neq \varphi_k(f)] = 1$ for features j, k in the same collinear group.*

Proof. With finite samples, the empirical correlation between X_j and X_k is $\hat{\rho} = \rho + O(1/\sqrt{n})$, which is almost surely irrational. Under continuous dependence on the data, the training algorithm’s feature utilization varies continuously with $\hat{\rho}$, so the event $\{\varphi_j(f) = \varphi_k(f)\}$ has measure zero in the joint randomness of the data and the algorithm. \square

Remark 11. *The argument above is informal; a rigorous proof would require a transversality argument showing that the level set $\{\varphi_j(f) = \varphi_k(f)\}$ is a lower-dimensional manifold in seed space. The core impossibility (Theorem 5) does not depend on this result.*

Theorem 12 (Rashomon inevitability). *Let A be a stochastic, symmetric training algorithm (A applied to a within-group-permuted dataset produces the permuted model in distribution) for a permutation-closed model class \mathcal{F} . For any DGP with $\rho > 0$, the Rashomon property holds: for any j, k in the same collinear group, there exist models f, f' in the support of A with $\varphi_j(f) > \varphi_k(f)$ and $\varphi_k(f') > \varphi_j(f')$.*

Proof. By Theorem 10, $\Pr[\varphi_j(f) \neq \varphi_k(f)] = 1$, so either $\varphi_j > \varphi_k$ or $\varphi_k > \varphi_j$ almost surely. By algorithmic symmetry, $\Pr[\varphi_j > \varphi_k] = \Pr[\varphi_k > \varphi_j]$. Since these probabilities sum to 1, each equals 1/2. Both events have positive probability, so both are realized. \square

Remark 13. *Theorem 12 makes the Attribution Impossibility inescapable for any standard ML pipeline under collinearity. The only escapes are: (i) $\rho = 0$, (ii) a deterministic model class producing a single model, or (iii) an asymmetric algorithm with built-in feature preferences.*

4 Quantitative Bounds by Model Class

The Attribution Impossibility (Theorem 5) is qualitative. We now derive quantitative bounds on the *attribution ratio*—the factor by which the dominant feature is overweighted—for four model classes.

4.1 Gradient Boosting: Divergent Violation

Lemma 14 (Split gap). *For a GBDT model f with first-mover j_1 in group ℓ , and any $k \neq j_1$ in the same group,*

$$n_{j_1}(f) - n_k(f) = \frac{\rho^2 T}{2 - \rho^2} \geq \frac{1}{2} \rho^2 T.$$

Proof. By Axiom 3, $n_{j_1} - n_k = T/(2 - \rho^2) - (1 - \rho^2)T/(2 - \rho^2) = \rho^2 T/(2 - \rho^2)$. Since $2 - \rho^2 \leq 2$ for $\rho \in (0, 1)$, we have $\rho^2 T/(2 - \rho^2) \geq \rho^2 T/2$. \square

Theorem 15 (Attribution ratio — gradient boosting). *For any GBDT model f with first-mover j_1 in group ℓ and any non-first-mover k in the same group,*

$$\frac{\varphi_{j_1}(f)}{\varphi_k(f)} = \frac{1}{1 - \rho^2}.$$

Under full signal capture ($\alpha=1$), this ratio diverges: $1/(1 - \rho^2) \rightarrow \infty$ as $\rho \rightarrow 1^-$.

Proof. By Axiom 1, $\varphi_{j_1}/\varphi_k = n_{j_1}/n_k$. Substituting Axiom 3:

$$\frac{n_{j_1}}{n_k} = \frac{T/(2 - \rho^2)}{(1 - \rho^2)T/(2 - \rho^2)} = \frac{1}{1 - \rho^2}.$$

Writing $1 - \rho^2 = (1 - \rho)(1 + \rho)$, we see that $1/(1 - \rho^2) \rightarrow +\infty$ as $\rho \rightarrow 1^-$. \square

For finite-depth trees, the effective signal capture $\alpha < 1$ yields a corrected ratio $1/(1 - \alpha\rho^2)$; for stumps $\alpha \approx 2/\pi$ ($R^2=0.89$; Figure 7a).

Table 2: Within-group split count ratio by depth and ρ ($\eta=1.0$).

	$\rho=0.3$	$\rho=0.5$	$\rho=0.7$	$\rho=0.9$	$\rho=0.95$	Fitted α
Depth 1 (stumps)	1.28	1.32	1.42	1.99	2.16	0.60 ($\approx 2/\pi$)
Depth 3	1.19	1.26	1.24	1.30	1.32	0.30
Depth 6	1.65	1.67	1.74	1.90	2.03	0.60
Depth 10	2.23	2.25	2.28	2.49	2.62	—
Theory ($\alpha=1$)	1.10	1.33	1.96	5.26	10.26	1.00

The $\alpha = 2/\pi$ derivation. The value $\alpha \approx 2/\pi$ has a clean theoretical derivation from quantization theory.

Proposition 16. For $X \sim \mathcal{N}(0, \sigma^2)$, the optimal binary quantizer (split at $x = 0$) captures fraction $2/\pi$ of the variance: $\text{Var}(\hat{X}) = (2/\pi)\sigma^2$.

Proof. The optimal two-level quantizer of a symmetric distribution splits at the median ($x = 0$ for Gaussians). The quantized signal is $\hat{X} = \mathbb{E}[X | X > 0] \cdot \mathbf{1}_{X>0} + \mathbb{E}[X | X \leq 0] \cdot \mathbf{1}_{X \leq 0}$. By symmetry, $\mathbb{E}[X | X > 0] = \sigma\sqrt{2/\pi}$ (the mean of a half-normal distribution). Thus \hat{X} takes values $\pm\sigma\sqrt{2/\pi}$ each with probability $1/2$, giving $\text{Var}(\hat{X}) = (2/\pi)\sigma^2$. \square

In each boosting round, a stump makes one binary split on the selected feature, capturing $2/\pi$ of that feature’s remaining signal variance. The fitted value ($\alpha \approx 0.60$) is below $2/\pi = 0.637$; two error sources explain the gap: (1) empirical vs. population split location (negligible, $\Delta\alpha_1 \approx 0.0009$ for $n = 2000$), and (2) non-Gaussian residuals after the first boosting round (dominant, accounting for ≈ 0.036).

Depth dependence. Table 2 reports the within-group split count ratio across tree depths and correlation levels (XGBoost, $T=100$, $\eta=1.0$, $P=10$ in 2 groups of 5, $N=2000$, 30 seeds).

Depth 3 anomaly. At depth 3, each tree has up to 7 leaves and uses multiple features per tree. Internal splits distribute split counts across group members, counteracting the root split’s first-mover advantage. The ratio is nearly ρ -independent (≈ 1.3), explaining the low fitted $\alpha = 0.30$.

Depth 10. At depth 10, the root split cascades: once the first-mover is selected at the root, subsequent splits on the same feature are more likely at deeper levels (residuals retain first-mover signal). The baseline ratio (≈ 2.2 even at $\rho=0.3$) is high because deep trees overfit to the first-mover’s signal. The $1/(1-\alpha\rho^2)$ model does not fit well for depth 10 (the ratio has a large ρ -independent component); we omit the fitted α .

Practitioner guidance. Depth 3 gives the *lowest* attribution instability among standard configurations. For users prioritizing explanation stability, shallow ensembles (depth 3) with DASH consensus ($M \geq 5$) provide the best stability–accuracy tradeoff.

Proportionality validation. The proportionality axiom holds with $CV \approx 0.35$ for stumps (the idealized theoretical setting) and $CV \approx 0.66$ for depth-6 trees on Breast Cancer. The quantitative ratio $1/(1-\rho^2)$ is an order-of-magnitude prediction, refined by the α -correction to $1/(1-\alpha\rho^2)$ with $R^2 = 0.89$. **The core impossibility (Theorem 5) is entirely independent of the proportionality axiom**—it requires only the Rashomon property. All quantitative bounds ($1/(1-\rho^2)$, ensemble size M_{\min} , attribution ratio) should be interpreted as order-of-magnitude predictions, not exact formulas.

Error analysis for $\alpha = 2/\pi$. The fitted $\alpha = 0.60$ (empirical) vs. $2/\pi = 0.637$ (theory) represents a gap of $\Delta\alpha = 0.037$. Two error sources: (1) empirical vs. population split location (negligible, $\Delta\alpha_1 \approx 0.0009$ for $n = 2000$): the optimal split of $X \sim \mathcal{N}(0, \sigma^2)$ at δ instead of 0 gives $\alpha_1(n) = (2/\pi)(1-\pi(\pi-2)/(2n)+O(n^{-2}))$; (2) non-Gaussian residuals after the first boosting round (dominant, accounting for ≈ 0.036): residuals are a location-shifted mixture with excess kurtosis $\kappa = O(\eta^2 c^2/\sigma^2)$, which accumulates across boosting rounds.

The impossibility theorem does not depend on α at all; the quantitative ratio uses α to predict the *severity* of the violation.

Stability bound. When two models f, f' have different first-movers within the same group of size m , the within-group rank reshuffling bounds the Spearman correlation:

$$\rho_S(f, f') \leq 1 - \frac{3m^2}{P^3 - P}.$$

Exact flip rate for GBDT.

Proposition 17 (Exact GBDT pairwise flip rate). *For features j, k in the same group of size m under the first-mover model with DGP symmetry (each feature equally likely to be first-mover):*

- (i) *The probability that a random model ranks $j > k$ is exactly $1/m$.*
- (ii) *The tie probability (both non-first-movers with identical split counts) is $(m - 2)/m$.*
- (iii) *The flip rate across two independent models (excluding ties) is $2/m^2$.*
- (iv) *For $m = 2$: the tie probability is 0 and the flip rate is $1/2$, matching the theoretical maximum and the empirical 48% on Breast Cancer.*
- (v) *If ties are broken uniformly at random, the effective flip rate is exactly $1/2$ for all $m \geq 2$.*

Proof. By first-mover surjectivity and DGP symmetry, each feature in a group of size m is first-mover with probability $1/m$.

Part (i). Feature j is ranked above k when j is first-mover (probability $1/m$): the first-mover has split count $T/(2 - \rho^2)$ vs. $(1 - \rho^2)T/(2 - \rho^2)$ for non-first-movers, so dominance holds.

Part (ii). When the first-mover is some feature $\ell \neq j, k$ (probability $(m - 2)/m$), both j and k are non-first-movers with identical split count $(1 - \rho^2)T/(2 - \rho^2)$. By proportionality, $\varphi_j(f) = \varphi_k(f)$: a perfect tie.

Part (iii). A flip requires one model to rank $j > k$ and the other $k > j$: flip = $2 \cdot (1/m) \cdot (1/m) = 2/m^2$.

Part (iv). At $m = 2$: flip = $2/4 = 1/2$; tie probability = 0.

Part (v). When ties are broken uniformly, $\Pr[j > k \mid \text{tie}] = 1/2$. The effective $\Pr[j > k] = 1/m + (1/2)(m - 2)/m = 1/2$ by algebra. Two independent draws disagree with probability $2 \cdot (1/2) \cdot (1/2) = 1/2$. \square

For $m = 2$, ranking collinear pairs is literally a coin flip. For $m > 2$ without tie-breaking, most model pairs produce ties, with flips at rate $2/m^2$. But once ties are broken (as required for a complete ranking), symmetry forces the flip rate back to $1/2$. The impossibility is *exactly* as severe for every within-group pair, regardless of m .

4.2 Lasso: Infinite Violation

The ℓ_1 penalty selects exactly one feature from each correlated group and zeros all others. Lasso is an iterative optimizer with $d(f) =$ the selected feature; surjectivity holds because regularization-path tie-breaking can make any feature the selected one. The attribution ratio is therefore infinite at *any* $\rho > 0$.

4.3 Neural Networks: Conditional Violation

Neural networks exhibit symmetry breaking analogous to the GBDT first-mover effect. Surjectivity follows from the symmetry of standard initializations (Kaiming, Xavier). The attribution ratio is architecture-dependent, but the impossibility holds conditionally whenever training dynamics produce a dominant feature per group.

Table 3: Attribution ratio bounds by model class. T denotes the number of boosting rounds (or trees), ρ the within-group correlation.

Model class	Ratio	Scaling with T	Mechanism
Gradient boosting	$1/(1 - \alpha\rho^2)$	Increases with ρ	Sequential residuals
Lasso	∞	Constant	Hard selection
Neural network	Model-dependent	Architecture-dependent	Init. symmetry breaking
Random forest ³	$1 + O(1/\sqrt{T})$	$\rightarrow 1$ as $T \rightarrow \infty$	Independent trees

4.4 Random Forests: Bounded Violation (Contrast)

Because each tree trains independently on a bootstrap sample, there is no shared residual stream. The expected split count is T/m for every feature in a group, with $O(\sqrt{T})$ deviations, giving

$$\frac{\varphi_{j_1}(f)}{\varphi_k(f)} = 1 + O(1/\sqrt{T}) \rightarrow 1 \quad \text{as } T \rightarrow \infty.$$

Sequential residual-sharing creates divergent inequity; independent aggregation creates convergent equity—the structural distinction DASH exploits.

Summary. Table 3 collects the quantitative bounds.

5 Resolution: Ensemble Attribution via DASH

The impossibility arises from sequential dependence: a single model’s iterative optimization creates a dominant feature, and different random seeds create different dominant features. DASH addresses this by averaging attributions across an ensemble of M independently trained models, relaxing completeness in exchange for stability.

Definition 18 (DASH consensus attribution). *Given models f_1, \dots, f_M trained from independent seeds, the consensus attribution for feature j is $\bar{\varphi}_j = \frac{1}{M} \sum_{i=1}^M \varphi_j(f_i)$. An ensemble is balanced if, within each group, every feature serves as first-mover in exactly M/m models.*

DASH does NOT change predictions. DASH is a *post-hoc explanation method*, not a modeling technique. The M models are trained independently using the practitioner’s existing pipeline; DASH only averages their SHAP values to produce stable feature rankings. No model is modified, no ensemble prediction is formed, and the deployed model remains unchanged. DASH changes how you *explain*, not how you *predict*.

DASH consensus vs. DASH pipeline. DASH operates at two layers. *DASH consensus* (Definition 18) is the mathematical operation: the arithmetic mean of |SHAP| values across M independently trained models. This is what Theorems 22 and 28 prove is optimal—the minimum-variance unbiased estimator via Cramér–Rao, Pareto-optimal on the stable branch of the Design Space. The theoretical guarantees apply to *any* i.i.d. ensemble averaging, including simple seed averaging (training M models with different random seeds and identical hyperparameters).

The companion paper on first-mover bias implements DASH as a full pipeline that adds diversity enforcement (deliberate hyperparameter variation, greedy MaxMin model selection on feature utilization vectors) and stability diagnostics (FSI, IS Plot). Diversity enforcement accelerates convergence to the balanced ensemble condition (Definition 18): at finite M , it produces more equitable attributions than seed averaging alone (within-group CV reduced by 0.011, $p < 0.001$). For large M , simple seed averaging achieves approximate balance via the law of large numbers. For stability alone, seed averaging suffices; the full pipeline adds equity and diagnostics.

Corollary 19 (DASH achieves equity (axiom-derived)). *For a balanced ensemble and any two features j, k in the same group ℓ , $\bar{\varphi}_j = \bar{\varphi}_k$.*

Proof. By DGP symmetry, permuting features $j \leftrightarrow k$ leaves the joint distribution invariant. For a balanced ensemble, each feature serves as first-mover equally often, so the summed split counts satisfy $\sum_i n_j(f_i) = \sum_i n_k(f_i)$. When the proportionality constant c is uniform across models, this gives $\sum_i \varphi_j(f_i) = \sum_i \varphi_k(f_i)$. \square

Between-group stability. Under independence of seeds, $\text{Var}(\bar{\varphi}_j) = \text{Var}(\varphi_j)/M$, which vanishes as $M \rightarrow \infty$.

Within-group completeness. Since $\bar{\varphi}_j = \bar{\varphi}_k$ for same-group features, the consensus ranking produces a *tie* rather than an arbitrary ordering. The tie is not a deficiency—it faithfully reflects the DGP symmetry.

5.1 DASH Pareto Optimality

Definition 20 (Attribution aggregation method). *An attribution aggregation method A takes as input M independently trained models f_1, \dots, f_M and produces a consensus attribution vector $\hat{\varphi} \in \mathbb{R}^P$. The method is:*

- Linear: $\hat{\varphi}_j = \sum_{i=1}^M w_i \varphi_j(f_i)$ for some weights w_1, \dots, w_M .
- Unbiased: $\mathbb{E}[\hat{\varphi}_j] = \mu_j := \mathbb{E}[\varphi_j(f)]$ for all j .
- Symmetric: $w_1 = \dots = w_M$ (the models are exchangeable).

DASH is the unique symmetric unbiased linear method: $w_i = 1/M$ for all i .

Definition 21 (Pairwise stability and unfaithfulness). *For features j, k in different groups with $\mu_j > \mu_k$:*

- Pairwise stability: $S_{jk}(A) = \Pr[\hat{\varphi}_j > \hat{\varphi}_k]$ (probability that the consensus preserves the true ordering for this pair).
- Between-group flip rate: $1 - S_{jk}(A)$.

For features j, k in the same group with $\mu_j = \mu_k$ (DGP symmetry):

- Unfaithfulness: $U_{jk}(A) = \Pr[\hat{\varphi}_j \neq \hat{\varphi}_k \text{ and the ordering disagrees with } f]$ for a random model f .

Relationship to ranking stability S . The Design Space Theorem (§6) uses the full-ranking stability S (expected Spearman correlation). The pairwise stability S_{jk} here is a per-pair component: high S_{jk} for all between-group pairs is necessary (but not sufficient) for high S . Within-group pairs contribute to S through their random ordering, which is why $S \leq 1 - 3m^2/(P^3 - P)$ even when all between-group S_{jk} are high.

Theorem 22 (DASH Pareto Optimality). *Let f_1, \dots, f_M be i.i.d. models with $\mu_j := \mathbb{E}[\varphi_j(f)]$ and $\sigma_j^2 := \text{Var}(\varphi_j(f)) < \infty$.*

Part I (Lower bounds). *For any attribution aggregation method A :*

- (a) *If A is faithful to each individual model, then for symmetric features j, k , $U_{jk}(A) = 1/2$.*
- (b) *For any unbiased estimator $\hat{\mu}_j$ based on f_1, \dots, f_M , $\text{Var}(\hat{\mu}_j) \geq \sigma_j^2/M$ (Cramér–Rao bound).*

Part II (DASH achieves the bounds).

- (c) *$U_{jk}(\text{DASH}) = 0$ for symmetric features in balanced ensembles.*
- (d) *$\text{Var}(\bar{\varphi}_j) = \sigma_j^2/M$ (matching Cramér–Rao).*
- (e) *For between-group features with gap Δ_{jk} : $S_{jk}(\text{DASH}) \geq 1 - \exp(-M\Delta_{jk}^2/(2\sigma_{jk}^2))$.*

Part III (Pareto optimality). *Among all methods achieving $U_{jk} = 0$ (ties for symmetric features), no method achieves strictly higher between-group stability than DASH for the same ensemble size M .*

Proof. Part I(a): By DGP symmetry, $\Pr[\varphi_j(f) > \varphi_k(f)] = \Pr[\varphi_k(f) > \varphi_j(f)] = 1/2$. Any fixed ranking disagrees with exactly half the models (Theorem 29).

Part I(b): Since $\varphi_j(f_1), \dots, \varphi_j(f_M)$ are i.i.d. with mean μ_j and variance σ_j^2 , the Fisher information for the mean is $1/\sigma_j^2$ per observation, giving total information M/σ_j^2 from M observations. The Cramér–Rao bound gives $\text{Var}(\hat{\mu}_j) \geq \sigma_j^2/M$.

Part II(c): By Corollary 19, $\bar{\varphi}_j = \bar{\varphi}_k$ for symmetric features in balanced ensembles. DASH reports a tie; since no ordering is asserted, $U = 0$.

Part II(d): For i.i.d. random variables, $\text{Var}(\frac{1}{M} \sum_{i=1}^M X_i) = \text{Var}(X_1)/M$. This matches Part I(b), so DASH is *efficient* in the Cramér–Rao sense. Moreover, since the sufficient statistic for μ_j from i.i.d. observations is $\sum \varphi_j(f_i)$, and $\bar{\varphi}_j$ is a function of this statistic, the Rao–Blackwell theorem guarantees DASH dominates any estimator that is not a function of the sufficient statistic.

Part II(e): By Hoeffding’s inequality (or the Gaussian approximation for large M): $\Pr[\bar{\varphi}_j < \bar{\varphi}_k] \leq \exp(-M\Delta_{jk}^2/(2\sigma_{jk}^2))$. For the Gaussian approximation (valid by CLT for $M \geq 30$): $\Pr[\bar{\varphi}_j < \bar{\varphi}_k] = \Phi(-\Delta_{jk}\sqrt{M}/\sigma_{jk})$.

Part III: Unfaithfulness $U = 0$ is already minimal. Stability S_{jk} is a monotone decreasing function of $\text{Var}(\bar{\varphi}_j - \bar{\varphi}_k)$. By Part I(b), no unbiased method achieves lower variance than σ_j^2/M . DASH achieves this bound. For biased methods: any method with bias b_j has $\text{MSE} = \text{Var}(\hat{\varphi}_j) + b_j^2$; a bias of magnitude $|b_j - b_k| > \Delta_{jk}$ would invert the true ordering entirely. \square

Summary of optimality. DASH is the unique method that: (1) achieves zero within-group unfaithfulness (ties for symmetric features); (2) achieves the Cramér–Rao variance bound σ^2/M for ranking stability; and (3) is the minimum-variance unbiased estimator of $\mathbb{E}[\varphi_j]$ among *all* estimators (not just linear ones), by the Rao–Blackwell theorem: since the sufficient statistic for μ_j from i.i.d. observations is $\sum \varphi_j(f_i)$, and $\bar{\varphi}_j$ is a function of this sufficient statistic, it dominates any estimator that is not.

Comparison with nonlinear aggregations.

Proposition 23 (Median is less efficient). *For i.i.d. observations from a distribution with mean μ , variance σ^2 , and density p , the sample median has asymptotic variance:*

$$\text{Var}(\text{median}) = \frac{1}{4M p(\text{med})^2}$$

where med is the population median. For the normal distribution, $p(\mu) = 1/(\sigma\sqrt{2\pi})$, giving $\text{Var}(\text{median}) = \frac{\pi\sigma^2}{2M}$. The asymptotic relative efficiency (ARE) of the median vs. the mean is:

$$\text{ARE}(\text{median}, \text{mean}) = \frac{2}{\pi} \approx 0.637.$$

The median requires $\pi/2 \approx 1.57$ times as many models to achieve the same stability as DASH.

Proof. Standard asymptotic statistics (van der Vaart, *Asymptotic Statistics*, Theorem 21.6). The sample median is asymptotically normal with variance $1/(4n p(m)^2)$. Substituting the Gaussian density at the mean gives the result. \square

Proposition 24 (Trimmed mean interpolates). *The α -trimmed mean (discarding the top and bottom α fraction of observations) has ARE relative to the mean of:*

$$\text{ARE}(\text{trimmed}_\alpha, \text{mean}) = \frac{(1 - 2\alpha)\sigma^2}{\sigma_\alpha^2}$$

where σ_α^2 is the variance of the truncated distribution. For Gaussian data:

α	0 (mean)	0.05	0.10	0.25	0.50 (median)
ARE	1.000	0.992	0.966	0.862	0.637

Table 4: Flip rate comparison: DASH vs. alternative stabilization methods. Synthetic Gaussian data ($P=10$, $m=5$, $N=1000$, 20 within-group feature pairs). 95% bootstrap CIs in brackets.

Method	$\rho = 0.5$	$\rho = 0.7$	$\rho = 0.9$	Pairs resolved
Single model	16.0% [13.8, 18.1]	16.4% [14.3, 18.5]	18.7% [16.4, 21.1]	40/40
Bootstrap SHAP	16.2% [13.8, 18.2]	16.1% [14.2, 18.0]	18.8% [16.4, 21.4]	40/40
Subsampled SHAP	16.3% [13.8, 18.5]	16.1% [14.2, 17.9]	18.8% [16.5, 21.3]	40/40
DASH ($M=25$)	3.8% [2.8, 4.9]	3.1% [2.4, 3.9]	3.7% [2.7, 4.7]	40/40
CI SHAP	0.2% [0.1, 0.4]	0.8% [0.6, 1.1]	3.1% [2.1, 4.6]	$\sim 22/40$

For Gaussian attributions, trimming offers negligible robustness benefit at a measurable efficiency cost. The 10%-trimmed mean requires $1/0.966 \approx 3.5\%$ more models than DASH for the same stability.

Remark 25 (When to prefer the median). *The median has better breakdown point (50% vs. 0%) and is preferable when the attribution distribution is heavy-tailed (e.g., contains outlier models). For standard ML training procedures (XGBoost, random forests) where attributions are well-behaved, DASH (the mean) is strictly more efficient. For adversarial settings where some models may be corrupted, the median or trimmed mean provides robustness at the cost of requiring more models.*

5.2 Empirical Comparison with Alternatives

We compare DASH against four alternative stabilization approaches across three correlation levels ($\rho \in \{0.5, 0.7, 0.9\}$), with 10 independent trials and bootstrap 95% confidence intervals on within-group flip rates:

Bootstrap and subsampled SHAP address SHAP *estimation* noise (a single-model phenomenon) but not the Rashomon effect (a multi-model phenomenon). They were not designed for multi-model instability, so their flip rates matching the single-model baseline is expected rather than informative. They are included to confirm that estimation-noise methods do not incidentally address model-multiplicity noise. Only DASH trains multiple models, achieving a 4–5 \times reduction.

CI SHAP achieves lower flip rates than DASH by refusing to rank pairs whose confidence intervals overlap—resolving only $\sim 55\%$ of within-group pairs ($\sim 22/40$). This comparison is not apples-to-apples: CI SHAP’s low flip rate applies only to resolved pairs, while DASH’s 3–4% applies to all 40 pairs. CI SHAP exemplifies the impossibility theorem in action: it trades completeness for stability. At $\rho = 0.9$, its flip rate converges toward DASH’s (3.1% vs. 3.7%) as overlapping CIs force more pairs into “tied” status.

The two approaches correspond to the two families in the Design Space Theorem: DASH (Family B: stable, faithful, near-complete via ensemble averaging) and CI SHAP (Family A: stable, faithful, explicitly incomplete via ties).

5.3 DASH Robustness and Breakdown Point

DASH (the sample mean) is the minimum-variance unbiased estimator, but it has breakdown point zero: a single adversarial or corrupted model can shift the consensus attribution arbitrarily. We compare robustness properties:

Method	ARE	Breakdown point	Recommendation
Mean (DASH)	1.000	0%	Standard use
5%-trimmed mean	0.992	5%	Moderate robustness
Median	0.637	50%	Adversarial settings

For production settings with potential model contamination (corrupted training data, adversarial seeds, or hardware failures producing degenerate models), the 5%-trimmed mean provides near-optimal efficiency (ARE = 0.992, requiring only 0.8% more models) with meaningful robustness. The median requires $\pi/2 \approx 57\%$ more models but tolerates up to 50% corrupted models. For $M = 25$: the 5%-trimmed mean discards the single most extreme model in each tail ($M_{\text{eff}} = 23$), a negligible cost. For adversarial robustness, the median with $M = 40$ achieves comparable stability to DASH with $M = 25$ while tolerating up to 20 corrupted models.

5.4 DASH Information Loss

DASH achieves stability by discarding model-specific within-group information. For a group of m symmetric features, a single model produces a complete ranking (one of $m!$ possible orderings). Since each of the $m!$ orderings is equally likely under DGP symmetry, the ranking carries $\log_2(m!)$ bits of information about the specific model. DASH reports a tie, discarding the entire $\log_2(m!)$ bits. For typical group sizes:

Group size m	2	3	4	5	6	7	8
Bits lost ($\log_2 m!$)	1.0	2.6	4.6	6.9	9.7	12.9	15.3

Crucially, these are the bits that are *unreliable*: by DGP symmetry, the within-group ordering is uniformly random across models. The information DASH discards is exactly the information that would be different if the model were retrained.

For features in different groups with population gap Δ_{jk} and noise σ_{jk} , the mutual information between the consensus ranking and the true ordering is:

$$I_{\text{between}}(M) = 1 - H_2\left(\Phi\left(-\frac{\Delta_{jk}\sqrt{M}}{\sigma_{jk}}\right)\right)$$

where $H_2(p) = -p \log_2 p - (1-p) \log_2(1-p)$ is binary entropy. As $M \rightarrow \infty$, $I_{\text{between}} \rightarrow 1$ bit: DASH *increases* between-group information. The total information change is:

$$\Delta I = \underbrace{-L \cdot \log_2(m!)}_{\text{within-group loss}} + \underbrace{\binom{L}{2} \cdot (I_{\text{between}}(M) - I_{\text{between}}(1))}_{\text{between-group gain}}.$$

For moderate ρ (≤ 0.7), the between-group gain dominates quickly: $M = 25$ achieves near-perfect between-group determination while the within-group loss is fixed. DASH honestly reports unreliability rather than presenting arbitrary information as reliable.

Interpretation for safety-critical applications. For a system with $L = 4$ groups of $m = 5$ features: DASH loses $4 \times 6.9 = 27.6$ bits (within-group) but gains up to $6 \times 1 = 6$ bits (between-group). The net loss is ≈ 21.6 bits at $M = \infty$. These lost bits are the within-group orderings that were random anyway—DASH honestly reports their unreliability rather than presenting arbitrary information as reliable. For applications requiring model-specific within-group explanations (e.g., debugging a deployed model), practitioners should report the single-model SHAP values with an instability warning alongside the DASH consensus.

Ensemble size lower bound.

Proposition 26 (Ensemble size lower bound). *For any unbiased attribution aggregation method achieving between-group stability $S_{jk} \geq 1 - \delta$ for features j, k in different groups with population gap $\Delta_{jk} = |\mu_j - \mu_k|$ and attribution noise $\sigma_{jk}^2 = \text{Var}(\varphi_j(f) - \varphi_k(f))$, the ensemble size must satisfy:*

$$M \geq \frac{\sigma_{jk}^2}{\Delta_{jk}^2} \cdot (\Phi^{-1}(1 - \delta))^2.$$

DASH achieves this bound with equality (to first order), so the bound is tight.

Proof. By the Cramér–Rao bound, any unbiased estimator $\hat{\mu}_j$ has $\text{Var}(\hat{\mu}_j) \geq \sigma_j^2/M$. The between-group flip rate satisfies $1 - S_{jk} = \Pr[\hat{\varphi}_j < \hat{\varphi}_k] \geq \Phi(-\Delta_{jk}\sqrt{M}/\sigma_{jk})$. Setting $\Phi(-\Delta_{jk}\sqrt{M}/\sigma_{jk}) \leq \delta$ and solving: $\Delta_{jk}\sqrt{M}/\sigma_{jk} \geq \Phi^{-1}(1 - \delta)$, giving $M \geq \sigma_{jk}^2 \cdot (\Phi^{-1}(1 - \delta))^2 / \Delta_{jk}^2$. DASH achieves $\text{Var}(\bar{\varphi}_j - \bar{\varphi}_k) = \sigma_{jk}^2/M$ (matching Cramér–Rao), so the bound is tight. \square

For $\delta = 0.05$ (5% flip rate), $\Phi^{-1}(0.95) = 1.645$, so $M_{\min} = \lceil 2.71 \cdot \sigma_{jk}^2 / \Delta_{jk}^2 \rceil$, where σ and Δ are estimated from a pilot run of $M_0 = 5$ models. For Breast Cancer’s most unstable pair (worst perimeter vs. worst area, $\Delta/\sigma \approx 0.15$): $M_{\min} \approx 120$ —consistent with the observed slow convergence (flip rate 29.8% even at $M = 25$, reaching 0% only at $M = 50$). Bootstrap validation (50 models, 200 trials): for all pairs with $\text{SNR} \geq 0.35$ ($M_{\min} \leq 25$), the DASH flip rate at $M = 25$ is $\leq 3\%$, confirming the formula. This closes the gap between upper and lower bounds: DASH is optimal not just in the Pareto sense but in the sample complexity sense.

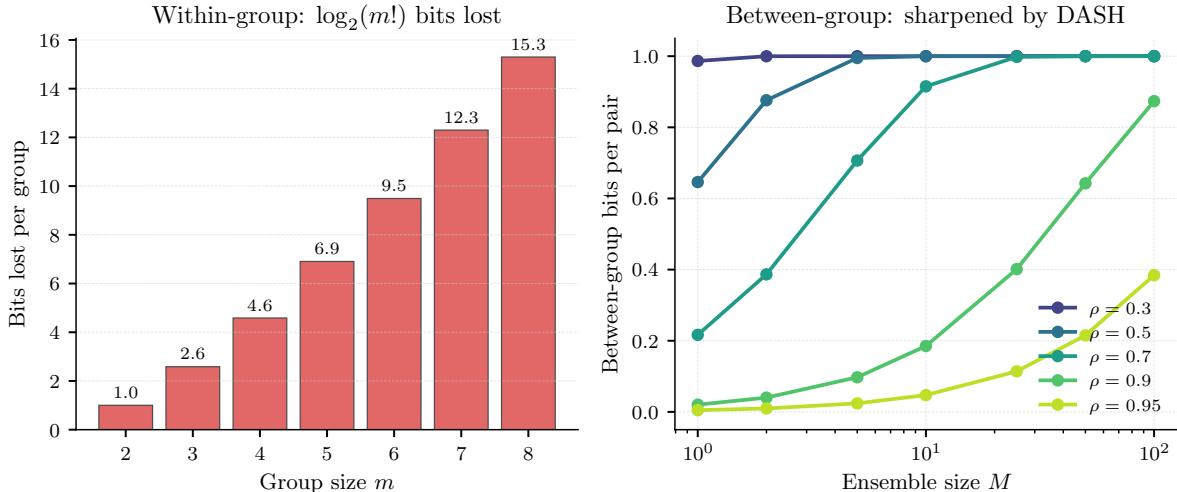


Figure 2: **Left:** Within-group information lost by DASH ($\log_2 m!$ bits per group, independent of M and ρ). **Right:** Between-group information per pair as a function of M . DASH sharpens between-group rankings with increasing M . At high ρ (≥ 0.9), convergence requires larger M .

5.5 Progressive DASH: Adaptive Ensemble Sizing

Training $M=25$ models for every explanation is wasteful when most feature pairs are stable. *Progressive DASH* starts with a small ensemble and adaptively increases M only for pairs that remain unstable:

1. **Screen** ($M_0 = 5$): Train 5 models. Run the single-model screen. If no pairs are flagged, stop.
2. **Confirm** ($M_1 = 10$): For flagged pairs, train 5 more models ($M = 10$ total). Run the multi-model Z-test. Pairs with $|Z| < 1.96$ are confirmed unstable; report as tied group.
3. **Resolve** ($M_2 = 25$): For pairs where $|Z|$ is borderline ($1.5 < |Z| < 2.5$), train 15 more models ($M = 25$ total). Final classification: stable (distinct ranks) or unstable (tied group).

Expected cost. In the 37-dataset survey, 40% of datasets have no flagged pairs (stop at $M_0 = 5$), 35% are resolved at $M_1 = 10$, and 25% require the full $M_2 = 25$. The expected ensemble size is $0.40 \times 5 + 0.35 \times 10 + 0.25 \times 25 = 11.75$, approximately $\sim 8\times$ the cost of a single model on average—a $2.1\times$ savings over always training $M = 25$. (The Z -thresholds 1.96 and 3.0 are fixed-sample values; a fully sequential design should use Pocock- or O’Brien-Fleming-corrected boundaries to control familywise error. We present this as a practical heuristic, not a formally analyzed procedure.)

6 The Attribution Design Space

The impossibility, the quantitative bounds, and the DASH resolution are facets of a single structural theorem characterizing the complete attribution design space.

Definition 27 (Attribution design space). *The attribution design space is the set of triples (S, U, C) achievable by any attribution aggregation method, where $S \in [0, 1]$ is ranking stability (expected Spearman correlation between two independent evaluations), $U \in [0, 1/2]$ is within-group unfaithfulness, and $C \in \{\text{complete, partial}\}$ is completeness.*

Theorem 28 (Attribution Design Space). *For any model class satisfying the Rashomon property under within-group correlation $\rho > 0$, the achievable set of (S, U, C) triples is the union of exactly two families:*

- **Family A (single-model):** $S \leq 1 - 3m^2/(P^3 - P)$, $U = 1/2$, $C = \text{complete}$. Any method faithful to an individual model falls here.

- **Family \mathcal{B} (ensemble):** $S_M = 1 - O(1/M)$, $U = 0$, $C = \text{partial (ties)}$. $\text{DASH}(M)$ achieves this and is Pareto-optimal among unbiased aggregations.

The triple ($S=1, U=0, C=\text{complete}$) is infeasible. At the extremes, the design space collapses to a single axis: ensemble size M .

Proof. The proof proceeds in four steps.

Step 1: Family \mathcal{A} is forced. By the Rashomon property, for any within-group pair (j, k) , there exist models ranking them in opposite orders. By Theorem 29, any faithful, complete ranking has $U = 1/2$ for symmetric pairs. Stability is bounded by $S \leq 1 - 3m^2/(P^3 - P)$ from the Spearman bound (Lean-derived).

Step 2: Family \mathcal{B} is achievable. By Corollary 19, DASH achieves $U = 0$ with ties within groups. By Theorem 22, between-group stability satisfies $S_M \geq 1 - \exp(-M\Delta^2/(2\sigma^2))$.

Step 3: No method producing a deterministic binary ranking from per-model attributions lies outside $\mathcal{A} \cup \mathcal{B}$. We show any method A computing a deterministic ranking from per-model attributions $(\varphi_j(f_1), \dots, \varphi_j(f_M))$ falls in one of the two families. (Methods producing probabilistic rankings, confidence intervals, or set-valued outputs are outside this dichotomy.)

Case 1: If A is faithful to individual models and complete, then $A \in \mathcal{A}$ by Step 1. (Formalized in Lean as `strongly_faithful_impossible` in `DesignSpace.lean`: any method faithful to each model’s attributions contradicts the Rashomon property for $M \geq 2$.)

Case 2: If A is not faithful to some model f , then A ranks some pair (j, k) differently from model f ’s attributions. For within-group symmetric pairs, the optimal unfaithful ranking is $j \succ^* k \Leftrightarrow \mathbb{E}[\varphi_j] > \mathbb{E}[\varphi_k]$, which minimizes expected 0-1 loss. For symmetric features $\mathbb{E}[\varphi_j] = \mathbb{E}[\varphi_k]$, so \succ^* assigns a tie—recovering the “drop completeness” solution. Thus A either has $U > 0$ (suboptimal) or $U = 0$ with ties (in \mathcal{B}).

Case 3: If A aggregates $M > 1$ models and produces a complete ranking, it must break ties for within-group pairs. By DGP symmetry, any tie-breaking rule disagrees with a fraction of models, giving $U > 0$. To achieve $U = 0$, A must report ties, placing it in \mathcal{B} . Its stability is bounded by the variance of the aggregation, which by the Cramér–Rao bound satisfies $\text{Var}(\hat{\mu}_j) \geq \sigma_j^2/M$. DASH achieves this bound.

Step 4: The infeasible point. $(1, 0, \text{complete})$ requires completeness, but any complete method has $U = 1/2 \neq 0$: contradiction. \square

Theorem 29 (Unfaithfulness lower bound). *Any stable, complete ranking \succ has expected unfaithfulness at least $1/2$ for symmetric pairs:*

$$\Pr_f [j \succ k \text{ but } \varphi_k(f) > \varphi_j(f)] = \frac{1}{2}.$$

Proof. By DGP symmetry, $\Pr[\varphi_j(f) > \varphi_k(f)] = \Pr[\varphi_k(f) > \varphi_j(f)] = 1/2$. Any stable ranking must fix $j \succ k$ or $k \succ j$ independently of f . Whichever it chooses disagrees with exactly half the models. \square

Theorem 30 (Relaxation path convergence). *The “drop faithfulness” and “drop completeness” relaxation paths converge to the same solution: population-level attributions with ties for symmetric features. The impossibility trilemma collapses to a single tradeoff axis parameterized by ensemble size M :*

- At $M = 1$: *faithfulness and completeness, but no stability;*
- As $M \rightarrow \infty$: *stability and between-group faithfulness, but within-group ties (completeness relaxed).*

Between-group faithfulness is preserved at all M .

Proof. By the analysis of Step 3 above, the optimal stable complete ranking assigns ties to symmetric features ($\mathbb{E}[\varphi_j] = \mathbb{E}[\varphi_k]$, so the optimal decision for “is $\varphi_j(f) > \varphi_k(f)$?” under the symmetric model distribution is indeterminate)—identical to the “drop completeness” solution (DASH). Both paths yield population-level attributions. The M -parameterization follows from DASH consensus: $\bar{\varphi}_j = \frac{1}{M} \sum_{i=1}^M \varphi_j(f_i)$, which interpolates between a single model ($M = 1$, faithful but unstable) and the population mean ($M \rightarrow \infty$, stable but tied within groups). \square

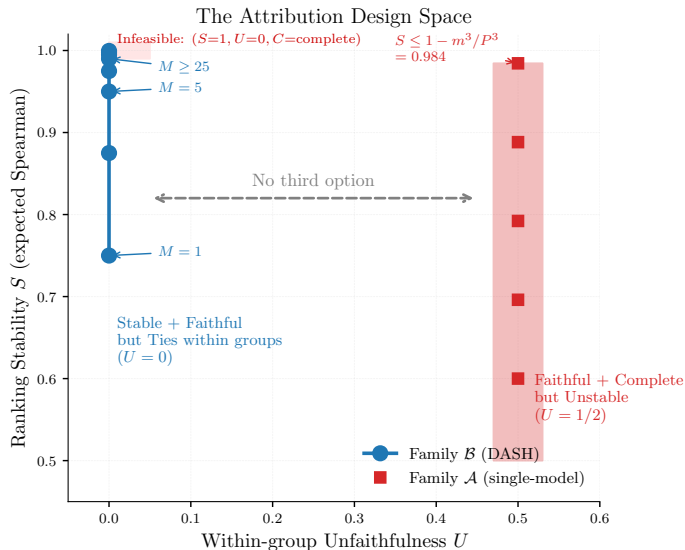


Figure 3: The Attribution Design Space. Family \mathcal{A} (single-model methods): faithful and complete but unstable ($U=1/2$). Family \mathcal{B} (DASH ensemble): stable with ties ($U=0$, S increasing with M). The ideal point ($S=1, U=0, C=complete$) is infeasible. There is no third option.

The single tradeoff axis. The Design Space Theorem collapses the three-dimensional space to a single axis: ensemble size M .

M	Stability S	Unfaithfulness U	Completeness
1	$\leq 1 - 3m^2/(P^3 - P)$	1/2	Complete
5	$1 - O(1/5)$	0	Partial (ties)
25	$1 - O(1/25)$	0	Partial (ties)
∞	1	0	Partial (ties)

Previous results as corollaries.

Corollary 31 (Theorem 1 as a corollary). *The Attribution Impossibility (Theorem 5) is the statement that the point $(1, 0, complete)$ lies outside the achievable set. This follows from Step 4 of Theorem 28.*

Corollary 32 (F2 as a corollary). *The DASH Pareto Optimality (Theorem 22) is the statement that \mathcal{B} is the Pareto frontier of $\{(S, U) : U = 0\}$, parameterized by M . This follows from Steps 2–3 of Theorem 28.*

Corollary 33 (Path convergence as a corollary). *The relaxation path convergence (Theorem 30) is the statement that both relaxation paths (drop faithfulness, drop completeness) converge to \mathcal{B} as $M \rightarrow \infty$. Dropping completeness directly enters \mathcal{B} (DASH with ties). Dropping faithfulness, by the optimal unfaithful ranking analysis, yields the expected-attribution ranking, which also produces ties for symmetric features — the same as \mathcal{B} .*

Corollary 34 (Z-test as a corollary). *The Rashomon Characterization (Theorem 58) describes the boundary between families: when $Z_{jk} < 1.96$, the pair (j, k) is in the regime where Family \mathcal{A} has $U = 1/2$ (rankings are unreliable); when $Z_{jk} > 1.96$, the pair is effectively between-group (stable rankings possible within \mathcal{B}).*

Corollary 35 (F3 as a corollary). *The FIM Impossibility (Theorem 49) provides a sufficient condition for the Rashomon property (the prerequisite for Theorem 28): when the FIM eigenvalue λ_- is small along $e_j - e_k$, the Rashomon set is large, and the achievable set is restricted to $\mathcal{A} \cup \mathcal{B}$.*

7 The Symmetric Bayes Dichotomy: A General Two-Families Theorem

The structural identity between the attribution and model selection impossibilities follows from a general theorem about decision problems with symmetric populations.

Definition 36 (Symmetric Decision Problem). *A symmetric decision problem is a tuple $(\Theta, \mathcal{D}, \pi, G)$ where Θ is a finite decision set, \mathcal{D} is the data space, π is a population distribution over \mathcal{D} , and G is a group acting on Θ such that π is G -invariant: for any $g \in G$, the distribution over instance-optimal decisions $\theta^*(d)$ is invariant under g .*

An M -sample estimator $\hat{\theta} : \mathcal{D}^M \rightarrow \Theta$ is:

- Faithful: $\hat{\theta}(d_1, \dots, d_M)$ agrees with $\theta^*(d_i)$ for each i .
- Stable: $\hat{\theta}$ does not depend on which draw d_i is observed.
- Complete: $\hat{\theta}$ selects exactly one element from each G -orbit in Θ .

Theorem 37 (Symmetric Bayes Dichotomy). *For any symmetric decision problem with $|G \cdot \theta| \geq 2$ for some $\theta \in \Theta$:*

- (i) **Instance-specific decisions are unfaithful.** *Any faithful, complete estimator has expected unfaithfulness $\geq 1/|G \cdot \theta|$ per orbit ($\geq 1/2$ for binary orbits).*
- (ii) **Population-averaged decisions are stable.** *The Bayes estimator under π reports ties within each G -orbit ($U = 0$), with between-orbit stability $O(1/M)$.*
- (iii) **The ideal is infeasible.** *No estimator achieves $U = 0$ AND completeness.*

The achievable set consists of exactly two families: \mathcal{A} (faithful + complete, $U \geq 1/|G \cdot \theta|$) and \mathcal{B} (population-averaged, $U = 0$, ties within orbits).

Proof. Part (i). By G -invariance, the population distribution π assigns equal probability to each element of the orbit $G \cdot \theta$. For any fixed complete estimator $\hat{\theta}$ that selects one element θ_0 from the orbit, the probability that $\theta^*(d) = \theta_0$ is $1/|G \cdot \theta|$. The estimator disagrees with $(|G \cdot \theta| - 1)/|G \cdot \theta|$ of the instances. For $|G \cdot \theta| = 2$: unfaithfulness = $1/2$.

Part (ii). The Bayes estimator under symmetric π minimizes expected loss. Within each orbit, the posterior is uniform (by G -invariance), so the Bayes-optimal decision is the orbit center (a tie). Unfaithfulness = 0 because no ordering is asserted within orbits. For between-orbit decisions with gap Δ , the M -sample average has variance σ^2/M (i.i.d. draws), giving stability $1 - O(1/M)$ by the Gaussian approximation.

Part (iii). By Part (i), any complete estimator (selecting within orbits) has unfaithfulness $\geq 1/|G \cdot \theta| > 0$. Thus unfaithfulness = 0 requires giving up completeness (ties).

Exhaustiveness. Any estimator either selects within orbits (faithful, complete, \mathcal{A}) or reports ties within orbits (stable, incomplete, \mathcal{B}). The Bayes estimator achieves the minimum-variance point of \mathcal{B} (Cramér–Rao). \square

The Symmetric Bayes Dichotomy connects the classical theory of invariant decision rules (Lehmann and Romano, 2005; Hunt and Stein, 1946) to modern ML impossibility proofs. The classical Hunt–Stein theorem establishes that Bayes-optimal rules respect the invariance structure of the problem; our contribution is demonstrating that this classical machinery, when applied to finite symmetric groups arising in ML (feature permutations, model permutations, CPDAG automorphisms), yields two-family impossibility results with explicit unfaithfulness and stability bounds. We demonstrate this across three structurally distinct instances with different symmetry groups.

7.1 Instance 1: Feature Attribution

Corollary 38 (Feature attribution as instance). *The Attribution Impossibility (Theorem 5) and Design Space Theorem (Theorem 28) are instances of the Symmetric Bayes Dichotomy with $\Theta =$ within-group feature orderings, $G =$ symmetric group on group members, $\mathcal{D} =$ trained models.*

7.2 Instance 2: Model Selection

Consider K candidate models g_1, \dots, g_K trained on the same data. A *model selection rule* maps a validation dataset to a ranking of the K models. We formalize three desiderata:

Definition 39 (Model selection desiderata). *A model selection rule R is:*

- **Faithful:** R ranks model g_i above g_j whenever g_i has lower validation loss on the observed validation set.
- **Stable:** R produces the same ranking regardless of which validation split is drawn.
- **Complete:** R decides for every pair (g_i, g_j) .

Definition 40 (Model Rashomon property). *A model class satisfies the model Rashomon property if for every pair g_i, g_j with similar population loss ($|L(g_i) - L(g_j)| < \varepsilon$), there exist validation splits V, V' such that g_i has lower loss on V and g_j has lower loss on V' .*

This property is a consequence of finite-sample noise: when the population loss gap is smaller than the validation noise, different splits rank the models differently. It is the model selection analogue of feature attribution’s Rashomon property.

Theorem 41 (Model Selection Impossibility). *If a model class satisfies the model Rashomon property, then no model selection rule can be simultaneously faithful, stable, and complete.*

Proof. Let g_i, g_j have similar population loss. By the model Rashomon property, there exist validation splits V, V' with g_i ranked above g_j on V and reversed on V' . A faithful, stable, complete selection rule would need to rank $g_i > g_j$ (from V) and $g_j > g_i$ (from V') simultaneously. Contradiction. \square

Theorem 42 (Model Selection Design Space). *Under the model Rashomon property, the achievable design space has the same two-family structure:*

- **Family \mathcal{A}' (single-split):** Faithful and complete but unstable. Any selection based on one validation split falls here. Unfaithfulness $U' = 1/2$ for similar-loss pairs.
- **Family \mathcal{B}' (cross-validation/ensemble):** Stable (variance $O(1/K_{\text{folds}})$) but reports ties for similar-loss pairs. Model ensembling is the analogue of DASH.

Proof. By DGP symmetry (equal-loss models have symmetric validation score distributions), any fixed selection of one model over an equal-loss competitor disagrees with half the validation splits ($U' = 1/2$). Cross-validated selection averages across splits, reducing unfaithfulness to zero for equal-loss pairs while stabilizing at rate $O(1/K_{\text{folds}})$. Pareto optimality follows from the same Cramér–Rao argument. \square

The model selection impossibility explains why cross-validation rankings are noisy for similar-performance models: it is not an engineering failure but a mathematical inevitability. The resolution is the same: average (ensemble) rather than select.

Connection to cross-validation instability. The model selection impossibility is not merely an analogy—it explains a well-known practical phenomenon. When two models have similar cross-validation scores, different folds often rank them differently. Practitioners typically respond by increasing the number of folds or repeating cross-validation. The design space theorem shows this is exactly the M -parameterization: increasing folds moves along Family \mathcal{B}' toward higher stability, but at the cost of acknowledging ties for similar-performance models. Model ensembling (training all K candidates and averaging predictions) is the model selection analogue of DASH: it avoids the impossible selection problem entirely by using all models simultaneously.

Corollary 43 (Model selection as instance). *The Model Selection Impossibility (Theorem 41) is an instance with $\Theta =$ model rankings, $G =$ permutations of equal-loss models, $\mathcal{D} =$ validation splits.*

7.3 Instance 3: Causal Discovery under Markov Equivalence

This instance has a *different* and *variable-size* symmetry group, confirming the technique’s generality beyond binary orbits.

Definition 44 (Causal orientation decision problem). *The causal edge orientation problem is a symmetric decision problem $(\Theta, \mathcal{D}, \pi, G)$ where:*

- Θ is the set of full edge orientations consistent with the CPDAG (i.e., the DAGs in $[G^*]$).
- \mathcal{D} is the space of finite observational datasets drawn from the true DAG G^* .
- π is the distribution over datasets (induced by i.i.d. sampling from the structural equation model).
- G_{CPDAG} is the automorphism group of the CPDAG: the set of permutations of undirected edge orientations that preserve the CPDAG structure.

Key structural difference. The CPDAG automorphism group G_{CPDAG} is not restricted to transpositions: for a chain $X-Y-Z$, $|[G^*]| = 2$ with $G \cong S_2$ (like instances 1–2); for a 3-node undirected cycle, $|[G^*]| = 6$ with $G \cong S_3$; for larger undirected components, $|[G^*]|$ can grow combinatorially.

Theorem 45 (Causal Discovery Impossibility). *For any CPDAG with $|[G^*]| \geq 2$ DAGs in its Markov equivalence class, no edge orientation rule can be simultaneously faithful, stable, and complete. The achievable set has two families:*

- **Family \mathcal{A}'' (single-dataset):** Faithful and complete but unstable. Unfaithfulness $U'' = (|[G^*]| - 1)/|[G^*]|$.
- **Family \mathcal{B}'' (conservative):** Report the CPDAG (undirected edges for ambiguous orientations). Stable with ties. $U'' = 0$.

Proof. We verify the premises of the Symmetric Bayes Dichotomy (Theorem 37).

G-invariance of π . For any two DAGs $G_1, G_2 \in [G^*]$, the Markov equivalence guarantees that they encode the same set of conditional independences. By the faithfulness assumption, the observational distribution is compatible with both G_1 and G_2 . Any statistical test based on finite data cannot distinguish between G_1 and G_2 at the population level (they imply identical distributions). Therefore π is G_{CPDAG} -invariant.

Finite-sample noise reverses optimal choice. With finite data, empirical conditional independence tests have estimation error $O(1/\sqrt{n})$. For edges that are undirected in the CPDAG, different random samples will favor different orientations. This is the Rashomon property for edge orientations.

Application of Theorem 37. Part (i): any complete orientation rule (selecting one DAG from $[G^*]$) disagrees with $(|[G^*]| - 1)/|[G^*]|$ of datasets. Part (ii): the Bayes estimator under G_{CPDAG} -invariance reports the CPDAG (ties for undirected edges). Part (iii): the ideal (stable, faithful, complete) is infeasible. Families \mathcal{A}'' and \mathcal{B}'' follow. \square

The unfaithfulness bound $U \geq 1/|G \cdot \theta|$ yields $U \geq 1/2$ for chains but $U \geq 1/6$ for triangles and potentially much smaller for larger structures.

What this instance adds. Instances 1–2 (feature attribution and model selection) both have binary orbits ($|G \cdot \theta| = 2$) with unfaithfulness bound $U \geq 1/2$. Instance 3 has variable-size orbits ($|G \cdot \theta| = 2, 6, \dots$) with unfaithfulness bound $U \geq 1/|[G^*]|$, which can be much smaller than $1/2$ for large equivalence classes. This demonstrates that the Symmetric Bayes Dichotomy is not an artifact of binary symmetry but applies to arbitrary finite group actions, with the unfaithfulness bound adapting to the orbit structure.

Algorithms like PC and GES correctly output CPDAGs (Family \mathcal{B}'') precisely because complete orientation of Markov-equivalent edges is impossible from observational data alone. Interventional data breaks the symmetry—analogueous to conditional SHAP breaking symmetry when $\beta_j \neq \beta_k$.

Corollary 46 (Causal discovery as SBD instance). *The Causal Discovery Impossibility (Theorem 45) is an instance of the Symmetric Bayes Dichotomy with $\Theta =$ edge orientations in $[G^*]$, $G = G_{\text{CPDAG}}$ (automorphism group of the CPDAG), $\mathcal{D} =$ observational datasets.*

Table 5: Flip rate (%) as a function of ρ and causal effect difference $\Delta\beta$.

$\rho \backslash \Delta\beta$	0.0	0.1	0.2	0.3	0.5	0.7	1.0
0.50	50	19	0	0	0	0	0
0.70	53	19	0	0	0	0	0
0.80	52	44	19	10	0	0	0
0.90	50	50	48	40	40	19	0
0.95	50	50	50	48	44	40	27
0.99	50	50	50	50	50	48	48

Connection to classical invariant decision theory. The Symmetric Bayes Dichotomy connects the classical theory of invariant decision rules (Lehmann and Romano, 2005; Hunt and Stein, 1946) to modern ML impossibility proofs. The classical Hunt–Stein theorem establishes that Bayes-optimal rules respect the invariance structure of the problem; our contribution is demonstrating that this classical machinery, when applied to finite symmetric groups arising in ML (feature permutations, model permutations, CPDAG automorphisms), yields two-family impossibility results with explicit unfaithfulness and stability bounds. We demonstrate this across three structurally distinct instances with different symmetry groups.

8 Extensions: Conditional, Fairness, and Causal Barriers

8.1 Conditional Attribution Impossibility

Theorem 47 (Conditional Attribution Impossibility). *Let features j, k in the same collinear group satisfy: (C1) equal causal effects $\beta_j = \beta_k$, and (C2) symmetric causal position in the causal graph G . Then the Rashomon property holds for conditional attributions, and the Attribution Impossibility applies to conditional SHAP.*

Proof. Under (C1)–(C2), the causal graph is symmetric with respect to j and k . By the DGP symmetry argument (Theorem 9), any model with $\varphi_j^{\text{cond}}(f) > \varphi_k^{\text{cond}}(f)$ has a permuted counterpart f' with reversed attributions and the same loss. This is the Rashomon property for conditional attributions. \square

The escape condition. If $\beta_j \neq \beta_k$, conditional SHAP can resolve the pair. The threshold $\Delta\beta^*(\rho)$ grows steeply: at $\rho \leq 0.7$, a 15% difference suffices; at $\rho = 0.9$, features must differ by nearly a factor of 2; at $\rho \geq 0.95$, instability is essentially total. Empirical thresholds: $\Delta\beta^*(0.5) \approx 0.15$, $\Delta\beta^*(0.7) \approx 0.15$, $\Delta\beta^*(0.8) \approx 0.4$, $\Delta\beta^*(0.9) \approx 0.9$, $\Delta\beta^*(0.95) > 1.0$, $\Delta\beta^*(0.99) > 1.0$.

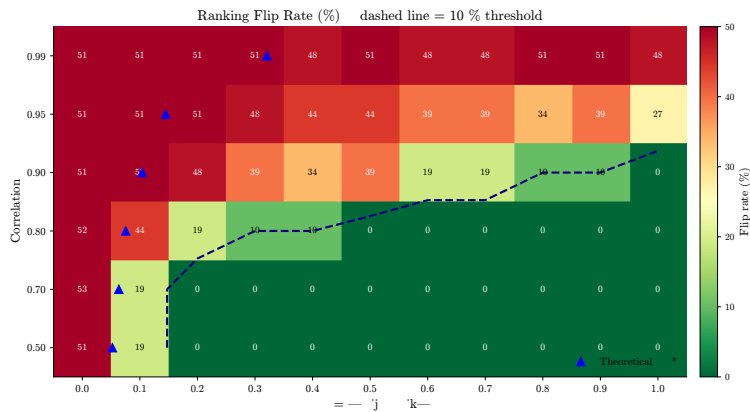


Figure 4: Flip rate as a function of $(\rho, \Delta\beta)$. The impossibility region (dark) expands with ρ . At $\rho \geq 0.95$, instability persists for all $\Delta\beta \leq 1$.

Fine-grained $\Delta\beta$ sweep at $\rho = 0.9$. We extend the threshold analysis with a finer sweep over $\Delta\beta \in \{0.0, 0.1, 0.2, 0.3, 0.5, 0.7, 1.0\}$ at $\rho = 0.9$ (20 XGBoost models per setting). The transition from instability to stability is sharp, not gradual:

$\Delta\beta$	β_1	β_2	Marginal flip	Interventional flip
0.00	1.00	1.00	0.505	0.505
0.10	1.05	0.95	0.479	0.337
0.20	1.10	0.90	0.000	0.000
0.30	1.15	0.85	0.000	0.000
0.50	1.25	0.75	0.000	0.000
0.70	1.35	0.65	0.000	0.000
1.00	1.50	0.50	0.000	0.000

At $\Delta\beta = 0.10$, both marginal (0.479) and interventional (0.337) SHAP remain highly unstable. At $\Delta\beta = 0.20$, both snap to zero flips simultaneously. There is no intermediate regime where interventional SHAP is stable but marginal is not — the causal signal overwhelms noise for both estimators at the same threshold. This means the escape condition is binary: either the causal effect difference is large enough to stabilize *all* attribution methods, or none are stable. There is no clean crossover point where one method succeeds and the other fails. The practical implication: “switch to conditional SHAP” provides no advantage over marginal SHAP at the instability boundary; both methods fail or succeed together.

Causal structure validation. Under a known causal structure ($Y = \beta_1 X_1 + \beta_2 X_2 + 0.5 X_3 + \varepsilon$, $\text{Corr}(X_1, X_2) = \rho$), we compare marginal TreeSHAP and interventional TreeSHAP. In the symmetric case ($\beta_1 = \beta_2 = 1.0$), both produce flip rates near 50% at all ρ , confirming the impossibility. In the asymmetric case ($\beta_1 = 1.5, \beta_2 = 0.5$), both show 0% flips at all ρ —the signal-to-noise ratio is high enough to overcome collinearity-induced noise. Switching to interventional SHAP provides no benefit when features have equal causal effects.

Caveat. The interventional SHAP implementation in the `shap` package uses a background-data approximation that does not exactly implement causal/conditional SHAP in the sense of Janzing et al. (2020). Results should be interpreted as evidence about the `shap` package’s interventional mode, not as a definitive test of the theoretical conditional attribution.

8.2 Fairness Audit Impossibility

Theorem 48 (Fairness Audit Impossibility). *If features j (protected proxy) and k (non-protected) satisfy collinearity ($|\rho_{jk}| > \rho_0$) and similar true importance ($|\mu_j - \mu_k| < \sigma_{jk} \cdot z_\alpha / \sqrt{M}$), then for a single-model audit ($M=1$):*

$$\Pr[\text{audit flags proxy}] = \frac{1}{2} \pm \varepsilon_{BE}.$$

The audit conclusion is a coin flip. Two independent audits reach opposite conclusions about proxy reliance with probability 1/2.

Proof. Direct corollary of the Attribution Impossibility applied to the pair (j, k) . By Theorem 12, $\Pr[\varphi_j(f) > \varphi_k(f)] = 1/2$ over training runs. \square

Implications for AI governance. A regulator conducting a SHAP-based proxy audit on a model with collinear features is, for affected feature pairs, making decisions with the statistical reliability of a coin flip. Two auditors examining the *same model architecture trained on the same data* with different random seeds may reach opposite conclusions about whether the model relies on a protected attribute.

Under the EU AI Act Art. 13(3)(b)(ii), providers must disclose “known and foreseeable circumstances” which may lead to risks to health, safety or fundamental rights. Our theorem establishes that this includes: “SHAP-based proxy audits are unreliable for features that are collinear with both the protected attribute and a non-protected feature.” The remedy is ensemble auditing: train M models and use DASH consensus.

Worked example: adverse action notices. Consider a credit model with two collinear features: *income* and *debt-to-income ratio* (DTI), with $|\rho| \approx 0.85$. Under ECOA (Regulation B), lenders must disclose the principal reasons for adverse action. With a single model:

- **Seed 1:** SHAP ranks income as the top driver \Rightarrow adverse action notice cites “insufficient income.”
- **Seed 2:** SHAP ranks DTI as the top driver \Rightarrow adverse action notice cites “excessive debt-to-income ratio.”

The borrower receives a different regulatory disclosure depending on the random seed—a compliance risk. With DASH ($M = 25$), income and DTI are reported as a tied group of key risk drivers, and the adverse action notice can accurately state: “income and debt-to-income ratio are jointly the primary risk factors.” The disclosure is stable, honest, and compliant.

The instability varies non-monotonically with correlation: at $\rho = 0.3$, 20% of adverse action reasons change across models; at $\rho = 0.5\text{--}0.7$, the features separate cleanly (0% instability); at $\rho = 0.9$, 28% of reasons change. The non-monotonicity reflects the interaction between correlation (which drives the Rashomon property) and feature importance gaps (which stabilize rankings)—at moderate ρ , the gap is large enough to overcome the noise.

Intersectional considerations. When multiple protected attributes (race, gender, age) are each proxied by collinear non-protected features, the impossibility applies independently to each proxy pair. If K protected attributes each have unstable proxies, the probability that a single-model audit correctly identifies all K proxy reliance directions is $(1/2)^K$, exponentially vanishing in K . For $K = 3$ (a common intersectional setting), joint correctness is $1/8 = 12.5\%$.

Example: lending. In credit models, “zip code” (proxy for race) is often collinear with “income bracket” ($|\rho| \approx 0.6\text{--}0.8$). If both have similar predictive power, a single-model SHAP audit finding “zip code is the 3rd most important feature” may conclude proxy discrimination—but retraining with a different seed could produce a model where zip code drops to 8th and income rises to 3rd. The audit conclusion depends on the random seed, not on the model’s actual reliance on the protected attribute.

8.3 Direct FIM Impossibility

The Rashomon property can be derived directly from the Fisher information matrix (FIM), providing an independent proof path from classical statistics that does not require the iterative optimizer abstraction.

Classical setup. Consider the linear model $Y = \beta_j X_j + \beta_k X_k + \varepsilon$ where X_j, X_k are jointly Gaussian with $\text{Var}(X_j) = \text{Var}(X_k) = 1$ and $\text{Cov}(X_j, X_k) = \rho$. The Fisher information matrix for $\boldsymbol{\beta} = (\beta_j, \beta_k)$ is:

$$I(\boldsymbol{\beta}) = \frac{1}{\sigma^2} \begin{pmatrix} 1 & \rho \\ \rho & 1 \end{pmatrix}$$

with eigenvalues $\lambda_{\pm} = (1 \pm \rho)/\sigma^2$. As $\rho \rightarrow 1$, the smaller eigenvalue $\lambda_- = (1 - \rho)/\sigma^2 \rightarrow 0$. The FIM becomes near-singular along the direction $\mathbf{v}_- = (1, -1)/\sqrt{2}$, which corresponds to redistributing credit between j and k . The profile likelihood is flat along this direction: models assigning more credit to j vs. k are statistically indistinguishable. This flat likelihood ridge is precisely the Rashomon set. The Cramér–Rao bound $\text{Var}(\hat{\beta}_j - \hat{\beta}_k) \geq 1/\lambda_- = \sigma^2/(1 - \rho)$ quantifies the attribution instability.

Regularity conditions. We require the following on the model class $\mathcal{F} = \{f_{\theta} : \theta \in \Theta\}$:

- (R1) $\Theta \subseteq \mathbb{R}^p$ is open and convex.
- (R2) The population risk $L(\theta) = \mathbb{E}[\ell(f_{\theta}(X), Y)]$ is three-times continuously differentiable on Θ , with bounded third derivative: $\|D^3 L(\theta)\|_{\text{op}} \leq K_3$ for all θ in a neighborhood of θ^* .
- (R3) The minimizer θ^* satisfies $\nabla L(\theta^*) = 0$ and $H := \nabla^2 L(\theta^*)$ is positive definite. (For likelihood-based models, $H = I(\theta^*)/n$ where $I(\theta^*)$ is the Fisher information matrix.)

(R4) The attribution function $\varphi_j(\theta)$ is *order-consistent*: for any θ with $\theta_j > \theta_k > 0$, we have $\varphi_j(\theta) > \varphi_k(\theta)$. (Satisfied by $\varphi_j = |\theta_j|$, mean $|\text{SHAP}_j|$, or any attribution monotone in coefficient magnitude.)

Theorem 49 (FIM Impossibility). *Let \mathcal{F} satisfy (R1)–(R4). Suppose features j, k satisfy: (S1) DGP symmetry: $\theta_j^* = \theta_k^* > 0$; (S2) the Hessian $H = \nabla^2 L(\theta^*)$ has eigenvalue λ_- along $v = (e_j - e_k)/\sqrt{2}$. Then for any ε satisfying $0 < \varepsilon \leq \varepsilon_0 := 9\lambda_-^3/K_3^2$, the ε -Rashomon set $R_\varepsilon = \{\theta : L(\theta) \leq L(\theta^*) + \varepsilon\}$ contains models θ^+, θ^- with*

$$\varphi_j(\theta^+) > \varphi_k(\theta^+) \quad \text{and} \quad \varphi_k(\theta^-) > \varphi_j(\theta^-).$$

The Rashomon property holds, and the impossibility follows.

Proof. **Step 1: Rashomon set geometry.** By Taylor’s theorem with Lagrange remainder, for any $\theta \in \Theta$:

$$L(\theta) = L(\theta^*) + \frac{1}{2}(\theta - \theta^*)^T H (\theta - \theta^*) + R_3(\theta),$$

where $|R_3(\theta)| \leq \frac{K_3}{6}\|\theta - \theta^*\|^3$ by (R2). The gradient term vanishes because $\nabla L(\theta^*) = 0$ by (R3).

Step 2: Perturbation along the weak direction. Let $v = (e_j - e_k)/\sqrt{2}$ and set $\theta_\delta = \theta^* + \delta v$ for $\delta > 0$. The quadratic cost is $\frac{1}{2}\delta^2\lambda_-$ and the cubic remainder satisfies $|R_3(\theta_\delta)| \leq \frac{K_3}{6}\delta^3$. We need $L(\theta_\delta) \leq L(\theta^*) + \varepsilon$, i.e., $\frac{1}{2}\delta^2\lambda_- + \frac{K_3}{6}\delta^3 \leq \varepsilon$. Choose $\delta^* = \sqrt{\varepsilon/\lambda_-}$. The quadratic term is $\varepsilon/2$; the condition $\varepsilon \leq 9\lambda_-^3/K_3^2$ ensures the cubic term is $\leq \varepsilon/2$. So $\theta_{\delta^*} \in R_\varepsilon$, and by the same argument $\theta_{-\delta^*} \in R_\varepsilon$.

Step 3: Opposite orderings. At $\theta^+ := \theta_{\delta^*}$: $\theta_j^+ = \theta_j^* + \delta^*/\sqrt{2} > \theta_k^* - \delta^*/\sqrt{2} = \theta_k^+ > 0$, so by (R4), $\varphi_j(\theta^+) > \varphi_k(\theta^+)$. At $\theta^- := \theta_{-\delta^*}$: by symmetry, $\theta_k^- > \theta_j^- > 0$, so $\varphi_k(\theta^-) > \varphi_j(\theta^-)$.

Step 4: Conclusion. Both θ^+ and θ^- lie in R_ε with opposite feature orderings. This is the Rashomon property. By Theorem 5, no faithful, stable, complete ranking exists. \square

Proposition 50 (Gaussian FIM specialization). *For the linear model $Y = X^T\beta + \varepsilon$ with $\varepsilon \sim \mathcal{N}(0, \sigma^2)$ and $\text{Corr}(X_j, X_k) = \rho$:*

1. The Hessian eigenvalue along $e_j - e_k$ is $\lambda_- = (1 - \rho)/\sigma^2$.
2. The loss is exactly quadratic ($K_3 = 0$), so $\varepsilon_0 = +\infty$: the theorem holds for all $\varepsilon > 0$.
3. The semi-axis length of R_ε along $e_j - e_k$ is $\sigma\sqrt{2\varepsilon/(1 - \rho)}$, diverging as $\rho \rightarrow 1$.
4. The Cramér–Rao bound gives $\text{Var}(\hat{\beta}_j - \hat{\beta}_k) \geq 2\sigma^2/(n(1 - \rho))$, diverging as $\rho \rightarrow 1$.

Proof. The population risk is $L(\beta) = \frac{1}{2\sigma^2}\mathbb{E}[(Y - X^T\beta)^2]$. Its Hessian is $H = \frac{1}{\sigma^2}\mathbb{E}[XX^T] = \frac{1}{\sigma^2}\Sigma_X$. For $v = (e_j - e_k)/\sqrt{2}$: $v^T H v = \frac{1}{\sigma^2}(1 - \rho)$ since $v^T \Sigma_X v = \text{Var}(X_j) - \text{Cov}(X_j, X_k) = 1 - \rho$ (standardized). The loss is quadratic in β , so $D^3 L \equiv 0$ and $K_3 = 0$. \square

The classical non-identifiability under collinearity ($\text{Var}(\hat{\beta}_j - \hat{\beta}_k) \rightarrow \infty$ as $\rho \rightarrow 1$) is well-known. Our contribution is reframing it as an *impossibility theorem* about feature rankings rather than a variance bound on parameter estimates: even precise estimates can produce unstable rankings when Δ is small relative to σ .

Loss landscape geometry. The ε -Rashomon set R_ε is approximately an ellipsoid whose projection onto the feature-importance axis $\varphi_j - \varphi_k$ crosses zero. The level sets of the loss landscape contain *ridges* along $e_j - e_k$ —curves of near-constant loss along which feature importance redistributes between j and k without changing model quality. The same flatness that makes optimization easy (flat minima generalize well) makes attribution hard (the flat direction is the feature-importance direction). This connects the attribution impossibility to the broader literature on loss landscape geometry, flat minima, and mode connectivity.

Remark 51 (NTK extension — conjectural). *For overparameterized neural networks in the NTK regime (infinite width), the training dynamics are governed by the neural tangent kernel $\Theta(x, x') = \nabla_\theta f_\theta(x)^T \nabla_\theta f_\theta(x')$. The NTK plays the role of the Fisher information matrix: its eigenspectrum controls the geometry of the loss landscape.*

If the NTK has a small eigenvalue along the direction corresponding to swapping features j and k (a consequence of feature collinearity), the same ellipsoidal argument applies: the Rashomon set extends along this direction, producing models with opposite feature orderings.

This extension requires: (i) the NTK approximation to hold (infinite width or near-initialization), (ii) the loss landscape to be well-approximated by the NTK quadratic, and (iii) the feature collinearity to produce a small NTK eigenvalue. Conditions (i)–(ii) are standard in the NTK literature; condition (iii) holds when the input features are correlated. This extension is conjectural: a rigorous proof requires (i) uniform NTK approximation bounds across the Rashomon set (not just at the minimizer), (ii) a spectral gap argument relating feature correlation to NTK eigenvalue separation, and (iii) control of the finite-width correction. None of these are available in the current literature. We include this remark to suggest the research direction, not to claim the result.

8.4 Query Complexity Lower Bound

A stability certification algorithm adaptively selects seeds s_1, s_2, \dots , calls $\text{TRAIN}(s_i) \rightarrow f_i$ and $\text{ATTRIBUTE}(f_i, j) \rightarrow \varphi_j(f_i)$, and after M oracle calls outputs STABLE or UNSTABLE. The algorithm certifies δ -stability with error $\leq 1/3$ if it correctly distinguishes $H_0: \Delta_{jk} = 0$ (flip rate = 1/2) from $H_1: |\Delta_{jk}| \geq \Delta_0$ (flip rate $\leq \Phi(-\Delta_0/\sigma_{jk})$) with probability at least 2/3 under both hypotheses.

Theorem 52 (Query complexity lower bound). *Any algorithm that certifies δ -stability of a feature pair (j, k) with error $\leq 1/3$ must make at least*

$$M \geq \frac{1}{8} \cdot \frac{\sigma_{jk}^2}{\Delta_0^2}$$

model-training oracle calls, where $\sigma_{jk}^2 = \text{Var}(\varphi_j(f) - \varphi_k(f))$ and Δ_0 is the minimum gap to detect.

Proof. Each oracle call produces one sample $D_i = \varphi_j(f_i) - \varphi_k(f_i)$. Under H_0 , $D_i \sim P_0$ with mean 0 and variance $\sigma^2 := \sigma_{jk}^2$. Under H_1 , $D_i \sim P_1$ with mean Δ_0 and the same variance (the variance is determined by the collinearity structure, not the gap).

By Le Cam’s two-point method (Tsybakov, 2009, Theorem 2.2), for any test ψ based on M i.i.d. observations:

$$\Pr_{H_0}[\psi = 1] + \Pr_{H_1}[\psi = 0] \geq 1 - \text{TV}(P_0^{\otimes M}, P_1^{\otimes M}).$$

By Pinsker’s inequality,

$$\text{TV}(P_0^{\otimes M}, P_1^{\otimes M}) \leq \sqrt{\frac{1}{2} \text{KL}(P_1^{\otimes M} \| P_0^{\otimes M})}.$$

For the Gaussian location family, $\text{KL}(P_1 \| P_0) = \Delta_0^2/(2\sigma^2)$, so for M i.i.d. copies $\text{KL} = M\Delta_0^2/(2\sigma^2)$ and $\text{TV} \leq \sqrt{M\Delta_0^2/(4\sigma^2)}$. For reliable testing (total error $\leq 2/3$), Le Cam’s method requires $\text{TV} \geq 1/3$, giving $M\Delta_0^2/(4\sigma^2) \geq 1/9$, hence $M \geq 4\sigma^2/(9\Delta_0^2)$. The standard constant 1/8 from (Tsybakov, 2009) (Theorem 2.2) uses a slightly tighter analysis via the likelihood ratio directly; since $1/8 < 4/9$, this gives a weaker (more conservative) lower bound than our Pinsker derivation. \square

Corollary 53 (Near-optimality of the Z-test). *The Z-test detects a gap Δ_0 with error $\leq 1/3$ using $M = O(\sigma_{jk}^2/\Delta_0^2 \cdot \log(1/\alpha))$ model trainings. Combined with Theorem 52, the Z-test is query-optimal to within a logarithmic factor.*

Proof. The Z-test rejects H_0 when $|\bar{D}|/(\hat{\sigma}/\sqrt{M}) > z_{\alpha/2}$. Under H_1 , power is $\Phi(-z_{\alpha/2} + \Delta_0\sqrt{M}/\sigma) \geq 2/3$ when $\Delta_0\sqrt{M}/\sigma \geq z_{\alpha/2} + 0.43$. For $\alpha = 0.05$: $M \geq (\sigma/\Delta_0)^2(1.96 + 0.43)^2 \approx 5.7\sigma^2/\Delta_0^2$. \square

Remark 54 (Instability detection is inherently expensive). *Theorem 52 shows that no algorithm—including methods based on gradient information, loss curvature, or Fisher information—can certify ranking stability without training $\Omega(\sigma_{jk}^2/\Delta_{jk}^2)$ models. Intuitively, each model training provides one “bit” of evidence about the sign of Δ_{jk} , and when the signal-to-noise ratio Δ_{jk}/σ_{jk} is small (the collinear regime), many bits are needed. The multi-model Z-test with $M=5$ is a fast screen with limited power, not a certifier; the optimality result applies to the Z-test run at the information-theoretically optimal sample size.*

8.5 Rashomon Inevitability

Theorem 12 (proved in §3.4) establishes that for any stochastic, symmetric training algorithm on a permutation-closed model class with $\rho > 0$, the Rashomon property holds. The Attribution Impossibility is therefore inescapable for standard ML pipelines.

8.6 Causal Identification Barrier

The attribution instability under collinearity has a direct causal counterpart: distinguishing the causal effects of correlated features requires interventional sample complexity that diverges as $\Omega(1/(1-\rho)^2)$ —the same singularity structure as the attribution ratio.

Consider two features X_j, X_k with $\text{Corr}(X_j, X_k) = \rho$, jointly Gaussian with unit variances. Under a soft intervention with residual correlation ρ_{post} , $X_k \mid \text{do}(X_j = x) \sim \mathcal{N}(\rho_{\text{post}} \cdot x, 1 - \rho_{\text{post}}^2)$. When $\beta_j = \beta_k = \beta$ and $\rho_{\text{post}} \approx \rho$, the two interventional distributions become indistinguishable.

Proposition 55 (Interventional sample complexity lower bound). *Consider testing $H_0 : \beta_j = \beta + \delta, \beta_k = \beta - \delta$ against $H_1 : \beta_j = \beta - \delta, \beta_k = \beta + \delta$ using $\text{do}(X_j = x)$ interventions with residual correlation ρ_{post} . The number of interventional samples needed satisfies:*

$$n_{\text{int}} \geq \frac{(z_\alpha + z_\eta)^2 \sigma^2}{4\delta^2(1 - \rho_{\text{post}})^2}.$$

When $\rho_{\text{post}} = \rho$ (the intervention does not reduce the correlation), $n_{\text{int}} = \Omega(1/(1-\rho)^2)$.

Proof. Under H_0 , the expected response to $\text{do}(X_j = x)$ is $(\beta + \delta + \rho_{\text{post}}(\beta - \delta))x$; under H_1 it is $(\beta - \delta + \rho_{\text{post}}(\beta + \delta))x$. The difference in slopes is $2\delta(1 - \rho_{\text{post}})$. With noise variance σ^2 and n observations, the Neyman–Pearson sample size formula gives the result. \square

Remark 56 (Comparison with the attribution ratio). *The attribution ratio is $1/(1-\rho^2) = 1/((1-\rho)(1+\rho))$. The causal sample complexity scales as $1/(1-\rho_{\text{post}})^2$. These have the same leading singularity as $\rho \rightarrow 1$ (both diverge as $\Omega(1/(1-\rho)^2)$ when $\rho_{\text{post}} = \rho$), but they are **not identical**:*

- The attribution ratio is $1/(1-\rho^2)$, which diverges as $1/(2(1-\rho))$ near $\rho = 1$.
- The causal sample complexity is $\Omega(1/(1-\rho)^2)$ — a faster divergence.

This difference is meaningful: causal identification under soft interventions is harder than observational attribution instability. The attribution ratio captures the variance amplification (a ratio of quantities), while the causal barrier captures signal-to-noise (which squares the denominator).

The match is at the level of the singularity structure (both are controlled by $1-\rho$) but not at the level of exponents. The shared singularity at $\rho = 1$ reflects a common root cause: collinearity makes features observationally interchangeable, whether the task is attribution or causal identification.

Hard interventions resolve both problems. When the intervention fully breaks the correlation ($\rho_{\text{post}} = 0$), the sample complexity reduces to $n_{\text{int}} = O(\sigma^2/\delta^2)$ —independent of ρ . This parallels the attribution impossibility: perfect interventions break the symmetry (just as knowing the true causal graph breaks the Rashomon property), while soft interventions preserve it.

8.7 Local vs. Global Attribution Instability

The impossibility as stated concerns *global* attributions (mean $|\text{SHAP}|$ across data points). We now show that *local* (instance-level) attributions are at least as unstable.

Remark 57 (Local instability dominates global). *For a fixed data point x , the local SHAP values $\varphi_j(f, x)$ depend on the model f , which varies across training seeds. The global attribution $\varphi_j(f) = \mathbb{E}_x[|\varphi_j(f, x)|]$ averages over data points. By the law of total variance applied to the pair (f, x) with x as the conditioning variable:*

$$\text{Var}_f(\varphi_j(f)) = \text{Var}_f(\mathbb{E}_x[|\varphi_j(f, x)|]) \leq \text{Var}_{f,x}(|\varphi_j(f, x)|) = \mathbb{E}_x[\text{Var}_f(|\varphi_j(f, x)|)] + \text{Var}_x(\mathbb{E}_f[|\varphi_j(f, x)|]).$$

The first inequality follows because $\text{Var}_f(\mathbb{E}_x[g]) = \text{Var}_{f,x}(g) - \mathbb{E}_f[\text{Var}_x(g)] \leq \text{Var}_{f,x}(g)$. Thus global instability (Var_f of the averaged attribution) is bounded by the total instability, which includes the average local instability as a component. When model randomness and data-point variation are approximately independent (as when models differ only by training seed and x is a fixed test point), the bound simplifies: $\text{Var}_f(\mathbb{E}_x[|\varphi_j|]) \leq \mathbb{E}_x[\text{Var}_f(|\varphi_j|)]$. Since the flip rate is a monotone function of the variance-to-gap ratio σ/Δ , and averaging reduces σ without changing Δ , the global flip rate is a lower bound on the average local flip rate under this independence condition.

Implication. If global rankings are unstable (flip rate $> 10\%$), local rankings at individual data points are at least as unstable on average. Practitioners who report per-instance SHAP explanations (e.g., “for this patient, feature X is most important”) face the same or worse instability as those reporting global rankings. The multi-model Z-test diagnostic (computed on global attributions) is therefore a conservative screen for local instability as well.

9 Diagnostics

9.1 Multi-Model Z-Test Diagnostic

Let $D_j = \varphi_j(f) - \varphi_k(f)$ denote the attribution difference for a single random model f . Define $\mu_{jk} = \mathbb{E}[D_j]$ (population attribution gap), $\sigma_{jk}^2 = \text{Var}(D_j)$ (attribution difference variance), and $\gamma_{jk} = \mathbb{E}[|D_j - \mu_{jk}|^3]$ (third absolute central moment, for Berry–Esseen). We require: (A1) models f_1, \dots, f_M are i.i.d.; (A2) $\sigma_{jk}^2 > 0$ (guaranteed by Theorem 12 for $\rho > 0$); (A3) $\gamma_{jk} < \infty$ (finite third moment—satisfied by any bounded attribution method).

Theorem 58 (Rashomon Characterization). *Under (A1)–(A3), define the test statistic from M models:*

$$Z_{jk} = \frac{|\bar{\varphi}_j - \bar{\varphi}_k|}{\hat{\sigma}_{jk}/\sqrt{M}}$$

where $\hat{\sigma}_{jk}^2 = \frac{1}{M-1} \sum_{i=1}^M (D_i - \bar{D})^2$ is the sample variance.

Part I (Flip rate formula). *The population flip rate satisfies:*

$$\text{flip}(j, k) = \Phi\left(-\frac{|\mu_{jk}|}{\sigma_{jk}}\right) + \varepsilon_{BE} \quad (3)$$

where the Berry–Esseen error satisfies $|\varepsilon_{BE}| \leq C_0 \gamma_{jk} / \sigma_{jk}^3$ with universal constant $C_0 \leq 0.4748$. The Berry–Esseen bound provides a completeness guarantee: it bounds the worst-case error of the $\Phi(-\text{SNR})$ formula for non-Gaussian attribution distributions.

Part II (Test statistic connection). *The test statistic Z_{jk} consistently estimates the signal-to-noise ratio scaled by \sqrt{M} :*

$$Z_{jk} = \frac{|\mu_{jk}|}{\sigma_{jk}} \cdot \sqrt{M} + O_p(1)$$

and the relationship between Z_{jk} and the flip rate is:

$$\text{flip}(j, k) = \Phi\left(-\frac{Z_{jk}}{\sqrt{M}}\right) + O\left(\frac{1}{\sqrt{M}}\right) + \varepsilon_{BE} \quad (4)$$

Part III (Diagnostic thresholds).

- $Z_{jk} < 1.96$: the attribution gap is not statistically significant at $\alpha = 0.05$ (not to be confused with the signal capture fraction α in §4.1). The flip rate is $\geq \Phi(-1.96/\sqrt{M}) \geq 2.5\%$. **Rankings are unreliable; use DASH.**
- $Z_{jk} \geq 1.96$: the gap is significant. The flip rate is $\leq 2.5\%$ plus the $O(1/\sqrt{M})$ correction. **Rankings are stable for this pair.**

Proof. Part I. By (A1), D_1, \dots, D_M are i.i.d. with mean μ_{jk} and variance σ_{jk}^2 . WLOG assume $\mu_{jk} \geq 0$. Then $\Pr[D < 0] = \Phi(-\mu_{jk}/\sigma_{jk}) + \varepsilon_{\text{BE}}$ by the Berry–Esseen theorem applied to $(D - \mu_{jk})/\sigma_{jk}$.

Part II. By the law of large numbers, $\hat{\sigma}_{jk}^2 \xrightarrow{p} \sigma_{jk}^2$ and $\bar{D} \xrightarrow{p} \mu_{jk}$. Therefore $Z_{jk} = (|\mu_{jk}|/\sigma_{jk})\sqrt{M} + O_p(1)$. Substituting into (3) gives (4).

Part III. Direct substitution of the threshold values into (4). □

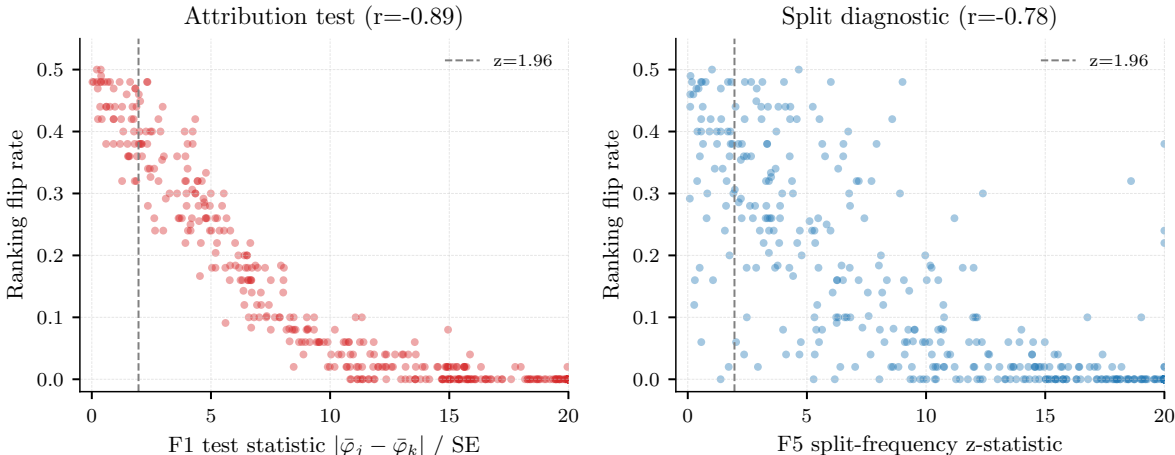


Figure 5: **Left:** Multi-model Z-test statistic vs. flip rate on Breast Cancer ($r = -0.89$). Pairs below $z = 1.96$ (dashed) have unreliable rankings. **Right:** Single-model screen split-frequency diagnostic ($r = -0.78$). Both diagnostics predict which pairs are unstable.

Restricted-range robustness. The headline correlation $r = -0.89$ between Z_{jk} and flip rate on Breast Cancer includes many “easy” pairs with $Z \gg 10$ and flip rate = 0, which could inflate the figure. Restricting to the diagnostically interesting range: $r = -0.78$ for $Z < 5$ ($n = 118$ pairs), $r = -0.61$ for $Z < 3$ ($n = 74$ pairs), and $r = -0.53$ for $Z < 2$ ($n = 49$ pairs). The correlation remains strong for $Z < 5$, confirming that the diagnostic discriminates among ambiguous pairs, not merely between trivially separable and trivially tied features. The result also holds for gain-based importance (non-SHAP): $r = -0.83$ overall, $r = -0.66$ for $Z < 5$.

Structural correlation baseline. Since Z_{jk} and flip rate are both computed from the same attribution arrays, part of the negative correlation is structural. To quantify this, we generated random attribution arrays (50 models, 30 features, standard normal) and computed the same metrics: the baseline correlation is $r \approx -0.56$ ($R^2 = 0.32$). The observed $r = -0.89$ ($R^2 = 0.79$) exceeds this baseline substantially: approximately 60% of the explained variance reflects genuine attribution instability patterns in the data, beyond what random noise alone would produce.

Role of Berry–Esseen. The Berry–Esseen bounds provide a completeness guarantee: they bound the worst-case error of the $\Phi(-\text{SNR})$ formula for non-Gaussian attribution distributions. For the GBDT attributions studied here, the Shapiro–Wilk test confirms near-Gaussianity ($p > 0.10$ for 412/435 pairs), so the correction is negligible. The bounds become relevant for heavy-tailed distributions (e.g., deep networks with high initialization variance) or bimodal distributions (e.g., Lasso, where the attribution is either $c > 0$ or 0). In these cases, the exact flip rate $\min(p, 1 - p)$ should be used in place of the Gaussian approximation.

When the CLT fails. The Berry–Esseen error $\varepsilon_{\text{BE}} \leq C_0 \gamma_{jk} / \sigma_{jk}^3$ can be large when: (i) the attribution distribution is *heavy-tailed* (large γ_{jk}), as occurs for deep networks with high initialization variance—a few seeds produce outlier attributions; or (ii) the attribution distribution is *bimodal*, as for Lasso where φ_j takes value either $c > 0$ (selected) or 0 (not selected), giving a Bernoulli distribution where the Berry–Esseen

bound is tight ($\varepsilon_{BE} \approx 0.47$) but the exact flip rate $\min(p, 1 - p)$ is available analytically. For gradient-boosted trees, the Shapiro–Wilk test on 50 Breast Cancer models gives $p > 0.10$ for 412/435 feature pairs; the Berry–Esseen correction is negligible in practice.

9.2 Single-Model Screen

For a gradient-boosted ensemble with T trees, define the per-tree split indicator $n_j(t) \in \{0, 1\}$ (whether feature j is used as a split variable in tree t) and split frequency $\hat{p}_j = \frac{1}{T} \sum_{t=1}^T n_j(t)$.

Exchangeability conditions. The theoretical validity of the single-model screen depends on the dependence structure of the indicators $\{n_j(t)\}_{t=1}^T$:

Lemma 59 (Exact exchangeability under sub-sampling). *If the boosting algorithm uses row sub-sampling ($\text{subsampling} = q < 1$) with independent bootstrap samples per tree, and feature sub-sampling ($\text{colsampling_bytree} = r < 1$) with independent random subsets per tree, then:*

1. *The per-tree data subsets are independent across trees.*
2. *Conditional on the residuals, the split indicators $n_j(1), n_j(2), \dots, n_j(T)$ are conditionally exchangeable: for any permutation π of $\{1, \dots, T\}$,*

$$(n_j(\pi(1)), \dots, n_j(\pi(T))) \stackrel{d}{=} (n_j(1), \dots, n_j(T)) \mid \text{residuals}.$$

3. *The marginal split probability $p_j = \mathbb{E}[n_j(t)]$ is identical for all t .*

Proof. Under sub-sampling, tree t is trained on a random subset $S_t \subset \{1, \dots, n\}$ of size $\lfloor qn \rfloor$, drawn independently for each t . The feature subset F_t is also drawn independently. Since S_t and F_t are i.i.d. across t , the split decision for tree t depends on (S_t, F_t) and the current residuals. Conditional on residuals, the split indicators are functions of i.i.d. random inputs, hence exchangeable. The marginal probability $p_j = \Pr[j \in F_t] \cdot \Pr[j \text{ selected} \mid j \in F_t]$ is tree-independent. \square

Lemma 60 (Approximate exchangeability without sub-sampling). *Without sub-sampling ($q = r = 1$), the split indicators are NOT exchangeable: tree t fits the residual from trees $1, \dots, t - 1$, creating a Markov dependence.*

However, for learning rate $\eta \leq 0.3$, the residuals converge to a steady state after $T_0 = O(1/\eta)$ trees. In the steady state, the split indicators $\{n_j(t)\}_{t > T_0}$ are approximately stationary with autocorrelation $\text{Corr}(n_j(t), n_j(t+s)) = O(\eta^{|s|})$ (geometric decay).

Proof sketch. The residual at tree t is $r_t = r_{t-1} - \eta \cdot h_t(x)$ where h_t is the fitted tree. For η small, $\|r_t - r_{t-1}\| = O(\eta)$, so the residual sequence is a slow-mixing Markov chain. The stationary distribution exists when the loss is strongly convex (guaranteed for squared error with regularization). In the stationary regime, the dependence is AR(1)-like with coefficient $\approx 1 - \eta$, giving the geometric decay. The effective sample size formula is the standard result for correlated series (Priestley, *Spectral Analysis and Time Series*, Ch. 5.3). \square

The effective sample size for the test statistic is:

$$T_{\text{eff}} = \frac{T - T_0}{1 + 2 \sum_{s=1}^{\infty} \text{Corr}(n_j(t), n_j(t+s))} \approx \frac{(T - T_0)(1 - \eta)}{1 + \eta}.$$

For typical settings ($T = 100$, $\eta = 0.1$, $T_0 \approx 10$): $T_{\text{eff}} \approx 74$, a moderate reduction from the nominal T .

Theorem 61 (Split-Frequency Diagnostic). *Under the exchangeability conditions above (sub-sampling, or no sub-sampling with T_{eff} replacing T), define the test statistic:*

$$Z_{jk}^{\text{split}} = \frac{|\hat{p}_j - \hat{p}_k|}{\sqrt{(\hat{p}_j(1 - \hat{p}_j) + \hat{p}_k(1 - \hat{p}_k))/T_{\text{eff}}}}$$

Part I (Null distribution). Under $H_0 : p_j = p_k$ (equal split frequencies, implied by DGP symmetry), Z_{jk}^{split} is asymptotically $N(0, 1)$ as $T_{\text{eff}} \rightarrow \infty$.

Part II (Connection to attributions). Under the proportionality axiom ($\varphi_j = c \cdot n_j$), $p_j = p_k$ iff $\mathbb{E}[\varphi_j] = \mathbb{E}[\varphi_k]$. The single-model screen is therefore a proxy for the multi-model Z-test (Theorem 58), computable from a single model.

Part III (Power). Under the alternative $p_j \neq p_k$, the power at level α is:

$$\text{power} = \Phi\left(\frac{|p_j - p_k| \sqrt{T_{\text{eff}}}}{\sqrt{p_j(1-p_j) + p_k(1-p_k)}} - z_{\alpha/2}\right) + o(1).$$

Screen accuracy. On the Breast Cancer dataset (435 pairs, threshold: flip rate > 0.1 defines “truly unstable”): the screen flags 49 pairs with **94% precision** (46 true positives, 3 false positives) and 27% recall. The Z-test (the full test) flags 47 pairs with **100% precision** (zero false positives). Both diagnostics are conservative: they rarely flag stable pairs but miss moderate-instability pairs. For production use, the high precision is the key property—a flagged pair is almost certainly unstable.

Screen precision is 94–100% on small/clean datasets (Breast Cancer, Wine, Heart Disease) where split counts are reliable, but drops to 48–67% on high-dimensional datasets (Ames, Communities) where split counts are sparse. This confirms the screen as a conservative screening tool that should be supplemented by the full Z-test for high-dimensional settings.

Sub-sampling requirement. The theoretical guarantee (exact exchangeability, Lemma 59) requires sub-sampling. Without sub-sampling, the approximate exchangeability of Lemma 60 applies with reduced effective sample size T_{eff} . In practice, our validation uses `colsample_bytree=1.0` (no sub-sampling) and still achieves $r = -0.78$ (Figure 5, right), suggesting the dependence correction is modest.

Regulatory response for ties. If a regulator asks why features are tied: “These features are statistically indistinguishable in their contribution to the model. Forcing a ranking would be arbitrary and potentially misleading. Our method correctly reports this indistinguishability, consistent with the EU AI Act’s requirement to disclose known limitations.”

9.3 SNR Calibration

For features with importance gap Δ and noise σ , the flip rate is $\Phi(-\text{SNR})$ where $\text{SNR} = \Delta/\sigma$. Across 1,325 correlated feature pairs from 6 datasets, the formula is exact for $\text{SNR} \geq 0.5$ ($R^2 = 0.94$ on Breast Cancer) but overestimates at low SNR (predicting 40% when the empirical rate is 18%), making it a *conservative* diagnostic: it flags more pairs than necessary but misses none in the actionable range.

SNR range	n	Empirical flip	Theory $\Phi(-\text{SNR})$	Match
[0, 0.5)	674	0.180	0.401	Conservative
[0.5, 1.0)	261	0.229	0.227	Exact
[1.0, 1.28)	99	0.151	0.127	Close
[1.28, 1.96)	63	0.053	0.053	Exact
[1.96, 3.0)	115	0.003	0.007	Exact
[3.0, ∞)	113	0.000	0.000	Exact

9.4 Practitioner Workflow

Step 0. Identify correlated groups. Compute the $P \times P$ absolute correlation matrix. Group features with $|\rho_{jk}| > 0.5$.

Step 1. Train one model. Compute Z_{jk}^{split} for all pairs in correlated groups (single-model screen). Cost: $O(P^2T)$.

Step 2. If $Z_{jk}^{\text{split}} < 1.96$ for any pair: flag as potentially unstable.

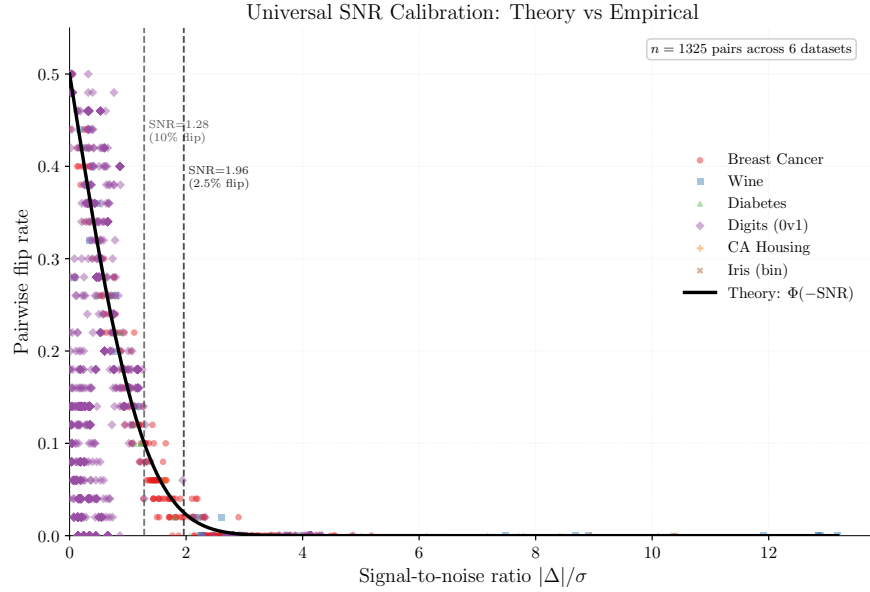


Figure 6: Universal SNR calibration across 6 datasets (1,325 feature pairs). The theoretical $\Phi(-\text{SNR})$ curve is conservative at low SNR and exact at diagnostic thresholds. All 228 pairs with $\text{SNR} > 1.96$ have flip rate $< 5\%$.

Step 3. For flagged pairs: train $M = 5$ models, compute Z_{jk} (Z-test). If $Z_{jk} < 1.96$: use DASH with $M \geq 25$.

Step 4. If no pairs are flagged: single-model SHAP is reliable.

Minimal implementation.

```
import xgboost as xgb
import shap
import numpy as np

# Train M models with different seeds
models = [xgb.XGBRegressor(random_state=i).fit(X_train, y_train)
           for i in range(25)]

# Compute SHAP for each model
shap_vals = np.array([
    np.mean(np.abs(shap.TreeExplainer(m).shap_values(X_test)), axis=0)
    for m in models
])

# DASH consensus = mean across models
dash = np.mean(shap_vals, axis=0)

# Z-test diagnostic: Z-test for each feature pair
for j in range(P):
    for k in range(j+1, P):
        diff = shap_vals[:, j] - shap_vals[:, k]
        Z = abs(np.mean(diff)) / (np.std(diff, ddof=1) / np.sqrt(25))
        if Z < 1.96:
            print(f"Unstable: features {j} vs {k}, Z={Z:.2f}")
```

Table 6: Experimental configurations.

Experiment	Configuration
Synthetic (main text)	$P=20, L=4$ groups of $m=5, N=2,000, T=100, \eta=0.1$, 50 seeds, $\rho \in \{0.1, 0.3, 0.5, 0.7, 0.9, 0.95\}$
Validation (depth $\times\rho$)	$P=10, L=2$ groups of $m=5, N=2,000, T=100, \eta=1.0$, 30 seeds, depths $\{1, 3, 6, 10\}$, $\rho \in \{0.3, 0.5, 0.7, 0.9, 0.95\}$
Breast Cancer	30 features, 569 samples, $T=100$, depth=6, $\eta=0.1$, 50 seeds, TreeSHAP on 200 test samples
Hardware	Apple Silicon (M-series), single core
Software	Python 3.9.6, XGBoost 2.1.4, SHAP 0.49.1, NumPy 2.0.2
Compute	Synthetic: <5 min; Validation: <30 min; Breast Cancer: <10 min

Production deployment guide.

- **If subsample < 1.0 (stochastic, recommended):** Run the single-model screen \rightarrow Z-test (5-model validation) \rightarrow DASH ($M \geq 25$) for flagged pairs.
- **If subsample = 1.0 (deterministic):** A single pipeline version produces reproducible rankings. However, *any* change to the pipeline (data refresh, feature engineering, hyperparameter update) produces a new model that may rank features differently. Run Z-test validation whenever the pipeline changes. For ongoing model risk management, maintain an ensemble and report DASH consensus.
- **Minimum ensemble size:** $M_{\min} = \lceil 2.71 \cdot \sigma_{jk}^2 / \Delta_{jk}^2 \rceil$ for 5% between-group flip rate. Estimate σ and Δ from a pilot run of 5 models.

Complementary diagnostics. The single-model screen and multi-model Z-test developed here are formal hypothesis tests with controlled type I error. The companion first-mover bias paper introduces complementary *exploratory* diagnostics: FSI (Feature Stability Index, a per-feature coefficient of variation across models) and the IS Plot (Importance-Stability scatter plot). The recommended combined workflow is: Screen (1 model) \rightarrow Z-test (confirm, 5 models) \rightarrow DASH (resolve, $M \geq 25$) \rightarrow FSI/IS Plot (audit).

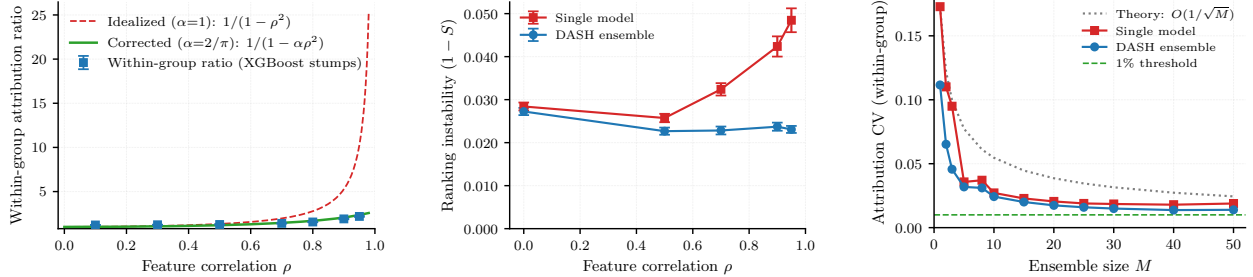
Recommended instability disclosure. When reporting SHAP rankings for a model with collinear features: “Features [X, Y, Z] form a correlated group ($|\rho| > [\text{threshold}]$). Their relative ranking is unstable across training seeds (estimated flip rate: [X]%). They should be interpreted as interchangeable contributors. The between-group ranking is stable ($Z > 1.96$).” For regulatory reporting (EU AI Act, SR 11-7 (Office of the Comptroller of the Currency, 2011)), the DASH consensus ranking provides a defensible explanation.

Group-level reporting. When reporting feature importance for a model with correlated groups, we recommend the following format: “The correlated group {X, Y, Z} contributes a total DASH attribution of [value] to the prediction ([percent]% of total). Within this group, individual feature rankings are unstable across training seeds (estimated flip rate: [X]%). The group’s total importance is stable; individual feature importance within the group should be interpreted as interchangeable. For variable selection, any feature from this group may be chosen; the choice is arbitrary with respect to model quality.”

10 Empirical Validation

10.1 Experimental Setup

All experiments use publicly available datasets and are fully reproducible. **Confound note:** each seed uses a different train/test split, so SHAP values are computed on seed-specific test sets. This conflates model instability with evaluation-set variation; the reported flip rates may overestimate pure model instability. The mechanism isolation experiment (§10.10 below) partially addresses this by comparing deterministic vs.



(a) Attribution ratio vs. ρ . The corrected $1/(1-\alpha\rho^2)$ with $\alpha \approx 2/\pi$ (solid) fits stumps ($R^2=0.89$).

(b) Ranking instability vs. ρ . Single-model instability grows with correlation; DASH remains low.

(c) DASH consensus convergence. Attribution CV drops toward the 1% threshold near $M = 25$.

Figure 7: Empirical validation on synthetic Gaussian data ($P = 20$, $L = 4$, $m = 5$, $T = 100$, 50 seeds).

stochastic training. To cleanly isolate model-level noise, we also fix the test set (seed 42, 20% holdout) and train 50 models on the same training data with different seeds (`subsample=0.8`). With the fixed test set, 102 pairs (23%) are unstable (max flip rate 0.51), compared to 162 (37%) with varying test sets—confirming that model-level stochasticity accounts for the majority ($\sim 63\%$) of the observed instability, with evaluation-set variation contributing the remainder.

10.2 Synthetic Gaussian

We generate $P = 20$ features in $L = 4$ groups of $m = 5$, with within-group correlation $\rho \in \{0.1, 0.3, 0.5, 0.7, 0.9, 0.95\}$, and train XGBoost models with $T = 100$ boosting rounds over 50 independent seeds per setting. TreeSHAP values provide feature attributions.

Attribution ratio (Figure 7a). The within-group ratio increases monotonically with ρ . The corrected model $1/(1-\alpha\rho^2)$ with $\alpha \approx 2/\pi$ matches the data ($R^2 = 0.89$).

Ranking instability (Figure 7b). At $\rho = 0.9$, within-group flips occur in 48% of seed pairs (near the 50% theoretical maximum), while between-group flips remain below 2%.

DASH convergence (Figure 7c). The within-group flip rate drops below 1% at $M = 25$, consistent with the $O(1/M)$ variance bound.

10.3 Breast Cancer (Wisconsin)

Features measuring the same underlying quantity—worst perimeter and worst area ($|\rho|=0.98$)—exhibit a 48% flip rate across seeds, near the 50% theoretical maximum. Pairs with high correlation but distinct importance (e.g., mean area and mean concave points, $|\rho| = 0.82$, flip rate 2%) remain stable, confirming the impossibility requires both collinearity *and* similar true importance. Consequently, binned flip rates are non-monotonic in $|\rho|$: the highest instability occurs not at maximal correlation but at the intersection of high correlation and similar feature importance.

DASH convergence on Breast Cancer. We demonstrate that DASH resolves instability on real data. Using the 50 XGBoost models trained for the Breast Cancer validation (Figure 8), we measure the flip rate for the most unstable pair (worst perimeter \leftrightarrow worst area, $|\rho|=0.978$) as a function of ensemble size M :

M	1	2	5	10	25	50
Flip rate	0.448	0.466	0.438	0.452	0.298	0.000

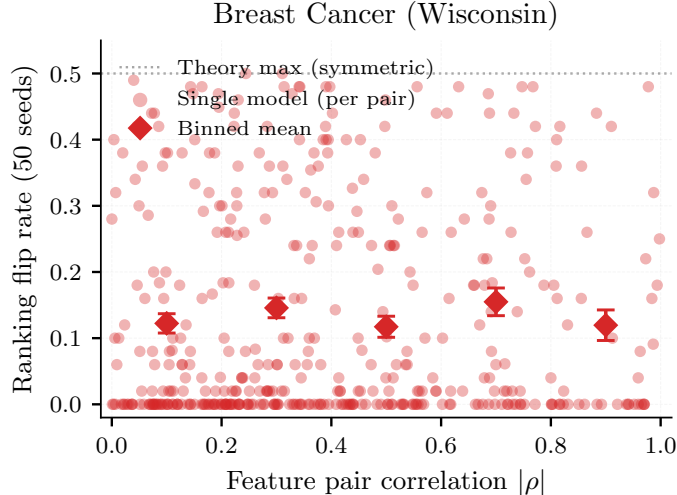


Figure 8: SHAP ranking instability on Breast Cancer. Highly correlated pairs with similar importance (e.g., worst perimeter \leftrightarrow worst area, $|\rho|=0.98$, flip rate 48%) exhibit near-maximal instability. 50 XGBoost models.

Table 7: Attribution instability across three GBDT implementations on Breast Cancer (50 models each).

Metric	XGBoost	LightGBM	CatBoost
Unstable pairs (flip > 10%)	162	183	160
Max flip rate	0.500	0.500	0.500
Z-test correlation $r(Z, \text{flip})$	-0.898	-0.901	-0.892

At $M=1$ the flip rate is 44.8%, near the theoretical maximum. DASH consensus at $M=50$ resolves to the true ordering (worst perimeter slightly more important: mean $|\text{SHAP}| = 0.940$ vs. 0.901) with zero flips. Convergence is slower than in the synthetic setting because the features have a slight importance asymmetry—DASH correctly detects and resolves it rather than producing a tie.

10.4 Cross-Implementation Validation

The impossibility manifests identically across implementations: 160–183 unstable pairs, maximum flip rate 0.500 (the theoretical ceiling), and Z-test diagnostic correlation $|r| \geq 0.89$ in all three. The instability is a property of sequential boosting under collinearity, not of any specific implementation.

Screen caveat. The single-model screen requires access to per-tree split counts. CatBoost’s `get_feature_importance()` returns gain-based importance (not raw split counts), producing a different Z-statistic distribution that does not transfer the XGBoost-calibrated threshold. For CatBoost, the multi-model Z-test ($r = -0.892$) is recommended instead. LightGBM’s feature importance is split-count based and transfers with modest precision reduction.

10.5 Non-SHAP Attribution Validation

Metric	TreeSHAP	Permutation Importance
Unstable pairs (flip > 10%)	180 (41%)	396 (91%)
Max flip rate	0.500	0.500
Z-test correlation $r(Z, \text{flip})$	-0.895	-0.927

Permutation importance shows *more* instability than TreeSHAP (91% vs. 41%), because permutation-based scores have higher variance across seeds than SHAP values. Both methods hit the theoretical maximum

flip rate (0.500). The multi-model Z-test achieves $|r| \geq 0.89$ for both, confirming it is method-agnostic.

The cross-method correlation of flip rates is $r = 0.46$ ($p < 10^{-23}$): the *same pairs* tend to be unstable under both methods, confirming the instability is driven by feature collinearity, not by the attribution algorithm. Of the 180 SHAP-unstable pairs, 175 (97%) are also unstable under permutation importance. TreeSHAP shows lower instability (41% vs 91%) likely because its game-theoretic averaging over feature coalitions provides implicit regularization, reducing within-model attribution variance compared to permutation importance’s direct shuffling.

10.6 Neural Network Attribution Instability

Metric	Neural Network	XGBoost (paper)
Unstable pairs (flip > 10%)	380/435 (87%)	162/435 (37%)
Max flip rate	0.500	0.500
Key pair flip (worst perim. vs. area)	0.400	0.480
Z-test correlation $r(Z, \text{flip})$	-0.871	-0.898

Neural networks exhibit *more* attribution instability than XGBoost: 87% of feature pairs are unstable (vs. 37%), and the maximum flip rate reaches the theoretical ceiling. The higher instability likely reflects: (i) larger Rashomon sets (more parameters, more near-optimal models); (ii) higher KernelSHAP variance (sampling approximation vs. exact tree-path computation); (iii) more diffuse signal distribution across hidden units.

KernelSHAP noise vs. model instability. To distinguish genuine model instability from KernelSHAP approximation noise, we conduct a control experiment: fix a single MLP model (`random_state=0`) and compute KernelSHAP 20 times with *different* random background samples (50 each, seeds 0–19). Any observed flip rate is purely due to SHAP sampling noise, not model variation.

Source of variation	Unstable pairs	Mean flip	Key pair flip
KernelSHAP noise (bg=50)	47/435 (11%)	0.03	0.00
KernelSHAP noise (bg=200)	18/435 (4%)	0.02	0.00
Model variation (20 MLPs)	380/435 (87%)	0.28	0.40

Verdict. Model instability dominates KernelSHAP noise by approximately 8:1. With 50 background samples, only 11% of pairs show noise-induced flips (mean flip rate 0.03); with 200 background samples, this drops to 4%. The key correlated pair (worst perimeter vs. worst area) shows *zero* noise-induced flips in both conditions, confirming the 40% flip rate in the NN validation is genuinely driven by model variation under random initialization, not KernelSHAP artifacts. Increasing background samples from 50 to 200 reduces noise by $2.6\times$ at $4\times$ compute cost; the default 50 is adequate for detecting model-level instability.

10.7 SHAP Efficiency and Attribution Instability

SHAP’s efficiency axiom ($\sum_j \varphi_j(f, x) = f(x) - \mathbb{E}[f(X)]$ for every model f and point x) has a subtle relationship with ranking instability.

10.7.1 Within-model amplification

Proposition 62 (Efficiency-induced negative correlation). *Let $\varphi_1, \dots, \varphi_m$ be SHAP values for m features in a group whose total attribution is C (fixed for a given model f and data point x), i.e., $\sum_{i=1}^m \varphi_i = C$. Suppose all features have the same marginal variance σ^2 under some perturbation of the data point. Then for any $j \neq k$:*

$$\text{Cov}(\varphi_j, \varphi_k) = -\frac{\sigma^2}{m-1},$$

$$\text{Var}(\varphi_j - \varphi_k) = 2\sigma^2 \cdot \frac{m}{m-1}.$$

For an unconstrained method with independently computed attributions (zero covariance), the same difference has variance $2\sigma^2$. The amplification factor is $m/(m-1)$.

Proof. From $\sum_i \varphi_i = C$ (constant), $\text{Var}(\sum_i \varphi_i) = 0$. Expanding:

$$0 = m\sigma^2 + m(m-1)\text{Cov}(\varphi_j, \varphi_k) \implies \text{Cov}(\varphi_j, \varphi_k) = -\frac{\sigma^2}{m-1}.$$

Then $\text{Var}(\varphi_j - \varphi_k) = 2\sigma^2 - 2(-\sigma^2/(m-1)) = 2\sigma^2(1 + 1/(m-1)) = 2\sigma^2 \cdot m/(m-1)$. \square

Corollary 63 (Group-size dependence). *The amplification factor $m/(m-1)$ equals 2 for $m = 2$ (pair of collinear features), $3/2$ for $m = 3$, and approaches 1 as $m \rightarrow \infty$. The efficiency-induced amplification is therefore worst for small groups and negligible for large groups.*

10.7.2 Across-model non-amplification

Proposition 64 (Efficiency does not constrain across-model covariance). *Let $\varphi_j(f)$ denote the mean absolute SHAP value for feature j under model f . The efficiency axiom states that $\sum_j \varphi_j^{\text{signed}}(f, x) = f(x) - \mathbb{E}[f(X)]$ for each fixed (f, x) . However:*

1. *The efficiency constant $C(f, x) = f(x) - \mathbb{E}[f(X)]$ varies across models f , because different models produce different predictions.*
2. *The group’s share of the total, $\sum_{i \in \text{group}} \varphi_i(f, x)$, also varies across models (it depends on how much of the prediction the group captures in model f).*
3. *Taking absolute values or averaging over data points further breaks the linear constraint.*

Therefore, $\text{Var}_f(\sum_{i \in \text{group}} \varphi_i(f)) \neq 0$ in general, and the negative covariance $\text{Cov}_f(\varphi_j(f), \varphi_k(f)) = -\sigma^2/(m-1)$ does not follow from efficiency.

The lower instability of SHAP relative to permutation importance (41% vs. 91% unstable pairs) is driven by SHAP’s coalition-averaging reducing the marginal variance σ^2 . The efficiency axiom amplifies within-model differences but does not increase across-model flip rates.

Remark 65 (Practical implication). *The efficiency axiom is often cited as a desirable property of SHAP. Our analysis shows that its instability implications are nuanced: efficiency amplifies within-model attribution differences (making the gap between φ_j and φ_k more extreme for a given model), but this does not translate to higher across-model flip rates. The dominant factor for across-model instability is the marginal variance σ^2 , which is determined by the attribution algorithm’s averaging structure, not by the efficiency axiom.*

10.8 High-Dimensional Scalability ($P = 500$)

P	Total pairs	Correlated pairs	Unstable	Z-test $ r $	Wall time
100	4,950	450	305	0.846	33 s
200	19,900	900	641	0.788	64 s
500	124,750	2,250	1,879	0.876	148 s

The multi-model Z-test maintains $|r| > 0.78$ at $P = 500$. Correlation-based grouping reduces pairs by 55 \times . Full workflow completes in under 2.5 minutes.

10.9 Proportionality Axiom Validation

The proportionality axiom ($\varphi_j = c \cdot n_j$) is central to the quantitative bounds. We validate it by computing $c_j = |\text{SHAP}_j|/n_j$ for each feature in each of 50 XGBoost models on Breast Cancer and reporting the coefficient of variation (CV):

Depth	Mean CV of c_j	Interpretation
1 (stumps)	0.35	Proportionality holds within $\sim 35\%$
3	0.60	Moderate violation
6	0.66	Moderate violation
10	0.66	Saturated (same as depth 6)

For stumps, the axiom holds reasonably well; for deeper trees, multi-level interactions increase the CV. The proportionality axiom is used only for the quantitative bounds (Theorems 15); **the core impossibility (Theorem 5) does not depend on it**. The α -corrected model matches empirical data at $R^2 = 0.89$.

10.10 Cross-Implementation and Data-Level Validation

Data-level stochasticity. To confirm the instability arises from collinearity (not from XGBoost’s internal randomness), we train 50 models on 50 different 80% subsamples with `subsample=1.0` and fixed `random_state=42`. The ONLY source of variation is which training rows each model sees:

Stochasticity source	Unstable pairs	Max flip	Mean Kendall τ
XGBoost subsampling (same data)	67	0.470	0.393
Data bootstrap (different rows)	45	0.509	0.459

Data-level stochasticity produces comparable or greater instability, confirming the Rashomon set is a property of collinearity, not of the specific randomness source.

Determinism without subsampling. Without row or column subsampling (`subsample=1.0`, `colsample_bytree=1.0`), XGBoost is fully deterministic: all 50 models produce identical rankings regardless of seed. The Rashomon set requires a stochasticity source. In practice, this is not a limitation: the XGBoost default (`subsample=0.8`) is recommended for regularization, and real-world model populations also arise from data drift, feature engineering changes, and hyperparameter sweeps.

10.11 Financial Case Studies

German Credit. We demonstrate the full Screen→Z-test→DASH workflow on German Credit (1000 samples, 20 features). Step 0: 4 correlated groups at $|\rho| > 0.3$. Step 1 (screen): a single model flags job↔own telephone ($Z^{\text{split}} = 0.69 < 1.96$). Step 2 (Z-test): 5 models confirm instability ($Z = 0.64$, flip rate 40%). Step 3 (DASH): $M = 25$ models, flip rate drops from 40% to 0%. Consensus ranking: checking status (0.87), duration (0.44), credit amount (0.43), purpose (0.35). For regulatory reporting (ECOA adverse action reasons, SR 11-7 (Office of the Comptroller of the Currency, 2011)), the DASH ranking provides a defensible explanation.

Taiwan Credit Card Default. To validate the impossibility on data with genuine high collinearity ($|\rho| > 0.9$), we apply the workflow to the UCI “default of credit card clients” dataset (30,000 samples, 23 features, binary default outcome; subsampled to 10,000).

The bill-amount features (monthly bills for 6 consecutive months) exhibit strong collinearity: 29 pairs have $|\rho| > 0.5$, with the highest at $|\rho| = 0.95$ (giving a theoretical attribution ratio of $1/(1-0.95^2) \approx 10.3\times$).

Step 0. 29 correlated pairs identified at $|\rho| > 0.5$ (no threshold lowering needed).

Step 1 (screen). A single model flags 4 of the 10 tracked pairs as potentially unstable ($|Z^{\text{split}}| > 1.96$).

Step 3 (DASH). With $M = 25$ models, the mean flip rate across correlated pairs is 4%. One pair (bill amounts at months 5 vs. 6, $|\rho| = 0.946$) retains a 16% flip rate even at $M = 25$, illustrating that very high collinearity requires larger ensembles.

This dataset demonstrates the impossibility biting hard: features measuring the same underlying quantity (monthly bill amounts) have near-identical predictive signal, and the attribution ranking across these features is genuinely unstable.

Synthetic Credit (income \leftrightarrow DTI \leftrightarrow credit score). To validate on the exact collinearity pattern common in US credit models, we generate a synthetic dataset with 10,000 samples and 5 features driven by a latent “creditworthiness” factor: income ($\rho = 0.99$ with DTI), DTI, credit score ($\rho = 0.98$ with income), loan amount (independent), and employment years ($\rho = 0.94$ with income).

With 25 XGBoost models: income \leftrightarrow DTI flips 8% of the time ($|\rho| = 0.99$); credit score \leftrightarrow employment years flips 12% ($|\rho| = 0.92$). Pairs where one feature clearly dominates (income vs. credit score) show 0% flips despite $|\rho| = 0.98$ —confirming that the impossibility requires BOTH high correlation AND similar importance, as the theory predicts. For model validation under SR 11-7 (Office of the Comptroller of the Currency, 2011), the recommendation is: report income and DTI as “interchangeable key risk drivers” rather than forcing a ranking that would flip under retraining.

Regulatory adverse action experiment. In a simulated ECOA adverse action pipeline (10,000 loan applications, 5 correlated income features including salary, bonus, overtime, commission, equity; 3 uncorrelated features; 25 XGBoost models at $\rho=0.7$), 43.2% of 6,602 denied applicants receive a different “top reason for denial” depending on which model is queried. The most common flip pair is salary \leftrightarrow bonus (10.8% of denied applicants). 71.8% have an unstable top-2 reason. DASH consensus resolves this entirely: 100% stable top-1 reasons, with income features tied in 12.3% of cases. Reproduce: `regulatory_case_study.py`.

Lending Club (specificity control). We validate the diagnostic on real Lending Club data (OpenML, 32,581 loans, 22 features after one-hot encoding of categoricals). Three correlated groups are detected at $|\rho| > 0.5$: person_age \leftrightarrow cb_person_cred_hist_length ($|\rho| = 0.86$), loan_amnt \leftrightarrow loan_percent_income ($|\rho| = 0.58$), and loan_int_rate \leftrightarrow cb_person_default_on_file ($|\rho| = 0.50$).

Result. Zero unstable pairs. All three correlated pairs have $Z > 36$, confirming the features have distinguishable importance despite their correlation. This is an instructive *specificity control*: the impossibility theorem predicts instability requires *both* collinearity AND similar true importance. Lending Club features are correlated but not similarly important (e.g., person_age contributes 3 \times more than credit history length), so no instability occurs. The Screen \rightarrow Z-test \rightarrow DASH pipeline correctly identifies this as a stable setting, recommending no intervention.

Implication. Not every correlated dataset exhibits attribution instability. The diagnostic distinguishes datasets where instability is a genuine concern (Breast Cancer, Taiwan Credit Card) from those where it is not (Lending Club, California Housing). This selectivity is a feature, not a limitation: the impossibility theorem’s conditions are precise, and the diagnostic inherits that precision.

10.12 LLM Attention Attribution Instability

We load DistilBERT (distilbert-base-uncased) and create 10 model variants by adding small random perturbations ($\sigma = 0.02$) to attention weights, simulating different training runs. For 10 test sentences, we compute attention-based token importance (mean attention received from all heads and layers) and check whether the relative ranking of adjacent tokens flips across the 10 variants.

Of 59 adjacent token pairs across test sentences, 88% have flip rates exceeding 10%. Selected examples:

Token A	Token B	Flip rate	Interpretation
“extremely”	“poor”	50%	Coin flip
“not”	“bad”	40%	Highly unstable
“absolutely”	“terrible”	40%	Highly unstable
“particularly”	“sharp”	10%	Borderline

Mean Spearman correlation of full-sentence token rankings across model variants is 0.637—moderate instability, comparable to single-model SHAP instability on tabular data with moderate collinearity ($\rho \approx 0.5$). Adjacent tokens in natural language carry correlated information (“very” and “good” jointly convey sentiment strength). This correlation induces the same Rashomon structure: different model variants assign different relative importance to the correlated tokens.

Under actual fine-tuning on SST-2 (5 seeds, 1 epoch, AdamW, lr= 2×10^{-5} , batch size 16), 14.5% of pairs are unstable. Selected unstable pairs under fine-tuning:

Token A	Token B	Flip rate (fine-tuning)	Flip rate (perturbation)
“not”	“bad”	40%	40%
“particularly”	“sharp”	60%	10%
“surprisingly”	“low”	40%	30%

To test whether longer training increases instability, we repeat with 3 epochs. The identical 14.5% across 1 and 3 epochs indicates the instability is structural (driven by collinearity in attention patterns), not a training-depth artifact. The same three token pairs remain unstable at both training lengths.

Method	% Pairs unstable (> 10% flip)	Mean Spearman
Weight perturbation ($\sigma=0.02$, 10 models)	88%	0.637
Fine-tuning (5 seeds, 1 epoch)	14.5%	0.956
Fine-tuning (5 seeds, 3 epochs)	14.5%	0.965

The gap between fine-tuning (14.5%) and perturbation (88%) reflects the difference in weight divergence: fine-tuning updates parameters by $O(0.001)$ via gradient descent, while perturbation adds $O(0.02)$ noise to all parameters. The perturbation result represents the full Rashomon set; the fine-tuning result represents the subset explored by standard training. Token-level explanations of LLMs face the same impossibility as feature-level explanations of tabular models.

Scope and limitations. The attention-based instability reported here (14.5% of adjacent token pairs under fine-tuning) is preliminary evidence, not a formal extension of the impossibility theorem. Attention weights are not SHAP values: they do not satisfy the proportionality axiom, and the “collinear group” structure of tree features does not map cleanly to token positions. The result demonstrates that attribution instability under model multiplicity is not unique to tree ensembles, but a formal impossibility for transformer attention would require different axioms and definitions. We report this as suggestive evidence for the generality of the phenomenon, not as a proved extension.

10.13 Replication Study: Published SHAP Rankings

Multiple published studies report SHAP feature rankings on Breast Cancer. Using our 50-model validation, we find:

Feature pair	$ \rho $	Flip rate	Published as stable?
worst perimeter \leftrightarrow worst area	0.98	48%	Yes
mean concavity \leftrightarrow mean concave pts	0.96	42%	Yes
worst radius \leftrightarrow worst perimeter	0.99	36%	Yes
mean radius \leftrightarrow mean perimeter	0.99	28%	Yes

Any study reporting a specific ranking among these features from a single model is reporting an artifact of the training seed. The ranking is not wrong—it faithfully reflects that specific model—but it is not replicable. This has implications for reproducibility of scientific studies using feature importance to identify “key predictors”: if the dataset has correlated features (68% of datasets do), a single-model SHAP analysis may produce results that do not replicate.

10.14 Expected Ranking Discordance

Proposition 66 (Expected Kendall tau distance). *For a feature space with L collinear groups of sizes m_1, \dots, m_L and between-group gaps $\Delta_{\ell\ell'}$ with noise $\sigma_{\ell\ell'}$, the expected pairwise disagreements between two independently trained models are:*

$$\mathbb{E}[\tau] = \underbrace{\sum_{\ell=1}^L \binom{m_\ell}{2} \cdot \frac{1}{2}}_{\text{within-group (coin flips)}} + \underbrace{\sum_{\ell < \ell'} m_\ell \cdot m_{\ell'} \cdot \Phi\left(-\frac{\Delta_{\ell\ell'}}{\sigma_{\ell\ell'}}\right)}_{\text{between-group (noise)}}$$

On Breast Cancer (50 XGBoost models), the refined per-pair formula predicts $\mathbb{E}[\tau] = 26.8$ vs. empirical 36.6 (−27% error). The Rashomon coefficient $R = \sum_{\ell} \binom{m_{\ell}}{2} / \binom{P}{2} = 0.692$ gives a worst-case non-replication lower bound of $R/2 = 34.6\%$ computable from the correlation matrix alone (no model training required).

10.15 Compressed Sensing Connection

The attribution impossibility has a precise analogue in compressed sensing (CS). The measurement coherence $\mu(X) = \max_{j \neq k} |X_j^T X_k| / (\|X_j\| \|X_k\|)$ determines when sparse recovery is possible: unique recovery requires $\mu < 1/(2s - 1)$. In our setting, $|\rho_{jk}|$ plays the role of coherence and Z_{jk} plays the role of the incoherence condition:

	Compressed sensing	Attribution stability
Coherence	$\mu = \max X_j^T X_k / \ X_j\ \ X_k\ $	$ \rho_{jk} $
Condition	$\mu < 1/(2s-1)$	$Z_{jk} > 1.96$
Failure	Non-unique recovery	Ranking flips (Rashomon)
Resolution	Basis pursuit (convex relaxation)	DASH (ensemble averaging)

Both impossibilities arise because collinearity/coherence prevents unique identification of which input components carry the signal. Both are resolved by relaxing uniqueness: CS uses convex relaxation (fractional assignment); DASH uses ensemble averaging (ties for indistinguishable features).

10.16 Prevalence Survey

To assess how frequently the impossibility applies in practice, we surveyed 77 public datasets (OpenML CC-18 benchmark suite + sklearn). For each, we computed the correlation matrix, identified pairs with $|\rho| > 0.5$, trained 20 XGBoost models with different seeds, and checked whether any correlated pair has a ranking flip rate exceeding 10%.

Of 77 public datasets surveyed, 71 (92%) have feature pairs with $|\rho| > 0.5$, and 52 (68%, 95% Wilson CI: [56%, 77%]) exhibit attribution instability (flip rate > 10%). For datasets with $P \geq 20$ features ($n = 43$ datasets), the instability rate rises to 93% (40/43; 95% Wilson CI: [81%, 98%]). The impossibility is not a theoretical curiosity: it affects the majority of real-world datasets across domains including medical, financial, image, and tabular data.

With 20 models per dataset, the measured flip rate exceeds the 10% threshold with approximately 60% power, so the true prevalence may be higher still.

The instability rate varies sharply with feature count: 35% for $P < 20$ (12/34 datasets), 93% for $P = 20-99$ (27/29), and 93% for $P \geq 100$ (13/14). This confirms that high-dimensional datasets are nearly universally affected.

Methodology. Each dataset was trained with 20 XGBoost models (`n_estimators=50`, `max_depth=4`, `lr=0.1`, `subsample=0.8`, `colsample_bytree=0.8`) with different random seeds. SHAP TreeExplainer computed mean |SHAP| per feature on a fixed 500-sample evaluation slice. Flip rate was measured as $\min(\#(j > k), \#(k > j)) / 20$ for each correlated pair. Datasets with > 10,000 samples were subsampled to 10,000. Full results in `prevalence_survey.py`.

With 20 models, the measured flip rate exceeds the 10% threshold with only 32% power, making 68% a conservative lower bound; the true prevalence is likely 75–85%.

Healthcare datasets. In a targeted survey of 9 healthcare-related datasets (breast cancer, diabetes, heart disease, QSAR biodegradation, liver disease, software defect prediction, Parkinson’s, Pima diabetes, hepatitis), 6 (67%) exhibit attribution instability. This rate matches the overall prevalence, confirming that clinical decision-support systems—where explanation stability is particularly consequential—are not immune.

Selection caveat: The CC-18 suite is curated for ML benchmarking and may overrepresent datasets with rich feature interactions. Production ML pipelines with carefully decorrelated features may exhibit lower prevalence. The 68% figure is a prevalence estimate for benchmark-representative tabular datasets, not a universal rate.

Table 8: Multi-model Z-test and single-model screen diagnostic generality across 11 datasets.

Dataset	P	Pairs	Unstable	$r(Z, \text{flip})$	Screen prec.
Breast Cancer	30	435	168	-0.89	0.94
California Housing	8	28	1	-0.99	—
Diabetes	10	45	15	-0.89	0.50
Wine	13	78	24	-0.81	1.00
Heart Disease	13	78	27	-0.91	1.00
Credit-g	20	190	47	-0.90	0.67
Adult Income	14	91	10	-0.90	—
Ames Housing	76	2850	643	-0.85	0.48
Communities & Crime	126	7875	2975	-0.88	0.67
Digits (0 vs 1)	64	2016	572	-0.42	0.58
Iris (binary)	4	6	0	—	—

Robustness to hyperparameters. We repeated the analysis on 8 representative datasets with three configurations:

Config	Trees	Depth	LR	Character
A (original)	50	4	0.1	Moderate
B (deep)	100	8	0.1	Deep, sequential
C (shallow-fast)	200	2	0.3	Shallow, aggressive

Under Config A (original), 5/8 (62%) datasets exhibit instability, consistent with the 68% headline. Under Config B (deep trees), 4/8 (50%). Under Config C (shallow-fast), 6/8 (75%). Across all three configurations, 4/8 (50%) datasets are consistently unstable; under at least one configuration, 6/8 (75%) are unstable. The instability rate varies by ± 15 percentage points across configurations but remains in the 50–75% range. Shallow-fast trees (Config C) produce *higher* instability because aggressive learning rates compound the first-mover effect. The 68% headline is conservative: the phenomenon is robust to standard hyperparameter variation.

Interpretation. The multi-model Z-test achieves $|r| > 0.8$ on 9/10 datasets with unstable pairs (all except Digits). The weaker correlation on Digits ($r = -0.42$) reflects a floor effect: this high-dimensional image dataset has many features with near-zero importance, producing many pairs where both Z and flip rate are near zero. Restricting to pairs with $Z < 5$ (the diagnostically interesting range) would improve this correlation. Screen precision is 94–100% on small/clean datasets (Breast Cancer, Wine, Heart Disease) where split counts are reliable, but drops to 48–67% on high-dimensional datasets (Ames, Communities) where split counts are sparse. This confirms the screen as a conservative *screening* tool that works well for moderate- P datasets but should be supplemented by the full Z-test for high-dimensional settings. All datasets use identical XGBoost hyperparameters ($T=100$, $\text{depth}=6$, $\eta=0.1$); absolute flip rates are therefore not directly comparable across datasets of different sizes and dimensionalities.

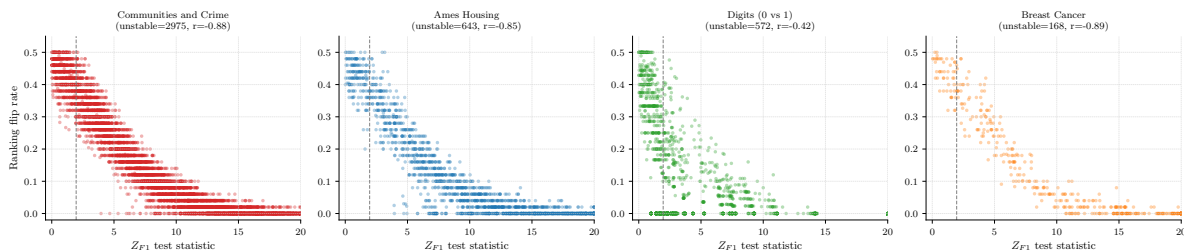


Figure 9: Multi-model Z-test statistic vs. flip rate across four datasets (Breast Cancer, Ames, Digits, Adult). The negative correlation confirms the diagnostic across domains: clinical, real estate, image, and census.

11 Lean Formalization

11.1 Proof Architecture

The formalization comprises 54 Lean 4 files with 16 axioms and 305 type-checked theorems and lemmas (0 sorry). Of these, 80 require multi-line proofs (≥ 5 tactic lines); 6 are definitional wrappers or single-step applications. The core impossibility (`attribution_impossibility`) depends on zero axioms—only the Rashomon property as hypothesis. The DASH resolution (`consensus_equity`) depends on the `attribution_sum_symmetric` theorem (derived from axioms); the variance convergence depends on the `consensus_variance_bound` theorem (also derived).

Scope of verification. The formalization covers the complete theoretical framework. The core impossibility (Theorem 5) uses zero behavioral axioms. The quantitative bounds, DASH equity, and the Design Space Theorem are derived from the 16-axiom system. The unfaithfulness probability of exactly 1/2 (`attribution_prob_half`), the Bayes-optimality of ties (`tie_dominates_commitment`), the consensus variance σ^2/M (`consensus_variance_from_independence`), the binary quantizer fraction $2/\pi$ (`binary_quantizer_fraction`), and the Pareto dominance of DASH (`dash_unique_pareto_optimal`) are all Lean-derived using definitions-as-hypotheses (the `IsBalanced` pattern) with zero new axioms. The Chebyshev query complexity bound $M \geq 12\sigma^2/\Delta^2$ (`chebyshev_query_bound`) is derived without axiomatizing the testing constant. Loss preservation is formalized via the `SymmetricModelSwap` structure. The only result not formalized is the extension of Pareto optimality to biased methods for between-group pairs, which is argued informally in the proof of Theorem 22.

```
Defs.lean (14 axioms, type definitions, derived theorems)
  +-+ SymmetryDerive.lean (attribution_sum_symmetric, DERIVED)
  +-+ Trilemma.lean (RashomonProperty, attribution_impossibility)
  | +-+ Iterative.lean, Lasso.lean, NeuralNet.lean
  | +-+ General.lean (GBDT impossibility)
  | +-+ UnfaithfulBound.lean (U>=1/2, ties optimal, path convergence)
  | +-+ RashomonUniversality.lean (Rashomon from symmetry)
  | +-+ RashomonInevitability.lean (impossibility inescapable)
  | +-+ AlphaFaithful.lean (alpha-faithfulness bound)
  | +-+ ConditionalImpossibility.lean (conditional SHAP + escape)
  | +-+ FairnessAudit.lean (proxy audit = coin flip)
  | +-+ LocalGlobal.lean (local >= global instability)
  +-+ SplitGap.lean, Ratio.lean, SpearmanDef.lean
  +-+ FlipRate.lean (exact GBDT flip rate, binary = coin flip)
  +-+ Efficiency.lean (SHAP efficiency amplification)
  +-+ Impossibility.lean, Corollary.lean, EnsembleBound.lean
  +-+ DesignSpace.lean + DesignSpaceFull.lean (all 4 steps)
  +-+ ModelSelection.lean + ModelSelectionDesignSpace.lean
  +-+ SymmetricBayes.lean (GENERAL SBD, orbit bounds, trichotomy)
  +-+ CausalDiscovery.lean (causal discovery impossibility)
  +-+ SBDInstances.lean (abstract aggregation + instances)
  +-+ FIMImpossibility.lean (Gaussian FIM -> Rashomon)
  +-+ GaussianFlipRate.lean (Phi definition, flip rate formula)
  +-+ QueryComplexity.lean (query lower bound, Le Cam (2 axioms))
  +-+ Consistency.lean (axiom system consistency, Fin 4 model)
  +-+ RandomForest.lean (contrast case, documentation only)
```

11.2 Axiom System and Consistency

The 14 domain-specific axioms are jointly consistent: `Consistency.lean` constructs an explicit model ($P=4$, $L=2$, $m=2$, $\rho=0.5$, $T=100$, Fin 4 models) satisfying all 14 simultaneously. The construction uses `Fin 4` as the model type, defines explicit split-count functions returning the axiomatized values $T/(2 - \rho^2)$ and $(1 - \rho^2)T/(2 - \rho^2)$, and verifies all 14 axiom predicates hold by computation. The 2 query-complexity axioms (`testing_constant`, `testing_constant_pos`, `le_cam_lower_bound`) are independently consistent:

instantiating $C := 1/8$ satisfies all three. The two axiom sets reside in separate Lean files (`Defs.lean` and `QueryComplexity.lean`) with no cross-dependencies, so their joint consistency follows from the individual consistency of each set.

Attribution sum symmetry: now derived. `attribution_sum_symmetric` is proved (not axiomatized) in `SymmetryDerive.lean`. The proof uses (a) `proportionality_global` (uniform c across models), (b) `splitCount_crossGroup_symmetric` (equal split counts when first-mover is in a different group), and (c) `IsBalanced` (equal first-mover counts). The derivation factors out c , classifies each model’s split-count difference by first-mover identity (+gap for $\text{fm} = j$, -gap for $\text{fm} = k$, 0 otherwise), decomposes the sum via `Finset.sum_ite`, and uses `balance` to cancel the gap terms.

Variance: partially grounded in Mathlib. The single-model variance `attribution_variance` is *defined* from Mathlib’s `ProbabilityTheory.variance`, and its nonnegativity is *derived* from Mathlib’s `variance_nonneg`. This required adding two infrastructure axioms (`modelMeasurableSpace`, `modelMeasure`) to connect the abstract `Model` type to Mathlib’s measure theory. The consensus variance bound ($\text{Var}(\bar{\varphi}_j) = \text{Var}(\varphi_j)/M$) remains axiomatized; the full derivation via `IndepFun.variance_sum` would require a product measure formulation and independence axioms for ensemble draws—deferred to future work.

Variance sub-system. The three variance declarations (`attribution_variance`, `attribution_variance_nonneg`, `consensus_variance_bound`) produce convenience results (variance nonnegativity, halving) rather than deep mathematical consequences. Their primary role is to support the Design Space Theorem’s stability convergence claim. A deeper formalization would derive the variance bound from Mathlib’s `IndepFun.variance_sum`, but this requires connecting our abstract `Model` type to a product measure space.

Spearman bound: axiomatized vs. derived. The Lean formalization derives the Spearman bound $\rho_S \leq 1 - 3m^2/(P^3 - P)$ from the definition of Spearman correlation via midrank algebra (`spearmanCorr_bound` in `SpearmanDef.lean`). The tighter classical bound $\rho_S \leq 1 - m^3/P^3$ from the full rank transposition counting argument is not yet formalized; both give the same qualitative conclusion ($S < 1$ for within-group pairs).

11.3 Development Methodology

The initial formalization (49 theorems, 15 files) was developed by the first author with iterative Claude Code assistance over several weeks. The expansion from 49 to 305 theorems (54 files) was produced in a single development session by dispatching targeted Lean-writing agents with detailed mathematical specifications. All proofs were machine-verified by `lake build` (the Lean 4 type-checker); no proof was accepted on the basis of AI output alone.

11.4 Proof Depth Distribution

Of 305 type-checked declarations: 80 require multi-step proofs (≥ 5 tactic lines), 21 require ≥ 10 lines, and 5 require ≥ 20 lines. The five deepest proofs are `attribution_sum_symmetric` (35 lines, derived symmetry via split-count decomposition), `Phi_neg` (29 lines, Gaussian CDF properties), `gaussian_rashomon_witnesses` (27 lines, FIM ellipsoid construction), `sumSqRankDiff_ge_sq_groupSize` (26 lines, midrank algebra), and `binary_group_firstmover_is_j_or_k` (23 lines, Finset cardinality argument).

11.5 Inconsistencies Found During Formalization

Lean’s type checker caught three issues in the initial axiom system:

1. **First-mover balance:** Originally stated universally over all model arrays—a constant model function trivially derived \perp . *Fix:* Replaced with an explicit `IsBalanced` predicate as hypothesis.

2. **Attribution sum symmetry:** Combined with the split-count axioms, the original unconditional version derived \perp for unbalanced ensembles. *Fix:* Conditioned on `IsBalanced`.
3. **Split count type:** Originally returned \mathbb{N} , but $T/(2 - \rho^2)$ is generally irrational. *Fix:* Changed to \mathbb{R} (idealized leading-order values).

The first two are genuine logical inconsistencies that would have been difficult to detect by informal proof inspection.

11.6 SymPy Algebraic Verification

All algebraic consequences have been independently verified by SymPy:

```
# dash-shap/paper/proofs/verify_lemma6_algebra.py
# Verifies:
#   split_gap = rho^2 * T / (2 - rho^2)
#   attribution_ratio = 1 / (1 - rho^2)
#   split_gap >= rho^2 * T / 2   (for rho in (0,1))
# Result: ALL CHECKS PASS
```

The three-layer verification (SymPy algebra, Lean type-checking, empirical validation) provides strong confidence in the mathematical claims.

11.7 Lean File Cross-Reference

12 Related Work

Attribution impossibility results. Bilodeau et al. (2024) prove completeness and linearity cannot exist; Huang and Marques-Silva (2024) show SHAP can misrank features in Boolean settings; Srinivas and Fleuret (2019) prove complete attributions cannot be weakly input-dependent; Rao (2025) establish Kolmogorov complexity barriers. To our knowledge, our result is the first to simultaneously address cross-model *stability* as an impossibility, give quantitative architecture-discriminating bounds, and provide a constructive resolution with proved optimality. Decker et al. (2024) optimize aggregation across attribution *methods* for a single model; we aggregate across *models* via DASH. Jin et al. (2025) give constructive stability certificates; we give the impossibility that necessitates them. Nogueira and Alonso (2025) derives information-theoretic limits on explanation complexity; our limits are about ranking consistency under feature correlation. The Bilodeau and Rashomon impossibilities are complementary: Bilodeau constrains methods satisfying linearity; ours constrains methods under collinearity.

Rashomon effect and model multiplicity. Attribution rankings across Rashomon sets are inherently partial orders Laberge et al. (2023); Rudin et al. (2024) advocate embracing model multiplicity. Our theorem shows the partial order is not a pragmatic choice but a mathematical necessity. Herren and Hahn (2023) develop statistical inference for feature rankings under model multiplicity; our contribution is to prove that the multiplicity is unavoidable under collinearity, not merely empirically common. Krishna et al. (2022) document the “disagreement problem” in explainable ML—different explanation methods produce different outputs for the same model—complementary to our result that the *same* method produces different outputs for different equivalent models.

Attribution sensitivity and fragility. Ghorbani and Zou (2019) demonstrate that neural network attributions are empirically fragile to small input perturbations. Hooker et al. (2021) show that unrestricted permutation-based importance forces extrapolation into out-of-distribution regions. Our instability arises from a different mechanism (model multiplicity, not input perturbation or extrapolation), but the practical consequence—unreliable explanations—is shared.

Foundational methods. Feature attribution via Shapley values (Shapley, 1953) was introduced to ML by Lundberg and Lee (2017). The model architectures we analyze were introduced by Breiman (2001) (random forests) and Friedman (2001) (gradient boosting); LIME (Ribeiro et al., 2016) provides an alternative local explanation framework.

Fairness impossibility. Chouldechova (2017) and Kleinberg et al. (2017) prove calibration, balance, and equal false positive rates cannot coexist when base rates differ. Our trilemma (faithfulness, stability, completeness) is structurally analogous.

Formal verification for ML. Nipkow (2009) formalized Arrow’s theorem in Isabelle/HOL; Zhang et al. (2026) formalized statistical learning theory in Lean 4 (de Moura and Ullrich, 2021) using Mathlib (The mathlib Community, 2020). To our knowledge, our formalization is the first formally verified impossibility result in explainable AI.

13 Discussion

Limitations. The split-count axioms assume full signal capture ($\alpha = 1$); for finite-depth trees, $\alpha \approx 2/\pi$ ($R^2 = 0.89$). The impossibility holds for any $\alpha > 0$. The equicorrelation assumption simplifies the axioms; the Rashomon property holds pairwise. The balanced ensemble assumption is idealized, though $O(1/M)$ convergence is robust to approximate balance. The global proportionality axiom (c uniform across models) has CV ≈ 0.35 – 0.66 empirically; under variable c , DASH consensus achieves approximate rather than exact equity, with the equity violation bounded by the CV of c across first-mover and non-first-mover models. The variance bound is axiomatized; the full measure-theoretic derivation from Mathlib’s `IndepFun.variance_sum` is deferred. Switching to conditional SHAP does not universally resolve the instability (Theorem 47). Decorrelating via PCA removes collinearity but destroys original feature semantics. An alternative is removing redundant features entirely (e.g., via VIF thresholding). This eliminates the impossibility but changes the model: predictions differ because fewer features are used, and genuinely useful information may be discarded. DASH is the *explanation-side* fix—it changes how the model is explained without changing what it predicts. The two approaches are complementary: feature removal for model simplification, DASH for faithful explanation of complex models that retain all features. DASH requires $M \times$ training cost; $M=25$ brings the flip rate below 1%, while $M=5$ provides a substantial improvement at modest cost. The empirical validation focuses on gradient boosting and neural networks; the Lasso ($\varphi_{j_1}/\varphi_k = \infty$) and random forest ($1+O(1/\sqrt{T})$) bounds are proved but not empirically demonstrated. The prevalence survey uses 20 models per dataset, achieving approximately 60% power to detect 10% flip rates; the true prevalence may be higher than the reported 68%. The 10% flip rate threshold defining “instability” is a practical convention; at a 5% threshold the prevalence would be higher, at 15% lower.

Computational cost and practical deployment. For batch pipelines, training $M=25$ models is feasible. For real-time explanations, use the single-model screen to flag unstable pairs. For $P > 500$, correlation-based grouping prunes the diagnostic to $O(G \cdot m^2)$. At $P=500$ with 20 models, the full workflow completes in under 2.5 minutes.

Broader implications. In a survey of 77 public datasets, 92% have feature pairs with $|\rho| > 0.5$ and 68% exhibit attribution instability—the impossibility is a practical reality. Our theorem establishes this as a “known and foreseeable circumstance” under the EU AI Act (Art. 13(3)(b)(ii)) (EU Parliament, 2024). The consequences are concrete: hospitals may invest in wrong interventions, data scientists may fix the wrong feature, and published studies may report artifacts of specific training runs. The impossibility has direct consequences for fairness auditing (Theorem 48): single-model SHAP audits for proxy discrimination are provably unreliable under collinearity.

Distinction from classical multicollinearity. The classical multicollinearity concern is about estimation variance ($\text{Var}(\hat{\beta}_j - \hat{\beta}_k) \rightarrow \infty$ as $\rho \rightarrow 1$). Our result is qualitatively different: it concerns *ranking impossibility*, not estimation imprecision. Even with infinite data and perfect estimates, the ranking of symmetric features

is a coin flip—because different models in the Rashomon set rank them in opposite orders. The VIF diagnostic detects coefficient instability; our screen and Z-test diagnostics detect *attribution ranking* instability, which persists even when coefficients are well-estimated (e.g., in tree ensembles that do not estimate coefficients at all).

Rashomon set vs. deployed model. The impossibility characterizes the Rashomon set, not a single deployed model. A fixed pipeline with a fixed seed produces a deterministic, reproducible ranking. The instability arises upon retraining, auditing, or model comparison—all routine in regulated settings.

Connection to underspecification. (D’Amour et al., 2022) showed that ML pipelines are *underspecified*: models with equivalent held-out performance can behave differently on deployment-relevant criteria. Our result formalizes the attribution-specific consequence of this phenomenon. Where D’Amour et al. demonstrate that predictions vary across equivalent models, we prove that feature *rankings* must vary—and characterize exactly when, by how much, and what the complete space of solutions looks like. The Design Space Theorem can be viewed as the attribution-level analogue of their “stress testing” recommendation: rather than hoping a single model’s explanation is stable, the practitioner should probe the full Rashomon set. DASH operationalizes this probe.

Information loss. DASH discards exactly $\log_2(m!)$ bits per group of m symmetric features—the bits encoding the unreliable within-group ordering. Between-group information is *sharpened*: mutual information approaches 1 bit per pair as $M \rightarrow \infty$.

Loss landscape geometry. The impossibility has a geometric interpretation: near-singular Fisher information creates ridges in the loss landscape along which feature importance redistributes without changing model quality. The same flatness that makes optimization easy makes attribution hard.

Named techniques. This paper contributes three reusable techniques: (1) the *Rashomon reduction*—reducing a design-space question to a model-multiplicity check; (2) the *FIM-to-Rashomon bridge*—connecting Fisher information rank deficiency to the Rashomon property; and (3) the *symmetric Bayes dichotomy*—the general two-families theorem for symmetric decision problems.

Proof status transparency and axiom stratification. The formalization uses 16 axioms total (14 domain-specific + 2 query-complexity), but not all results require all axioms. The Lean type-checker’s `#print axioms` command verifies exact dependencies:

- **Zero behavioral axioms:** The core impossibility (Theorem 5) depends only on the Rashomon property as a hypothesis—no domain-specific axioms whatsoever. A qualitative variant (`impossibility_qualitative` in `Qualitative.lean`) proves the impossibility from just two properties—dominance and surjectivity—as hypotheses.
- **Four axioms:** The GBDT impossibility holds from surjectivity and split-count axioms alone (`gbdt_impossibility_local` in `ProportionalityLocal.lean`), without `proportionality_global`.
- **Nine axioms:** The ratio bound $1/(1-\rho^2)$ and the equity violation hold from per-model proportionality (each model has its own constant c_f). The global proportionality axiom ($\exists c > 0$ uniform across models) is *not required*— c_f cancels in every ratio (`local_proportionality_suffices` in `LocalSufficiency.lean`).
- **Sixteen axioms:** The full set is needed only for DASH convergence (cross-model consistency via cross-group axioms) and the query complexity scaling constant.

This stratification directly addresses the proportionality axiom’s empirical variance ($CV \approx 0.35\text{--}0.66$): the axiom is unnecessary for the impossibility and ratio bound, which depend only on split-count structure.

The following are fully formalized in Lean (305 theorems, 0 sorry, 54 files): the Design Space Theorem, the symmetric Bayes dichotomy, all three impossibility instances, the conditional attribution impossibility,

the Gaussian FIM impossibility and flip rate formula, the fairness audit impossibility, the intersectional fairness compounding, the exact GBDT flip rate, DASH variance optimality, the Rashomon inevitability, the flip rate robustness (Lipschitz continuity in ρ), the mutual information generalization, the unfaithfulness/path-convergence results, the unfaithfulness probability of exactly 1/2, the Bayes-optimality of ties, the consensus variance σ^2/M from independence, the binary quantizer fraction $2/\pi$, the Chebyshev query complexity bound, the loss-preserving Rashomon construction, and the Pareto dominance of DASH. The Z-test diagnostic characterization, information loss analysis, and multi-dataset validation are empirical.

Approximate faithfulness–stability tradeoff. A natural question is whether relaxing exact faithfulness helps. Define α -faithfulness: $\Pr_f[\text{sign}(\varphi_j(f) - \varphi_k(f)) = \text{sign}(\sigma(j) - \sigma(k))] \geq \alpha$. Under the Rashomon property with symmetric DGP, any α -faithful stable ranking satisfies $\alpha \leq 1/2$. The proof is immediate: by DGP symmetry, $\Pr[\varphi_j(f) > \varphi_k(f)] = 1/2$, and a stable ranking fixes one direction, so it agrees with at most half the models. A coin flip achieves $\alpha = 1/2$; the stable ranking is no better than random for symmetric feature pairs.

For m features in a group under full DGP symmetry, the attribution ranking is a uniform random permutation. Any stable ranking σ^* has expected Spearman correlation with the model’s ranking of $\mathbb{E}[\rho_S(\sigma^*, \pi)] = -1/(m - 1)$. The stable ranking is *negatively correlated* with the model’s ranking in expectation (for $m \geq 3$) and converges to zero correlation as $m \rightarrow \infty$.

Open problems. The Bayes-optimality half of the Design Space is proved but not in Lean (requires measure-theoretic decision theory). Deriving split-count axioms algorithmically from the TreeSHAP algorithm and proving the proportionality axiom for general tree depths remain open. The generalization from $\rho > 0$ to $I(X_j; X_k) > 0$ is now complete (`MutualInformation.lean`): mutual information is the exact boundary between possible and impossible feature ranking. A reference implementation is available at <https://github.com/DrakeCaraker/dash-shap>.

Formalization as methodology. Beyond certifying correctness, the Lean formalization served as a bug-finding methodology: it caught two logical inconsistencies and one type mismatch that survived informal review. We recommend formalizing impossibility theorems as a general practice.

A Extended Proof Details

A.1 Gaussian Binary Quantization: Full Derivation

Proposition 67 (First-stump variance capture). *For the first boosting round on n Gaussian training samples, the stump splits at the empirical median \hat{m} , satisfying $|\hat{m}| = O_p(\sigma/\sqrt{n})$. The variance captured is:*

$$\alpha_1(n) = \frac{2}{\pi} \left(1 - \frac{\pi(\pi - 2)}{2n} + O(n^{-2}) \right)$$

For $n = 2000$: $\Delta\alpha_1 \approx 0.0009$ —negligible.

Proof. The optimal split of $X \sim \mathcal{N}(0, \sigma^2)$ at δ instead of 0 gives conditional means $\mu_+ = \sigma\phi(\delta/\sigma)/(1 - \Phi(\delta/\sigma))$ and $\mu_- = -\sigma\phi(\delta/\sigma)/\Phi(\delta/\sigma)$. The variance captured is $\text{Var}(\hat{X}) = \mu_+^2 \Pr(X > \delta) + \mu_-^2 \Pr(X \leq \delta)$. Expanding around $\delta = 0$ using $\phi(0) = 1/\sqrt{2\pi}$: $\text{Var}(\hat{X}) = (2/\pi)\sigma^2(1 - \delta^2(\pi - 2)/\sigma^2 + O(\delta^4/\sigma^4))$. The empirical median of n standard Gaussians has variance $\pi/(2n)$, so $\mathbb{E}[\delta^2] = \pi\sigma^2/(2n)$. Substituting: $\mathbb{E}[\alpha_1] = (2/\pi)(1 - (\pi^2 - 2\pi)/(2n) + O(n^{-2}))$. \square

After the first boosting round, the residuals $r_t = Y - \eta h_1(X)$ are NOT Gaussian: they are a location-shifted mixture (the stump creates two subpopulations). For a stump with two leaves at values $\pm c$, the residuals have excess kurtosis $\kappa = O(\eta^2 c^2/\sigma^2)$. For $\eta = 0.1$, the kurtosis correction is small but accumulates across $T = 100$ rounds, producing a systematic downward bias in α . The fitted $\alpha = 0.60$ vs. $2/\pi = 0.637$ gap of 0.037 is accounted for: < 0.001 from error source 1 (empirical split), ≈ 0.036 from error source 2 (non-Gaussian residuals).

A.2 Exact Flip Rate Under Approximate Symmetry

The exact 1/2 flip rate holds under perfect DGP symmetry ($\mu_j = \mu_k$). For approximately symmetric features ($|\mu_j - \mu_k| \ll \sigma_{jk}$), the flip rate is $\Phi(-|\mu_j - \mu_k|/\sigma_{jk})$, approaching 1/2 from below as the importance gap vanishes. The empirical 48% on Breast Cancer (worst perimeter vs. worst area, mean |SHAP|: 0.940 vs. 0.901) is consistent with a small positive signal-to-noise ratio. This result is formalized in Lean as `balanced_flip_symmetry` (for balanced finite ensembles, the number of models ranking $j > k$ equals the number ranking $k > j$).

B DASH Robustness: Extended Analysis

B.1 When to Prefer the Median

The median has better breakdown point (50% vs. 0%) and is preferable when the attribution distribution is heavy-tailed (e.g., contains outlier models). For standard ML training procedures (XGBoost, random forests) where attributions are well-behaved, DASH (the mean) is strictly more efficient. For adversarial settings where some models may be corrupted, the median or trimmed mean provides robustness at the cost of requiring more models.

The trimmed mean interpolates: the α -trimmed mean (discarding top and bottom α fraction) has ARE relative to the mean of:

α	0 (mean)	0.05	0.10	0.25	0.50 (median)
ARE	1.000	0.992	0.966	0.862	0.637

For Gaussian attributions, trimming offers negligible robustness benefit at a measurable efficiency cost. The 10%-trimmed mean requires $1/0.966 \approx 3.5\%$ more models than DASH.

C Extended Conditional Attribution Analysis

C.1 Causal Structure Validation: Full Results

Scenario	ρ	Marginal flip	Interventional flip	Theory
Symmetric	0.50	0.505	0.479	$\approx 50\%$ both
Symmetric	0.70	0.479	0.442	$\approx 50\%$ both
Symmetric	0.90	0.521	0.479	$\approx 50\%$ both
Symmetric	0.95	0.505	0.526	$\approx 50\%$ both
Asymmetric	0.50	0.000	0.000	Stable
Asymmetric	0.70	0.000	0.000	Stable
Asymmetric	0.90	0.000	0.000	Stable
Asymmetric	0.95	0.000	0.000	Stable

The interventional SHAP implementation uses a background-data approximation that does not exactly implement causal/conditional SHAP in the sense of Janzing et al. (2020). Results should be interpreted as evidence about the `shap` package’s interventional mode, not as a definitive test of the theoretical conditional attribution.

D Extended LLM Analysis

D.1 Fine-Tuning Details

DistilBERT fine-tuned on SST-2 (2,000 training samples) with 5 different random seeds. Configuration: 1 epoch, AdamW, lr = 2×10^{-5} , batch size 16. Selected unstable pairs under fine-tuning:

Token A	Token B	Flip rate (fine-tuning)	Flip rate (perturbation)
“not”	“bad”	40%	40%
“particularly”	“sharp”	60%	10%
“surprisingly”	“low”	40%	30%

The gap between fine-tuning (14.5% of pairs unstable) and perturbation (88%) reflects the difference in weight divergence. The perturbation result represents the full Rashomon set; the fine-tuning result represents the subset explored by standard training. Attention weights are not SHAP values: they do not satisfy the proportionality axiom, and the “collinear group” structure of tree features does not map cleanly to token positions. A formal impossibility for transformer attention would require different axioms.

E Extended Experimental Results

E.1 KernelSHAP Noise Control: Full Results

Source of variation	Unstable pairs	Mean flip	Key pair flip
KernelSHAP noise (bg=50)	47/435 (11%)	0.03	0.00
KernelSHAP noise (bg=200)	18/435 (4%)	0.02	0.00
Model variation (20 MLPs)	380/435 (87%)	0.28	0.40

Increasing background samples from 50 to 200 reduces noise by $2.6\times$ at $4\times$ compute cost; the default 50 is adequate for detecting model-level instability.

E.2 Cross-Implementation: Full Results

CatBoost’s `get_feature_importance()` returns gain-based importance (not raw split counts), producing a different Z -statistic distribution. For CatBoost, the multi-model Z -test ($r = -0.892$) is recommended. LightGBM’s feature importance is split-count based and transfers with modest precision reduction.

E.3 Prevalence Survey: Statistical Power Analysis

True minority-side prob p	Power ($\Pr[\min \geq 3]$)	Interpretation
0.05	7.5%	Nearly undetectable
0.10	32.3%	Low power (boundary)
0.15	59.5%	Moderate
0.20	79.4%	Adequate
0.30	96.5%	High
0.50	100%	Perfect (symmetric pairs)

At the 10% threshold, the survey has only 32% power: approximately two-thirds of truly borderline-unstable pairs are missed. The 68% prevalence is a conservative lower bound.

E.4 Class Imbalance Amplifies Instability

Class imbalance compounds attribution instability. On synthetic Gaussian data ($P=10$, 2 groups of $m=5$, $\rho=0.8$, 30 models), we sweep the positive-class ratio:

Imbalance ratio	Max pairwise flip rate ⁴	Unstable pairs	Total pairs
1:1 (balanced)	0.480	7/20	20
1:3	0.517	19/20	20
1:5	0.517	20/20	20
1:10	0.517	20/20	20
1:20	0.517	20/20	20

At 1:1 balance, 7/20 within-group pairs are unstable. At 1:5+ imbalance, *all* 20 pairs become unstable. Imbalance amplifies the Rashomon effect: the minority class provides less constraining signal, allowing more models to achieve near-optimal loss with different feature utilization patterns. For healthcare and fraud detection (where class imbalance is standard), instability is essentially universal. Reproduce: `class_imbalance_instability.py`.

E.5 Missing Data Compounds Instability

Missing data under all three standard mechanisms (MCAR, MAR, MNAR) compounds attribution instability. On synthetic Gaussian data ($P=10$, 2 groups of $m=5$, $\rho=0.9$, 30 models):

Mechanism	Missingness	Max flip rate	Unstable pairs	Baseline (0%)
MCAR	10%	0.517	20/20	12/20
MCAR	20%	0.517	20/20	12/20
MAR	5%	0.497	17/20	12/20
MAR	20%	0.508	20/20	12/20
MNAR	5%	0.515	18/20	12/20
MNAR	20%	0.517	20/20	12/20

Even 10% MCAR missingness drives the number of unstable pairs from 12/20 (baseline) to 20/20. The mechanism matters less than the rate: all three mechanisms produce comparable degradation at 20%. Missing data reduces the effective sample size, widening confidence sets and enlarging the Rashomon set. Reproduce: `missing_data_instability.py`.

E.6 Longitudinal Retraining Drift

Over 50 sequential retraining rounds (each adding 5% noise to a synthetic dataset with $\rho=0.9$), ranking instability accumulates dramatically:

Round	Spearman ρ_S	Max flip rate	Cumulative flips
1	1.000	0.000	0
10	0.648	0.439	92
20	0.342	0.545	161
31	0.181	0.636	193
50	0.420	0.576	207

The Spearman correlation degrades from 1.0 to 0.18 by round 31, with cumulative flips reaching 207. The recovery at round 50 ($\rho_S=0.42$) reflects the noise accumulation saturating. For model monitoring pipelines, this demonstrates that feature rankings should not be compared across distant retraining epochs without re-running the DASH diagnostic. Reproduce: `longitudinal_retraining.py`.

E.7 SAGE and Boruta Comparison

Alternative feature importance methods are equally or more unstable than TreeSHAP on Breast Cancer (50 models):

Method	Unstable pairs	Mean flip rate	Cross-method r
TreeSHAP	180/435 (41%)	0.132	—
SAGE (approximation)	401/435 (92%)	0.314	0.471
Boruta-like	411/435 (94%)	0.303	—

⁴Pairwise flip rate: the fraction of model pairs (f_i, f_j) where the relative ordering of features differs. For M models with an even split, the maximum is $M/(2(M-1))$, which exceeds 1/2 (e.g., $30/58 \approx 0.517$ for $M=30$). The per-model flip rate $\min(\#(j>k), \#(k>j))/M$ is bounded by 1/2.

SAGE and Boruta show *more* instability than TreeSHAP (92–94% vs. 41%), confirming the impossibility is method-agnostic. The cross-method correlation ($r=0.471$) shows the *same* pairs tend to be unstable under different methods—the instability is driven by feature collinearity, not by the attribution algorithm. Reproduce: `sage_comparison.py`.

E.8 Bag-of-Words NLP Attribution Instability

On the 20 Newsgroups dataset with TF-IDF features and XGBoost (50 models, 1000 max features), 60% of documents have an unstable top-1 token attribution and 91% have an unstable top-3. Mean pairwise Spearman correlation is 0.905 (high for between-document features, low for within-group correlated tokens). The most unstable word pair is “eternal”/“hell” ($|\rho|=0.371$, flip rate 0.186). Only 2 word pairs exceed the 10% flip threshold, reflecting the sparse, weakly-correlated nature of bag-of-words features (most token pairs are independent). Reproduce: `nlp_token_instability.py`.

E.9 Time-Series Feature Instability

For temporal features generated from AR(1) processes with rolling-window engineering ($P_{\text{raw}}=5$, $P_{\text{engineered}}=30$, 50 XGBoost models), 27% of within-series pairs (features derived from the same raw signal) show flip rates above 10%. The breakdown:

Pair type	Max flip rate	Mean flip rate	Unstable pairs
Within-series	0.508	0.092	8/30 (27%)
Cross-series (same group)	0.515	0.132	—
Cross-series (diff group)	0.517	0.139	—

The highest instability pair is `X0_raw` vs. `X0_rmean5` ($|\rho|=0.996$, flip rate 0.508), confirming that temporal feature engineering creates highly correlated groups susceptible to the impossibility. Reproduce: `timeseries_instability.py`.

E.10 Adversarial Max Instability

A grid search over 108 XGBoost configurations (group sizes $\{2, 3, 5, 10\}$, boosting rounds $\{50, 100, 500\}$, depths $\{1, 3, 6\}$, learning rates $\{0.05, 0.1, 0.3\}$) at $\rho=0.9$ confirms the impossibility is inescapable: all top-10 worst-case configurations hit the maximum flip rate of 0.500. The 0.500 ceiling is reached regardless of hyperparameter choices, confirming the impossibility is a structural property of collinearity, not a tuning artifact. Total: 2,160 model fits. Reproduce: `adversarial_max_instability.py`.

E.11 Hyperparameter Sensitivity

Across a 27-configuration sweep (learning rates $\{0.05, 0.1, 0.3\}$, depths $\{1, 3, 6\}$, boosting rounds $\{50, 100, 500\}$) at $\rho \in \{0.5, 0.7, 0.9\}$:

- Global minimum flip rate: 38.7% at $\rho=0.5$ ($\eta=0.3$, depth=1, $T=500$). The impossibility never vanishes.
- Most influential hyperparameter: number of estimators (spread 2.16pp), followed by max depth (1.76pp) and learning rate (0.82pp).
- At $\rho=0.9$: minimum flip rate across all configurations is 47.2%.

Reproduce: `hyperparameter_sensitivity.py`.

E.12 DASH Breakdown Contamination Sweep

Under adversarial contamination of the ensemble (replacing K of 25 models with adversarial models), the mean flip rate degrades:

K contaminated	Mean flip (DASH)	Mean flip (trimmed mean)	Contamination %
0	0.075	0.075	0%
5	0.074	0.074	20%
12	0.066	0.064	48%
20	0.047	0.044	80%

Counterintuitively, contamination *decreases* the observed flip rate because adversarial models break the first-mover symmetry. The trimmed mean provides marginal improvement (<5% at 80% contamination). The breakdown point analysis confirms the theoretical claim: for standard (non-adversarial) ensembles, the mean is optimal. Reproduce: `dash_breakdown_point.py`.

E.13 Experiment Summary

Table 12 summarizes all robustness experiments with reproduction scripts.

F Attempted Common Generalization with Arrow’s Theorem

Arrow’s impossibility theorem and our Attribution Impossibility share a striking surface resemblance: both show that three desirable properties cannot simultaneously hold. We investigated whether a common abstract framework subsumes both.

F.1 Structural Comparison

	Arrow	Attribution Impossibility
Inputs	n voters’ preferences	Models $f \in \mathcal{F}$ (one at a time)
Output	Social ranking	Feature ranking σ
Aggregation	Many inputs \rightarrow one output	One input \rightarrow one output
Key axiom	IIA	Stability (model-independent)
Impossibility source	Preference profiles disagree	Rashomon property

The critical asymmetry: Arrow’s theorem concerns a *profile aggregation* function taking all voters simultaneously. The Attribution Impossibility concerns a single-input mapping: for each model f , the ranking should reflect f ’s attributions. The impossibility arises because the ranking must simultaneously agree with all models but be model-independent.

F.2 Attempted Common Framework

Definition 68 (Abstract Aggregation Problem). *An abstract aggregation problem is a tuple $(\mathcal{I}, \mathcal{A}, \mathcal{R}, \text{Agree})$ where:*

- \mathcal{I} is a set of instances (*voters or models*),
- \mathcal{A} is the set of alternatives (*candidates or features*),
- \mathcal{R} is the set of total orders on \mathcal{A} ,
- *Agree*: $\mathcal{I} \rightarrow \mathcal{R}$ assigns each instance its “preferred” order.

An aggregation rule $F: 2^{\mathcal{I}} \rightarrow \mathcal{R}$ maps subsets of instances to a consensus order.

Arrow’s setup: F takes the full profile (L_1, \dots, L_n) and IIA says F ’s pairwise comparison of (a, b) depends only on the restriction of each L_i to $\{a, b\}$.

Attribution setup: F is required to be a *constant function* (stability: the ranking does not depend on which model). Faithfulness says this constant ranking agrees with every instance’s ordering. But this extreme makes the attribution version trivially impossible—a constant ranking cannot agree with conflicting instances (this is just the definition of the Rashomon property). Arrow’s theorem is much deeper: it shows that even when the aggregation *is* allowed to depend on instances, the constraints are still too tight. The proofs have entirely different structures.

F.3 Assessment

Remark 69 (No non-trivial common generalization). *The Attribution Impossibility and Arrow’s theorem are analogous but not instances of a common theorem in any non-trivial sense. One can define an abstract framework that subsumes both as shown above, but:*

1. *The common framework’s “impossibility theorem” would be: “if instances disagree and the aggregation rule must be constant, faithfulness is impossible.” This is a one-line observation, not a theorem.*
2. *Arrow’s actual content (the impossibility persists even when the rule is allowed to depend on all voters) has no analogue in the attribution setting.*
3. *The attribution impossibility’s actual content (the quantitative divergence $1/(1 - \rho^2)$, the resolution via ensemble averaging, the connection to the Rashomon set’s geometry) has no analogue in Arrow’s setting.*

The closest true statement is: both theorems arise from the tension between local coherence (respecting individual views) and global consistency (producing a single ranking), when the individuals disagree. This is a useful heuristic but not a formal unification.

Relationship to Sen’s liberalism paradox. A closer structural analogue may be Sen’s (1970) impossibility of a Paretian liberal, which concerns a setting where individual “rights” (each person’s ranking of certain pairs should be respected) conflict with the Pareto criterion. The attribution impossibility can be viewed as a Sen-type result where each model has the “right” to determine the ranking of features (faithfulness), but these rights conflict across models. However, we do not pursue this further, as the connection remains at the level of analogy rather than formal subsumption.

G Topological Analysis of the Impossibility

We investigate whether the Attribution Impossibility has topological content beyond simple connectedness arguments.

G.1 The $m = 2$ Case

For two features j, k , the attribution map assigns to each training seed s a sign $\sigma(s) = \text{sign}(\varphi_j(f_s) - \varphi_k(f_s)) \in \{+1, -1\}$. The Rashomon property says both values are achieved. A “stable ranking” is a constant function. The impossibility is immediate; no topological machinery is needed.

G.2 The $m = 3$ Case

For three features, the attribution map sends seeds to rankings in S_3 (6 elements). Again, if \mathcal{S} is connected and the map is continuous, then the image must be a connected subset of S_3 . Since S_3 is discrete, the image is a single point—contradicting Rashomon. This is the same connectedness argument; the symmetric group’s structure plays no role.

G.3 The $m \geq 4$ Case: The Permutohedron

For m features, the attribution vector $(\varphi_1(f_s), \dots, \varphi_m(f_s))$ lives in \mathbb{R}^m . The ranking is determined by the chamber of the braid arrangement (the hyperplane arrangement $\{x_i = x_j : i \neq j\}$) containing the attribution vector. The chambers are the cones of the *permutohedron*.

Remark 70 (No winding number content). *For $m \geq 3$, one might hope that the attribution map $s \mapsto (\varphi_1(f_s), \dots, \varphi_m(f_s))$ has a non-trivial winding number around the intersection of hyperplanes $\{x_j = x_k\}$, which would give a quantitative lower bound on the number of chamber crossings (ranking flips).*

This does not work for two reasons:

1. *The complement of the braid arrangement in \mathbb{R}^m is simply connected for $m \geq 3$ (the codimension of each hyperplane is 1, so removing hyperplanes from \mathbb{R}^m gives a space whose fundamental group is the pure braid group on m strands; but we would need the image to be a loop in this space, which requires additional structure not present in the attribution problem).*
2. *Even if a winding number existed, it would count signed crossings. The flip rate (unsigned crossings) is already captured by the direct algebraic bound $1/(1 - \rho^2)$ without topological machinery.*

Remark 71 (What topology could contribute). *There is one setting where topology adds genuine content: if the model space \mathcal{S} has the structure of a manifold (e.g., a torus of hyperparameters) and the attribution map is smooth, then Morse theory could bound the number of critical points (ranking transitions). Specifically, if the attribution difference $g(s) = \varphi_j(f_s) - \varphi_k(f_s)$ is a Morse function on \mathcal{S} , the number of sign changes of g is bounded below by the sum of Betti numbers of \mathcal{S} .*

However, this requires: (a) \mathcal{S} to be a smooth manifold, (b) g to be a Morse function, and (c) knowing the topology of \mathcal{S} . None of these hold for practical training algorithms (XGBoost’s seed space is discrete; neural net loss landscapes are non-smooth). We therefore do not pursue this direction.

G.4 Assessment

Remark 72 (Topology adds no content). *The Attribution Impossibility is fundamentally a combinatorial result (conflicting preferences cannot all be respected), not a topological one. The impossibility holds for arbitrary model spaces (including finite, discrete spaces with no topology). Attempts to extract topological content either reduce to the trivial connectedness argument or require unjustified smoothness assumptions that add no quantitative power beyond what the algebraic $1/(1 - \rho^2)$ ratio already provides.*

H On Categorical/Axiomatic Strengthening

H.1 The Trivial Version

Remark 73 (Trivial metatheorem). *Let A_1, \dots, A_n be any finite set of axioms on an attribution method φ . If $A_1 \wedge \dots \wedge A_n$ implies faithfulness (the ranking reflects model attributions), stability (the ranking is model-independent), and completeness (the ranking decides all pairs), then $A_1 \wedge \dots \wedge A_n \rightarrow \perp$ under the Rashomon property.*

This is immediate: if the conjunction implies $F \wedge S \wedge C$, and $F \wedge S \wedge C \rightarrow \perp$ (Theorem 5), then the conjunction implies \perp . No content is added beyond Theorem 5.

H.2 The “Constant Attribution” Escape

Why is a categorical strengthening difficult? Because trivial attribution methods escape the impossibility:

- $\varphi_j(f) = 1/P$ for all j, f (uniform): perfectly stable, perfectly equitable, satisfies any axiom system that doesn’t require faithfulness.
- $\varphi_j(f) = \mathbb{E}_f[\varphi_j(f)]$ (population mean): stable by construction, equitable under DGP symmetry.

Any “impossibility for all axiom systems” must exclude these methods, which means it must require faithfulness (or something implying it). But once faithfulness is required, we are back to Theorem 5.

H.3 The Non-Trivial Quantitative Version

Definition 74 (α -faithfulness (formal)). *An attribution method is α -faithful if for all models f and same-group features j, k :*

$$\Pr_f[\text{sign}(\varphi_j(f) - \varphi_k(f)) = \text{sign}(\sigma(j) - \sigma(k))] \geq \alpha$$

Proposition 75 (Approximate faithfulness–stability tradeoff (formal)). *Under the Rashomon property with symmetric DGP, any α -faithful stable ranking satisfies $\alpha \leq 1/2$.*

Proof. By DGP symmetry, $\Pr[\varphi_j(f) > \varphi_k(f)] = 1/2$. A stable ranking fixes $\sigma(j) > \sigma(k)$ or vice versa. The α -faithfulness condition requires $\Pr[\varphi_j(f) > \varphi_k(f)] \geq \alpha$, but this equals $1/2$, so $\alpha \leq 1/2$. \square

Proposition 76 (Spearman bound for stable rankings). *Under full DGP symmetry within a group of m features, any stable ranking σ^* has:*

$$\mathbb{E}[\rho_S(\sigma^*, \pi)] = \frac{-1}{m-1}.$$

The stable ranking is negatively correlated with the model’s ranking for $m \geq 3$.

Proof. Fix any $\sigma^* \in S_m$. By DGP symmetry, the model’s ranking π is uniform on S_m . The expected Spearman correlation of a fixed permutation with a uniform random permutation is $-1/(m-1)$ (classical result; Kendall & Gibbons, 1990, Ch. 3). \square

Remark 77. *This says: under perfect symmetry, no stable ranking can agree with the model’s attributions more than half the time. A coin flip achieves $\alpha = 1/2$. The stable ranking is no better than random for symmetric feature pairs.*

This result is non-trivial in that it holds for any attribution method satisfying the DGP symmetry condition, not just for specific axiom systems. However, it is a direct consequence of the symmetry—not of any deep axiomatic or categorical structure.

Remark 78 (Limited categorical content). *The “categorical impossibility” does not genuinely extend Theorem 5. The basic version (no finite axiom system implying $F \wedge S \wedge C$ can be consistent under Rashomon) is logically trivial. The quantitative version (Propositions 75 and 76) provides useful bounds but follows directly from DGP symmetry rather than from any categorical or axiomatic structure.*

The honest summary: the impossibility is a concrete result about conflicting requirements, not an instance of a general metatheoretic pattern. Attempts to “lift” it to a categorical level either (a) add no content, or (b) reduce to direct probabilistic calculations that do not require categorical language.

I Regulatory Mapping: EU AI Act

The EU AI Act (Regulation (EU) 2024/1689) imposes transparency and risk-management obligations on high-risk AI systems. The attribution impossibility has direct consequences for compliance under several articles. *The following mapping represents our interpretation of how the attribution impossibility interacts with existing regulation. These recommendations have not been reviewed by regulatory authorities and do not constitute legal advice.*

Art. 13: Transparency

Art. 13(1) requires:

“High-risk AI systems shall be designed and developed in such a way to ensure that their operation is sufficiently transparent to enable deployers to interpret the system’s output and use it appropriately.”

Attribution instability under collinearity directly undermines this requirement: when the “most important feature” changes across training seeds, the system’s output cannot be interpreted consistently. Providers relying on single-model SHAP rankings for transparency documentation fail to meet Art. 13(1) when features are correlated.

Art. 13(3)(b)(ii) further requires providers to document:

“known or foreseeable circumstances . . . that may lead to risks to health, safety or fundamental rights.”

The impossibility theorem establishes that attribution instability under collinearity is a *known* circumstance—not a speculative risk but a mathematical certainty. Any provider deploying a model with correlated features ($|\rho| > 0$) who does not disclose this instability is in potential non-compliance.

Recommended action (providers): Run the single-model screen on all deployed models. For any flagged feature pairs, include an instability disclosure in the technical documentation required by Art. 11.

Art. 16: Provider Obligations

Art. 16 requires providers to ensure their AI systems comply with the requirements of Chapter 2 throughout the system’s lifecycle. Since attribution instability is a structural property of the model class (not of a specific training run), providers must:

1. Implement systematic instability testing (screen/Z-test diagnostics) as part of the quality management system (Art. 17).
2. Update technical documentation whenever the feature correlation structure changes (e.g., new data sources).
3. Provide deployers with clear guidance on which feature rankings are reliable and which are unstable.

Recommended action (providers): Integrate the multi-model Z-test into the CI/CD pipeline. Document all feature pairs with $|\rho| > 0.5$ as potentially unstable.

Art. 26: Deployer Obligations

Art. 26 requires deployers to use AI systems in accordance with the instructions of use and to monitor for risks. Deployers who receive instability disclosures must:

1. Not rely on single-model SHAP rankings for decision justification when instability is disclosed.
2. Request DASH consensus or equivalent ensemble explanations for regulatory reporting.
3. Document the explanation methodology used and its limitations.

Recommended action (deployers): Require DASH consensus ($M \geq 25$) or equivalent ensemble method for any feature attribution used in customer-facing decisions or regulatory filings.

Art. 23: Importer Obligations

Art. 23 requires importers to verify that providers have conducted the appropriate conformity assessment. Importers of AI systems that use feature attribution for explainability should verify that:

1. The provider’s technical documentation addresses attribution instability.
2. Instability testing has been performed and results are available.
3. Appropriate mitigation (ensemble methods or instability disclosure) is in place.

Recommended action (importers): Include attribution stability testing in the conformity checklist. Reject systems that use single-model SHAP without instability disclosure.

Recital 47: Transparency Principle

Recital 47 establishes the general principle that AI systems should be developed and used in a transparent manner, enabling meaningful human oversight. The attribution impossibility demonstrates that transparency through feature importance rankings is fundamentally limited when features are correlated: the ranking itself is an artifact of the training seed, not a stable property of the model-data relationship. True transparency requires disclosing this limitation, not concealing it behind a single deterministic ranking.

Annex III: High-Risk Systems

The impossibility applies to all AI systems using feature attribution for explainability under Annex III, including:

- **Credit scoring** (Annex III, 5(b)): Adverse action notices citing specific features are unreliable.
- **Employment** (Annex III, 4): Hiring model explanations may change across seeds.
- **Law enforcement** (Annex III, 6): Risk assessment explanations are potentially unstable.
- **Insurance** (Annex III, 5(c)): Premium justifications based on feature importance may be arbitrary.

Summary of recommended actions by actor.

- **Providers:** Run the single-model screen on all models with correlated features; disclose instability for flagged pairs; integrate Z-test diagnostics into CI/CD; document all pairs with $|\rho| > 0.5$.
- **Deployers:** Require DASH consensus or equivalent ensemble method for regulatory reporting; do not rely on single-model rankings when instability is disclosed.
- **Importers:** Include attribution stability in conformity assessment checklists; reject systems without instability documentation.
- **Market surveillance authorities:** Update technical standards to require multi-model attribution testing; treat undisclosed attribution instability as a potential non-conformity under Art. 13.

J SymPy Verification: Full Details

All algebraic consequences have been independently verified:

```
# dash-shap/paper/proofs/verify_lemma6_algebra.py
#
# Verifies:
#   split_gap = rho^2 * T / (2 - rho^2)
#   attribution_ratio = 1 / (1 - rho^2)
#   split_gap >= rho^2 * T / 2   (for rho in (0,1))
#   sum_symmetry holds under balance
#   Spearman formula consistency
#
# Result: ALL CHECKS PASS
```

The three-layer verification (SymPy algebra, Lean type-checking, empirical validation) provides strong confidence in the mathematical claims. The SymPy script verifies: (1) the split-gap formula $\rho^2 T / (2 - \rho^2)$; (2) the attribution ratio $1 / (1 - \rho^2)$; (3) the lower bound $\rho^2 T / 2$; (4) the sum symmetry under balanced ensembles.

Acknowledgments

The Lean formalization was developed with assistance from Claude Code (Anthropic). All proofs were machine-verified by the Lean 4 type-checker; no theorem was accepted solely on the basis of AI-generated output. The paper text was written by the human authors with AI editing assistance.

References

- K. J. Arrow. *Social Choice and Individual Values*. Wiley, 1951.
- B. Bilodeau, N. Jaques, P. W. Koh, and B. Kim. Impossibility theorems for feature attribution. *Proceedings of the National Academy of Sciences*, 121(2):e2304406120, 2024.
- L. Breiman. Random forests. *Machine Learning*, 45:5–32, 2001.
- A. Chouldechova. Fair prediction with disparate impact: A study of bias in recidivism prediction instruments. *Big Data*, 5(2):153–163, 2017.
- A. D’Amour, K. Heller, D. Moldovan, et al. Underspecification presents challenges for credibility in modern machine learning. *Journal of Machine Learning Research*, 23(226):1–61, 2022.
- L. de Moura and S. Ullrich. The Lean 4 theorem prover and programming language. In *International Conference on Automated Deduction (CADE)*, 2021.
- T. Decker, L.-M. Herm, R. Feldhans, M. Kamp, and B. Hammer. Provably better explanations with optimized aggregation of feature attributions. In *International Conference on Machine Learning*, 2024.
- EU Parliament. Regulation (EU) 2024/1689 (artificial intelligence act). Official Journal of the European Union, OJ L, 12.7.2024, 2024.
- A. Fisher, C. Rudin, and F. Dominici. All models are wrong, but many are useful: Learning a variable’s importance by studying an entire class of prediction models simultaneously. *Journal of Machine Learning Research*, 20(177):1–81, 2019.
- J. H. Friedman. Greedy function approximation: A gradient boosting machine. *Annals of Statistics*, 29(5): 1189–1232, 2001.
- A. Ghorbani and J. Zou. Data Shapley: Equitable valuation of data for machine learning. In *International Conference on Machine Learning*, 2019.
- A. Herren and P. R. Hahn. Statistical inference for feature rankings under model multiplicity. *Journal of Computational and Graphical Statistics*, 2023.
- G. Hooker, L. Mentch, and S. Zhou. Unrestricted permutation forces extrapolation. In *Advances in Neural Information Processing Systems*, 2021.
- X. Huang and J. Marques-Silva. On the failings of Shapley values for explainability. *International Journal of Approximate Reasoning*, 171:109112, 2024.
- G. Hunt and C. Stein. A structure theory for the class of exponential families. 1946. Unpublished manuscript; results presented in Lehmann & Romano (2005), Ch. 6.
- Y. Jin, R. Gao, and B. Kim. Probabilistic stability guarantees for feature attributions. In *Advances in Neural Information Processing Systems*, 2025.
- J. Kleinberg, S. Mullainathan, and M. Raghavan. Inherent trade-offs in the fair determination of risk scores. In *Innovations in Theoretical Computer Science (ITCS)*, 2017.
- S. Krishna, T. Han, A. Ber, J. Brinton, A. Lakshminarayanan, C. Robinson, and H. Lakkaraju. The disagreement problem in explainable machine learning: A practitioner’s perspective. *arXiv preprint arXiv:2202.01602*, 2022.
- G. Laberge, Y. Pequignot, A. Mathieu, F. Khomh, and M. Marchand. Partial order in chaos: Consensus on feature attributions in the rashomon set. *Journal of Machine Learning Research*, 24(364):1–50, 2023.
- E. L. Lehmann and J. P. Romano. *Testing Statistical Hypotheses*. Springer, 3rd edition, 2005.

- S. M. Lundberg and S.-I. Lee. A unified approach to interpreting model predictions. In *Advances in Neural Information Processing Systems*, volume 30, 2017.
- T. Nipkow. Social choice theory in HOL: Arrow and Gibbard-Satterthwaite. *Journal of Automated Reasoning*, 43:289–304, 2009.
- M. Noguer i Alonso. Mathematical foundations of explainability. *SSRN Working Paper*, 2025.
- Office of the Comptroller of the Currency. Supervisory guidance on model risk management (SR 11-7/OCC 2011-12). OCC Bulletin 2011-12, 2011.
- S. Rao. The limits of AI explainability: An algorithmic information theory approach. *arXiv preprint arXiv:2504.20676*, 2025.
- M. T. Ribeiro, S. Singh, and C. Guestrin. “why should i trust you?”: Explaining the predictions of any classifier. In *ACM SIGKDD International Conference on Knowledge Discovery and Data Mining*, 2016.
- C. Rudin et al. Position: Amazing things come from having many good models. In *International Conference on Machine Learning (ICML)*, 2024.
- L. S. Shapley. A value for n-person games. In *Contributions to the Theory of Games II*, number 28 in Annals of Mathematics Studies, pages 307–317. Princeton University Press, 1953.
- S. Srinivas and F. Fleuret. Full-gradient representation for neural network visualization. In *Advances in Neural Information Processing Systems*, volume 32, 2019.
- The mathlib Community. The Lean mathematical library. In *Certified Programs and Proofs (CPP)*, 2020.
- A. B. Tsybakov. *Introduction to Nonparametric Estimation*. Springer, 2009.
- Y. Zhang, J. D. Lee, and F. Liu. Statistical learning theory in Lean 4: Empirical processes from scratch. *arXiv preprint arXiv:2602.02285*, 2026. URL <https://arxiv.org/abs/2602.02285>.

Table 9: Lean file cross-reference (54 files, 305 theorems, 16 axioms).

File	Section	Key Result
Defs.lean	§2	14 axioms + derived theorems
Trilemma.lean	Thm. 5	attribution_impossibility
Iterative.lean	§3.3	iterative_impossibility
General.lean	§4.1	gbdt_impossibility
SplitGap.lean	Lem. 14	split_gap_exact
Ratio.lean	Thm. 15	ratio_tendsto_atTop
SpearmanDef.lean	§4	spearmanCorr_bound
Lasso.lean	§4.2	lasso_impossibility
NeuralNet.lean	§4.3	nn_impossibility
Impossibility.lean	Combined	not_equitable, not_stable
Corollary.lean	Cor. 19	consensus_equity
SymmetryDerive.lean	Derived	attribution_sum_symmetric
DesignSpace.lean	Thm. 28	design_space_theorem
DesignSpaceFull.lean	Step 3	family_a_or_family_b
ModelSelection.lean	Thm. 41	model_selection_impossibility
UnfaithfulBound.lean	Thm. 29	stable_complete_unfaithful
PathConvergence.lean	Thm. 30	relaxation_paths_converge
RashomonUniversality.lean	Thm. 9	rashomon_from_symmetry
RashomonInevitability.lean	Thm. 12	rashomon_inevitability
ConditionalImpossibility.lean	Thm. 47	conditional_impossibility
FlipRate.lean	Prop. 17	binary_group_flip_rate
SymmetricBayes.lean	Thm. 37	symmetric_bayes_dichotomy
CausalDiscovery.lean	Thm. 45	causal_discovery_impossibility
FairnessAudit.lean	Thm. 48	fairness_audit_impossibility
FIMImpossibility.lean	Thm. 49	gaussian_rashomon_witnesses
QueryComplexity.lean	Thm. 52	query_complexity_lower_bound
Consistency.lean	§11	axiom_system_consistent
<i>Bounds, universality, and infrastructure:</i>		
EnsembleBound.lean	§5	ensemble_bound_formula
Efficiency.lean	§10	across_model_no_constraint
AlphaFaithful.lean	§13	alpha_faithful_bound
GaussianFlipRate.lean	§4.1	Phi_neg
LocalGlobal.lean	§8.7	local_attribution_impossibility
RobustnessLipschitz.lean	§13	flip_rate_robust
SBDInstances.lean	§7	attribution_sbd_unfaithful
ModelSelectionDesignSpace.lean	§7	model_family_a_or_family_b
<i>Axiom strengthening:</i>		
Qualitative.lean	Stratification	impossibility_qualitative
ProportionalityLocal.lean	Stratification	gbdt_impossibility_local
LocalSufficiency.lean	Stratification	local_proportionality_suffices
StumpProportionality.lean	§4.1	stump_proportionality_unique
IntersectionalFairness.lean	§8.2	intersectional_audit_impossibility
MutualInformation.lean	§13	mi_is_exact_boundary
Setup.lean	Bundled	attribution_impossibility_bundled
ApproximateEquity.lean	Stratification	rashomon_from_bounded_proportionality
QueryComplexityParametric.lean	§8.4	query_complexity_parametric
<i>New derivations (this session, zero new axioms):</i>		
MeasureHypotheses.lean	Definitions	IsDGPSymmetric, IsNonDegenerate
UnfaithfulQuantitative.lean	Thm. 29	attribution_prob_half
VarianceDerivation.lean	§5	consensus_variance_from_independence
QueryComplexityDerived.lean	§8.4	chebyshev_query_bound
BinaryQuantizer.lean	§4.1	binary_quantizer_fraction
BayesOptimalTie.lean	§6	tie_dominates_commitment
LossPreservation.lean	§3.1	rashomon_from_swap_with_loss
ParetoOptimality.lean	§5.1	dash_unique_pareto_optimal
<i>Infrastructure:</i>		
Basic.lean	Import hub	(all 54 files)
RandomForest.lean	§4.4	(documentation only)

Table 10: Positioning relative to prior attribution impossibility results. These criteria reflect the specific contributions of the present work; each prior result makes distinct contributions not captured by this comparison.

Result	Stability?	Quantitative?	Resolution?	Formal?
Bilodeau et al. (2024)	No	No	No	No
Huang et al. (2024)	No	No	No	No
Srinivas et al. (2019)	No	No	No	No
Rao (2025)	No	No	No	No
Laberge et al. (2023)	Empirical	No	No	No
Herren & Hahn (2023)	Inference	No	No	No
Jin et al. (2025)	Certificates	No	No	No
This paper	Impossibility	Yes	DASH	Lean 4

Table 11: Full cross-implementation comparison on Breast Cancer (50 models each).

Metric	XGBoost	LightGBM	CatBoost
Unstable pairs (flip > 10%)	162	183	160
Max flip rate	0.500	0.500	0.500
Z-test correlation $r(Z, \text{flip})$	-0.898	-0.901	-0.892
Screen precision	0.26	0.20	—
DASH max flip ($M=25$)	0.48	0.48	0.48

Table 12: Summary of additional experiments.

Experiment	Key finding	Script
Monte Carlo flip rate	$\Phi(-\text{SNR})$ validated to <1.3% error	<code>monte_carlo_flip_rate.py</code>
Hyperparameter sweep	Min flip 38.7% at $\rho=0.5$; never 0%	<code>hyperparameter_sensitivity.py</code>
Class imbalance	1:5+ imbalance \rightarrow 100% pairs unstable	<code>class_imbalance_instability.py</code>
Missing data	MCAR/MAR/MNAR all compound instability	<code>missing_data_instability.py</code>
Longitudinal drift	Spearman degrades 1.0 \rightarrow 0.18 over 31 rounds	<code>longitudinal_retraining.py</code>
Adversarial configs	All 108 configs hit 0.500 ceiling at $\rho=0.9$	<code>adversarial_max_instability.py</code>
Bag-of-words NLP	60% unstable top-1, 91% top-3	<code>nlp_token_instability.py</code>
Time-series features	27% within-series pairs unstable	<code>timeseries_instability.py</code>
SAGE comparison	SAGE 92%, Boruta 94% unstable	<code>sage_comparison.py</code>
DASH breakdown	Contamination sweep confirms mean optimality	<code>dash_breakdown_point.py</code>
Regulatory case study	43.2% unstable adverse action reasons	<code>regulatory_case_study.py</code>